

CRANIOFACIAL DEVELOPMENT OF
ZEBRAFISH AND OTHER
DANIONINAE, AND THE ROLES OF
THYROID HORMONE IN SHAPING THE
SKULL

Stacy Vy Nguyen

A dissertation
submitted to the Faculty of
the department of Biology
in partial fulfillment
of the requirements for the degree of
Doctor of Philosophy

Boston College
Morrissey College of Arts and Sciences
Graduate School

March 2024

ABSTRACT

CRANIOFACIAL DEVELOPMENT OF ZEBRAFISH AND OTHER DANIONINAE, AND THE ROLES OF THYROID HORMONE IN SHAPING THE SKULL

Stacy V. Nguyen

Advisor: Sarah K. McMenamin, Ph.D.

Proper bone development requires coordination and timing of specific morphogenetic events, and relative shifts in these temporal processes can change morphology. Thyroid hormone (TH) plays an important role in regulating the timing of vertebrate skeletogenesis, and the hormone induces the profound skeletal shape changes that occur during amphibian metamorphosis. Like humans, zebrafish do not undergo an ecological metamorphosis; yet TH is essential in coordinating postembryonic developmental processes. In particular, several elements of the craniofacial skeleton that continue to ossify and remodel during later stages of development are sensitive to TH titer. My aims focus on the role of TH in regulating skeletal growth and shape changes in zebrafish. To examine changes in the entire zebrafish skeleton during normal postembryonic development, I generated a skeletal reference of microCT scans of zebrafish ranging from early juvenile through adult stages (Chapter 2). After defining the normal changes that wild-type zebrafish undergo, I hypothesized that TH coordinates the developmental shape changes and determined the role of TH in stimulating developmental shape change in zebrafish skulls and its effects on skeletogenic cell populations (Chapter 3). Finally, I investigated whether phenotypes

induced by altered TH levels mirror some of the evolutionary diversity seen across Danioninae craniofacial skeletons (Chapter 4). My research elucidates the role of TH in the regulation of bone growth and shape change in a vertebrate system and provides new insights into the natural craniofacial diversity of Danioninae.

ACKNOWLEDGMENTS

This dissertation and body of work would not be possible without the love, support, and encouragement of many individuals whom I have had the profound privilege of having in my life.

First, thank you to my advisor and mentor Sarah McMenamain, for everything you have done for me during my time at Boston College and in your lab. Our countless discussions about science, research, and life have undoubtedly helped to shape the researcher I am today and the educator I hope to be tomorrow. Thank you for taking a chance on me, for giving me the opportunity to pave my own way, for reminding me that I deserve a seat at the table, and for always believing in me.

Thank you to my dissertation committee members, Vicki Losick, Shannon Fisher, Chris Kenaley, and MJ Gubbels, for the constructive conversations and insight on research and career ambitions alike.

Thank you to the Boston College Biology Department, especially Colette McLaughlin, Diane Butera, and Dina Goodfriend, for the never-ending support and words of encouragement. Thank you to the Higgins Hall staff, Kiel Smith, Chris Cardoso, John O'Grady, Walter Carberry, and many others, for your dedication and hard work. Thank you to the ACF staff, especially Todd and Nancy, for all your help with taking care of our zebrafish.

Thank you to the members of the McMenamain Lab, both past and present, that have made coming to lab every day an absolute joy and adventure. To my fellow grad students Melody and Eric, thank you for always lending a listening ear, having my back, and accompanying me on coffee runs. To Yinan and Anna, thank you for being my first

friends in lab. To Joan, thank you for keeping me situationally aware. To my first undergrads Mary and Raj, thank you for your patience and hard work as we built these projects together. To Emma and Rachel, thank you for always being in my corner. To Bella and Brendan, thank you for trusting me to be your unofficial lab mentor and for countless shenanigans. To Gabby and John, thank you for the best memories in the microCT bay. To Jenny, thank you for late-night work parties in lab. To Andrew and Deirdre, thank you for your friendship during the last chapter of my time in lab.

Thank you to all of my friends in Boston, California, and everywhere in between. Graduate school has been a long six years, but your friendship has kept me going despite the difficult challenges that have come and gone. To my 215 roommates Bryant and Meg, thank you for the best movie marathons and board game nights, and for being my family away from family. To Anthony, Vickie, Steve, Joy, Denny, and Darin, thank you for giving me a reason to look forward to Wednesdays. To Bethany, Stacy, Sarah, and Jade, thank you for your support in all my endeavors since we were teenagers. To Jueun, Rushi, and Jesse, thank you for your “just because” texts and phone calls that always brighten my day. To James and John, thank you for 7+ years of friendship.

Thank you to my mentors Fang Wang, Jennifer Ho-Chen, and Thomas Taylor for helping to make graduate school a reality. Your guidance and support gave me the confidence to pursue my career aspirations.

A sincere thank you to my family for their immeasurable love and support from the very beginning. Thank you to my brother, James Nguyen, for being my first friend and partner in crime. I am so grateful to have such a hardworking and caring brother in my life. Thank you to my parents, Andrew Anh Nguyen and Laura Liễu Nguyen, for

sacrificing everything for my future. Everything I do, I do with the hopes of making you proud. I would like to especially thank my mother for her endless words and acts of love and encouragement. I am the woman I am today because of you, and I am so lucky to have you as my role model and best friend. *Cám ơn Mẹ, con thương Mẹ.*

Lastly, thank you to my forever partner in life and favorite person, Alex Browman. It is truly difficult to put my immense gratitude into words. You are my biggest cheerleader, stats consultant, R troubleshooter extraordinaire, sounding board for all ideas, and so, so much more. I cannot imagine going through graduate school without our family by my side. You and Cole are my heart and my life, always.

TABLE OF CONTENTS

ABSTRACT	iv
ACKNOWLEDGMENTS	v
List of tables	xi
List of figures	xii
Table of abbreviations	xv
CHAPTER 1	1
Introduction: Craniofacial Development, Metamorphosis, and the role of Thyroid Hormone on Skeletogenesis	1
1.1 CRANIOFACIAL MORPHOLOGY THROUGHOUT DEVELOPMENT	2
1.2 DEVELOPMENTAL TIMING	2
1.3 METAMORPHOSIS AND THYROID HORMONE	3
1.4 METAMORPHOSIS IN TELEOSTS	4
1.5 THYROID HORMONE REGULATION AND ACTION	5
1.6 ZEBRAFISH AS A SKELETOGENESIS MODEL	7
1.7 ZEBRAFISH SKELETOGENESIS	8
1.8 THYROID HORMONE AND ZEBRAFISH SKELETOGENESIS	10
1.9 MICROCOMPUTED TOMOGRAPHY	12
1.10 GEOMETRIC MORPHOMETRICS	13
1.11 ZEBRAFISH BELONG TO THE SUBFAMILY DANIONINAE	15
1.12 RATIONALE AND RESEARCH QUESTIONS	15
Chapter 2	17
Skeletal changes in wild-type zebrafish during normal juvenile and adult development	17
2.1 INTRODUCTON	18
2.1.1 The zebrafish skeleton.....	18
2.1.2 Online repositories and resources	18
2.1.3 Rationale for and summary of this research.....	19
2.2 RESULTS	20
2.2.2 Zebrafish skeletons increase in density and volume throughout juvenile and adult growth.....	21
2.2.3 Segmentation of individual bones captures the association of each skeletal element in relation to others in 3D space.....	24
2.3 DISCUSSION	25
2.3.1 MicroCT technology as a tool for capturing shape change across developmental stages	25
2.3.2 Progressive ossification of skeletal elements during later stages of development..	26
2.3.3 The zebrafish skeleton continues to undergo shape changes during postembryonic development	26
2.3.4 The skeletal reference as a normal morphological baseline.....	27
2.4 MATERIALS AND METHODS	29
2.4.1 Fish rearing and measurement.....	29
2.4.2 MicroCT scanning and reconstruction	30
2.4.3 Quantification and segmentation.....	31
2.4.4 Interactive 3D PDFs and data accessibility.....	32

2.5	SUPPLEMENTAL DATA.....	34
Chapter 3	39
Thyroid hormone shapes the zebrafish craniofacial skeleton during juvenile and adult development	39
3.1	INTRODUCTION	40
3.1.1	Metamorphosis in teleosts.....	40
3.1.2	Thyroid hormone and its role during metamorphosis.....	40
3.1.3	Skeletogenesis & skeletogenic cell types.....	41
3.1.4	Responses of skeletogenic cell types to TH.....	42
3.1.5	Shape change during postembryonic development.....	43
3.1.6	Rationale for and summary of this research.....	43
3.2	RESULTS	44
3.2.1	2D morphometric analysis of specific craniofacial bones reveals that TH coordinates allometric shape change during development.....	44
3.2.1a	Tripus.....	44
3.2.1b	Lower Jaw.....	47
3.2.1c	Hyomandibula.....	50
3.2.1d	Pharyngeal jaws.....	53
3.2.2	3D morphometric analysis reveals the role of TH in shaping the overall head shape of zebrafish during normal development.....	55
3.2.3	The dermatocranium and jaw elements of the zebrafish craniofacial skeleton undergo the most change during juvenile and adult development.....	57
3.2.4	Thyroid hormone influences osteoblast and chondrocyte populations during early metamorphosis.....	58
3.3	DISCUSSION	62
3.3.1	TH regulates the rate of ossification of specific skeletal elements.....	62
3.3.2	The zebrafish skull undergoes shape changes during later stages of development that are sensitive to thyroid hormone.....	63
3.3.3	Comparing 2D and 3D morphometric analyses.....	63
3.3.4	Thyroid hormone alters osteoblast and chondrocytes cell populations.....	64
3.4	MATERIALS AND METHODS	65
3.4.1	Fish rearing and thyroid ablation.....	65
3.4.2	MicroCT scanning and 3D modeling.....	65
3.4.3	Landmarking and geometric morphometrics.....	66
3.4.4	Fluorescent Imaging.....	69
3.5	SUPPLEMENTAL DATA	70
CHAPTER 4	71
Craniofacial diversity across Danionins and effects of TH status on adult craniofacial morphology of two Danio species	71
4.1	INTRODUCTION	72
4.1.1	Using zebrafish and its relatives for research and craniofacial development.....	72
4.1.2	Danioninae phylogeny.....	72
4.1.3	Danioninae comparative studies.....	73
4.1.4	Danioninae use as research models.....	73
4.1.5	Fish craniofacial biology & craniofacial comparison between Danio rerio and other Danios.....	74
4.1.6	Role of TH in craniofacial skeleton development.....	75
4.1.7	Rationale for and summary of this research.....	75

4.2	RESULTS.....	76
4.2.1	Danioninae exhibit a range of craniofacial shapes.....	76
4.2.2	Centroid distance is correlated with phylogenetic distance	78
4.2.3	Thyroid hormone-altered heads have unique craniofacial skeletons	79
4.3	DISCUSSION	80
4.3.1	Diversity of Danioninae craniofacial head shapes and relationship to phylogeny .	80
4.3.2	Detecting specific differences in upper jaw morphology.....	81
4.3.3	Thyroid hormone stabilizes craniofacial phenotypes.....	82
4.4	MATERIALS AND METHODS.....	82
4.4.1	Fish rearing and preparation.....	82
4.4.2	MicroCT scanning and 3D modeling	83
4.4.3	Automatic landmarking and geometric morphometrics.....	84
4.5	SUPPLEMENTAL DATA.....	86
CHAPTER 5.....		89
Discussion: Research summary and future directions		89
5.1	RESEARCH SUMMARY & FUTURE DIRECTIONS	90
5.1.1	Research goals.....	90
5.1.2	A developmental framework for assessing disrupted phenotypes	90
5.1.3	Advancement of the understanding of the role of thyroid hormone in zebrafish skeletogenesis during postembryonic development	91
5.1.4	Insight into the craniofacial diversity of the Danioninae subfamily	93
5.1.5	Conclusion and future directions.....	95

List of tables

Supplemental Table 2.1. Summary of categories of sizes, sample numbers, and MorphoSource ID. -----	28
Supplemental Table 2.2. Information about every individual scanned. -----	29-30
Supplemental Table 2.3. Summary of statistical analyses for pairwise comparisons of vertebral canal widths in 12, 16, 20 and 24 mm SL zebrafish. -----	31-32
Supplemental Table 3.1. Summary of 3D landmarking scheme. -----	64
Supplemental Table 4.1 Centroid distance is correlated with phylogenetic distance. ----	79
Supplemental Table 4.2. Summary of species identification of species obtained from the pet trade. -----	101

List of figures

Figure 1.1 The life cycle of a teleost. -----	5
Figure 1.2 Thyroid hormone regulatory pathway and action on bone. -----	6
Figure 1.3 Ossification of craniofacial skeleton in zebrafish by calcein staining. -----	7
Figure 1.4 Postembryonic development in zebrafish. -----	9
Figure 1.5 Thyroid hormone regulates the development of several traits in zebrafish. --	10
Figure 2.1 Cross sections of microCT scans visualized in 3D Slicer. -----	19
Figure 2.2 Increasing skeletal density and volume with linear growth. -----	21
Figure 2.3 Quantified skeletal density and volume relative to linear growth. -----	22
Figure 2.4 Anatomy of the craniofacial skeleton. -----	23
Figure 2.5 Shape change of the lower jaw and caudal vertebrae. -----	25
Figure 2.6. DMSO-treated zebrafish have similar skeleton shape and bone density compared to wild-type zebrafish. -----	23
Figure 2.7 Manually measured standard lengths are closely correlated to digitally measured standard lengths. -----	28
Figure 2.8 Histogram showing size distribution of samples scanned. -----	29
Figure 2.9 Preview of interactive PDF with freely movable 3D models for 24 mm SL individual. -----	31
Figure 3.1 Specific features of the tripus are sensitive to developmental TH. -----	43
Figure 3.2 The tripus does not markedly change shape across developmental stages, but developmental TH titer changes the shape of the tripus. -----	44
Figure 3.3 Features of the lower jaw are sensitive to developmental TH. -----	46

Figure 3.4 The lower jaw changes shape during larval and juvenile development and this shape change is dependent on TH. -----47

Figure 3.5 Features of the hyomandibula are dependent on developmental TH. -----49

Figure 3.6 TH stimulates development of a mature shape in the hyomandibula. -----50

Figure 3.7 TH is required for adult shape in the pharyngeal jaws. -----52

Figure 3.8 Developmental TH sculpts the adult zebrafish skull. -----54

Figure 3.9 TH regulates the developmental trajectory of overall head shape in juvenile and adult zebrafish. -----55

Figure 3.10 The zebrafish skull expands in several dimensions during juvenile and adult development. -----56

Figure 3.11 Thyroid hormone regulates osteoblast populations in zebrafish skulls. -----57

Figure 3.12 Dorsal view of *collala* & *sp7* expression in 5.5mm SL euthyroid and hypothyroid zebrafish. -----58

Figure 3.13 Lateral view of *collala* & *sp7* expression in 5.5mm SL euthyroid and hypothyroid zebrafish. -----59

Figure 3.14 Ventral view of *collala* & *sp7* expression in 5.5mm SL euthyroid and hypothyroid zebrafish. -----60

Figure 3.15 Landmarks used for developmental morphometric analysis of four craniofacial bones. -----65

Figure 3.16 Landmarks used for developmental 3D morphometric analysis of overall head shape. -----66

Figure 4.1 Danioninae are a subfamily of Cyprinidae. -----75

Figure 4.2 Capturing craniofacial shape information with automatic 3D landmarking. --75

Figure 4.3 Danioninae have a spectrum of head and bone shapes. -----76

Figure 4.4 Thyroid hormone regulates craniofacial morphology in *Danio rerio* and *Danio albolineatus*. -----77

Figure 4.5 Thyroid hormone altered heads have unique craniofacial skeletons. -----78

Supplemental Figure 4.1 Centroid distance is correlated with phylogenetic distance. --84

Supplemental Figure 4.2 Centroid distance relationships are maintained between different templates used for automatic 3D landmarking. -----85

Supplemental Figure 4.3 Centroid distance relationships are maintained between 3000 and 6700 automatically placed 3D landmarks. -----86

Table of abbreviations

DMSO	dimethylsulfoxide
dpf	days post fertilization
microCT	microcomputed tomography
MTZ	metronidazole
PCA	principal component analysis
PFA	paraformaldehyde
SL	standard length
T3	triiodothyronine (active thyroid hormone)
T4	thyroxine (inactive thyroid hormone)
TH	thyroid hormone
TR	nuclear thyroid hormone receptor
TRE	thyroid hormone response element

CHAPTER 1

Introduction: Craniofacial Development, Metamorphosis, and the role of Thyroid Hormone on Skeletogenesis

1.1 CRANIOFACIAL MORPHOLOGY THROUGHOUT DEVELOPMENT

Changing the shape of craniofacial bones can greatly alter the ecological function of a vertebrate, and understanding how developmental processes sculpt skeletal phenotypes across the organisms life span can provide insight into evolutionary adaptations (Esteve-Altava & Rasskin-Gutman, 2015; Keer et al., 2022; Kyomen et al., 2023; S. McMenamin et al., 2017; Mork & Crump, 2015). In zebrafish, the transitions between developmental stages involves morphological and physiological changes, including ossification of essential craniofacial bones that allow for the onset of adult behaviors and adult feeding kinematics (Hernandez & Staab, 2015; McMenamin et al., 2017; Staab et al., 2012). The developmental timing of such ossification events is crucial for the proper formation of the bones, ensuring adaption to environmental conditions. Nonetheless our understanding of such transitions is incomplete, therefore I have addressed the following questions in my dissertation: 1) what changes does the zebrafish skeleton undergo during juvenile and adult development, 2) what is the role of thyroid hormone (TH) in stimulating developmental shape change in zebrafish skulls, and 3) do TH altered zebrafish skulls closely resemble the natural craniofacial diversity of the subfamily Danioninae.

1.2 DEVELOPMENTAL TIMING

Relative shifts in the timing of developmental processes can change the morphology of an organism (Bonett, 2021; Duboule, 1994). These relative shifts, known as heterochrony, involve the alteration of relative developmental growth rates or the relative timing of developmental processes and can lead to developmental extensions or truncations (Bonett, 2021). Developmental truncation results in progenesis, an early offset

of development, or neoteny, the slowed rate of development (Alberch et al., 1979). For example, paedomorphosis (the retention of larval traits into adult stages) in certain species of newts and salamanders is seen as an example both of reproductive progenesis (early sexual maturation), as seen in the palmate newt *Lissotriton helveticus*, and neoteny (delayed somatic development), of which the Ezo salamander *Hynobius retardatus* is a prime example (Denoël et al., 2019; Denoel & Joly, 2000; Okamiya et al., 2021). These modified ontogenetic pathways are dependent on relative growth rates in aquatic and terrestrial habitats (Denoël & Joly, 2000).

Skeletogenesis and bone remodeling normally occur in highly coordinated developmental sequences in which specific genes must be expressed in the correct location at the correct time (Delaurier et al., 2010; Witten et al., 2001). Coordination of different developmental events is necessary for the organization, patterning, and morphogenesis of many tissues, and heterochronic alterations can cause severe skeletal malformations (Fazzalari, 2008; Hammond et al., 2012). Craniosynostosis, the premature ossification of the cranial sutures, is an example of heterochrony in which there is an earlier shift in the timing of bone fusion due to increased expression of *runx2* (Esteve-Altava & Rasskin-Gutman, 2015). This results in the improper development of the frontal and parietal bones, affecting the growth and development of the underlying brain (Teng et al., 2018). Differences in palatal suture development via heterochronic shifts may also help to explain morphological differences between species (Goswami et al., 2013; Shibusawa et al., 2021).

1.3 METAMORPHOSIS AND THYROID HORMONE

A classic example of coordinated developmental timing, metamorphosis is a hormone-induced shift during postembryonic development, involving major changes in

morphology and physiology. In 1912, Gudernatsch discovered that thyroid hormone (TH) was responsible for amphibian metamorphosis after feeding thyroid gland extract to tadpoles (Brown & Cai, 2007). Since then, more than a century of research examined the mechanisms of TH signaling that are responsible for the profound morphological changes that occur during amphibian metamorphosis (Ruthsatz et al., 2020; Thambirajah et al., 2019). Numerous skeletal changes occur during amphibian metamorphosis, including the reduction of tail fins followed by the development of limbs (Thampi et al., 2018). Drastic metamorphic remodeling of the skull is dependent on developmental timing in which coordinated cell signaling results in the formation, reshaping, and fusion of skeletal elements (Vassilieva & Smirnov, 2021). In salamanders, heterochronic shifts in which somatic metamorphosis is delayed can lead to paedomorphosis. It has been shown that paedomorphosis can also arise from accelerating the rate gonadal development relative to somatic development (Bonett et al., 2014).

1.4 METAMORPHOSIS IN TELEOSTS

Encompassing over 30,000 known species, teleosts are bony ray-finned fishes that make up nearly half of all described vertebrate species. In teleosts, metamorphosis encompasses many life changes during larval, juvenile, and adult development, including alterations in morphology, ecology, and physiology (Fig 1.1, Fricke et al., 2023; McMenamin & Parichy, 2013). There is much diversity in these postembryonic transitions, during which some species experience major morphological changes comparable to (or more physiologically profound than) amphibian metamorphosis while others undergo more subtle transformations (McMenamin & Parichy, 2013). Such changes to morphology can allow the organism to exploit environments or niches that were previously inaccessible or

unsuitable at premetamorphic stages (Iwai & Tachiki, 2023). Hormones such as thyroid hormone play an important role in controlling these changes that occur during metamorphosis.

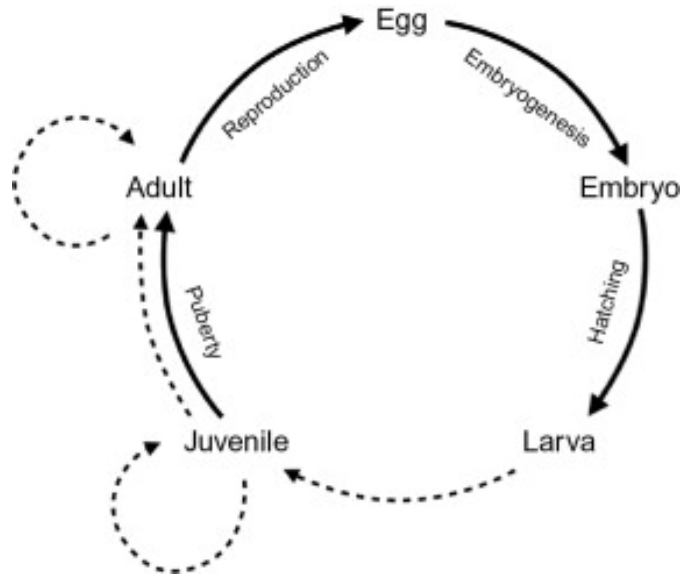


Figure 1.1 The life cycle of a teleost. Dashed lines represent possible periods of metamorphosis during the life cycle. Adapted from (McMenamin & Parichy, 2013).

1.5 THYROID HORMONE REGULATION AND ACTION

Regulation of systemic TH levels occurs through the hypothalamic-pituitary-thyroid axis (Tuchendler & Bolanowski, 2014). Thyroid releasing hormone is synthesized in the hypothalamus, signaling the production and release of thyroid stimulating hormone from the pituitary. This in turn binds to its receptor in the thyroid, signaling the production of TH in its inactive thyroxine (T₄) and active triiodothyronine (T₃) forms (Tuchendler & Bolanowski, 2014). Finally, active T₃ exerts its actions by binding to nuclear thyroid hormone receptors (TRs) (Fig 1.2, Kim & Mohan, 2013).

In target tissues, local TH action is regulated at three distinct levels by different types of regulators: transmembrane transporters such as MCT8 control the movement of TH in and out of the cell, deiodinases are enzymes that activate T4 and inactivate T3, and nuclear receptors play a major role in signaling (Vancamp & Darras, 2018; Waung et al., 2012). TH acts largely, although not exclusively, through TRs which interact together with co-activator or co-repressor complexes to bind response elements in the genome (Bakos et al., 2018; Waung et al., 2012). These receptors are ligand-inducible transcription factors that bind T3. Structurally, TRs function as homodimers or preferentially as heterodimers with other members of the same receptor family, most notably the retinoid X receptors (Vancamp et al., 2018). TRs stimulate transcription by binding to TH response elements (TREs) situated in regulatory regions of target genes (Chen et al., 2011).

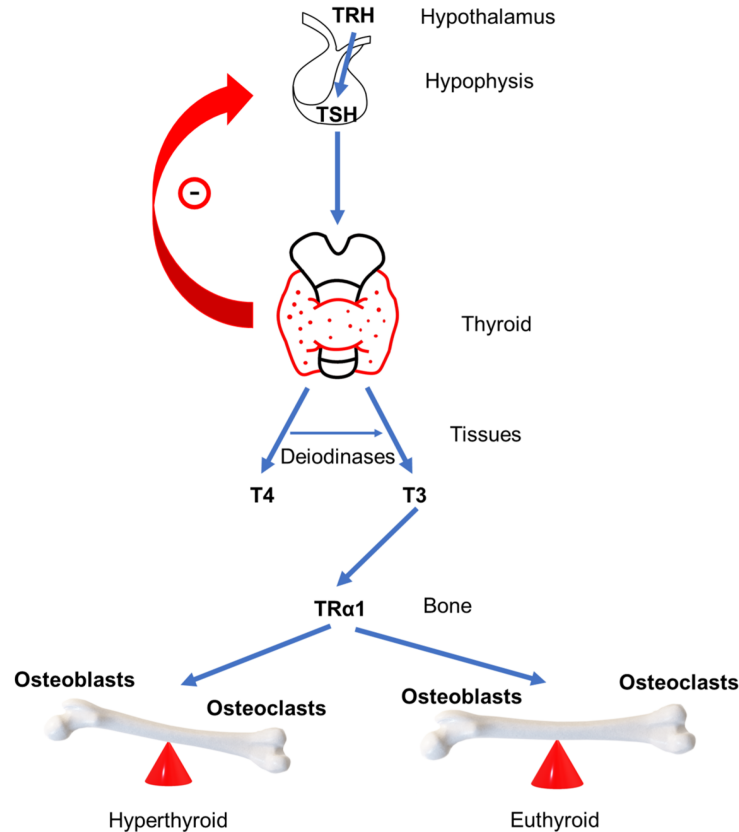


Figure 1.2 Thyroid hormone regulatory pathway and action on bone. TRH, thyroid releasing hormone; TSH, thyroid stimulating hormone; T4, thyroxine; T3, triiodothyronine; and TR α 1, thyroid hormone receptor α . Adapted from (Wahl et al., 2023).

1.6 ZEBRAFISH AS A SKELETOGENESIS MODEL

Zebrafish are a flexible tool for studying skeletogenesis. Their relatively small size, transparency during early stages of development, and ease of genetic manipulation make them a tractable model for vertebrate skeletogenesis. Zebrafish skeletons share several similarities with other vertebrate skeletons, including similar cell populations and types of ossification (Bruneel & Witten, 2015; Hammond et al., 2012). Current research continues to uncover the cellular and molecular mechanisms that drive skeletal morphogenesis in zebrafish.

A variety of mutant phenotypes in zebrafish serve as models for human bone disorders such as osteoporosis and osteogenesis imperfecta (Dietrich et al., 2021; Harris et al., 2014; Kwon et al., 2019a). Previous work in zebrafish has shed light on the basic developmental mechanisms and pathways that dictate skeletal development and maintenance (Tonelli et al., 2020; Yelick & Schilling, 2002). Previous research has elucidated the role of genes such as *runx2*, *sox9*, *tgfb2*, and *coll1a1* in zebrafish skeletogenesis (Delaurier et al., n.d.; Kimmel et al., 2010a; Kwon et al., 2019b). The majority of these studies that examine zebrafish skeletal morphology focused on either embryonic or adult stages of development and there remains a gap in knowledge about the intermediate juvenile stages in which many bones continue to undergo shape change (Henke et al., 2023; Kwon et al., 2019).

1.7 ZEBRAFISH SKELETOGENESIS

Constituting a majority of zebrafish skeleton, the ossification sequence of the craniofacial skeleton is well characterized, and many postembryonic stages are characterized by the ossification of specific skeletal elements (Fig 1.3, Bird & Mabee, 2003; Cubbage & Mabee, 1996, Parichy et al., 2009). In zebrafish, the metamorphosis of pigment patterns begins around 6 mm SL over the dorsal and ventral myotomes with the increasing appearance of metamorphic melanophores leading to the formation of primary stripes (Fig 1.4, Parichy, 2006). At the same time, skeletal elements including the basihyal, hyomandibula, branchiostegal rays, and supraoccipital are also actively ossifying in the zebrafish skull (Fig 1.3, Parichy et al., 2009).

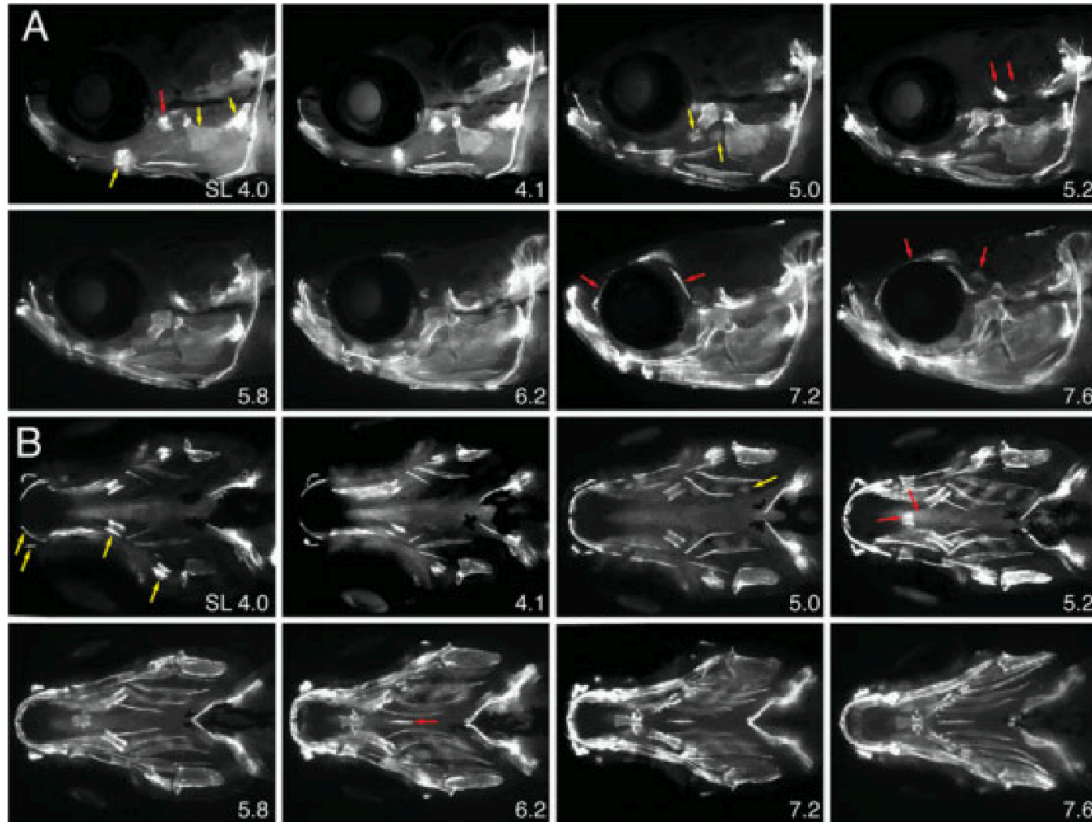


Figure 1.3 Ossification of craniofacial skeleton in zebrafish by calcein staining. Standard length is indicated in the bottom right on each image, and lateral views (panel A) and ventral views (panel B) are from the same individual. Select skeletal elements are indicated with arrows. A Panels : 4.0, quadrate, hyomandibula, opercle, ceratobranchial 5; 5.0, ceratobranchial 2, ceratobranchial 3; 5.2, prootic, basioccipital; 7.2, lateral ethmoid, pterosphenoid; 7.8, supraorbital, sphenotic; B Panels: 4.0, dentary, infraorbital, ceratohyal, hyomandibula (scored for lateral view); 5.0, ceratobranchial 4; 5.2, ventral hypohyals, basihyal; 6.2, urohyal; 8.0, infraorbital 1, dentary, ceratohyal. Adapted from (Parichy et al., 2009).

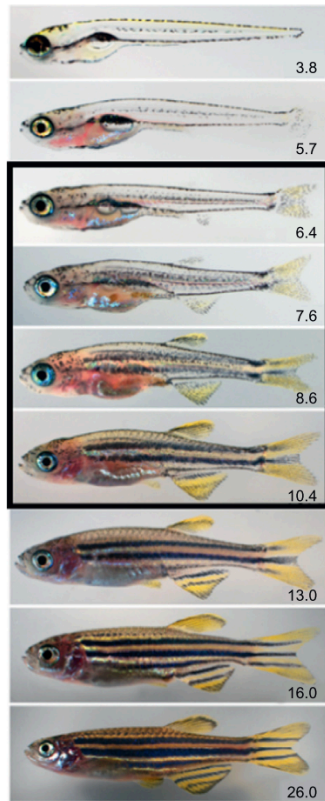


Figure 1.4 Postembryonic development in zebrafish. Standard length is indicated in the bottom right on each image, and peak metamorphic remodeling stages are outlined by the black box. Adapted from (McMenamin & Parichy, 2013).

1.8 THYROID HORMONE AND ZEBRAFISH SKELETOGENESIS

In zebrafish, thyroid follicles are present starting at ~60 hours post-fertilization as the embryo hatches (Alt et al., 2006). Conditional ablation of the thyroid follicles of the zebrafish transgenic line *Tg(tg:nVenus-v2a-nfnB^{wp.r18})* using metronidazole allows researchers to test the effects of TH on various aspects of postembryonic development (McMenamin et al., 2014). TH regulates body proportions in zebrafish, and hypothyroid (HypoTH) zebrafish show delayed growth patterns compared to wild-type zebrafish (Fig 1.5, Hu et al., 2019). Numerous studies have shown that blocking TH activity results in malformation of numerous skeletal elements in zebrafish such as the pharyngeal jaws and

premaxilla (Keer et al., 2019; McMenamin et al., 2017). In the zebrafish caudal fin, TH plays a role in proximodistal patterning regardless of fin size, inducing distal features such as segment shortening and branching of the fin ray (Harper et al., 2023). TH regulates the branching of the rays in the pectoral fins, and in HypoTH fish, these branches formed very distally or were absent from the fins (Ranieri, 2023).

Previous research has also shown that premature ossification of craniofacial elements such as the palatine, infraorbitals, and kinethmoid occurs under high levels of TH (Shkil et al., 2012). An anatomical assessment of the zebrafish skeleton compared the shape of specific bones in adults in wild-type, hypothyroid, and hyperthyroid conditions, finding alterations to morphology and ossification under both increased and decreased TH levels (Keer et al., 2019). The frontal and parietal bones of the dermatocranium ossify faster, overlapping more at the sutures than wild-type zebrafish, resembling craniosynostosis (Keer et al., 2019). The lower jaws of hyperthyroid (HyperTH) zebrafish are elongated, protruding past the upper jaw elements (Keer et al., 2019). What remains to be determined are the specific developmental trajectories that define intermediate morphologies of the entire zebrafish skeleton or specific craniofacial elements between juvenile and adult stages.

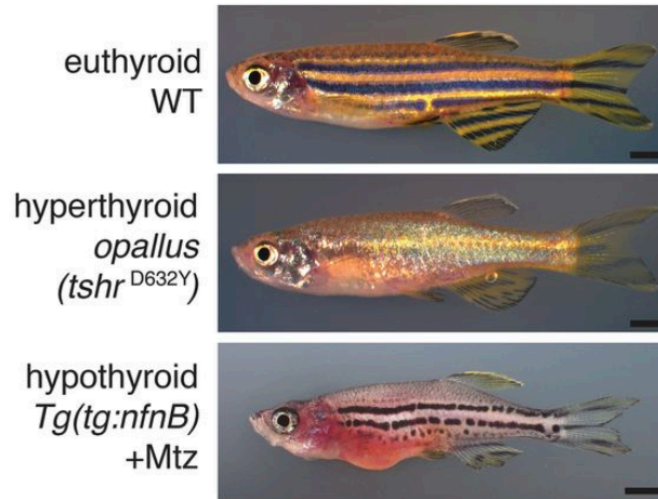


Figure 1.5 Thyroid hormone regulates the development of several traits in zebrafish. Wild-type (WT), hyperthyroid, and hypothyroid zebrafish phenotypes. Scale bars, 2 mm. Adapted from (McMenamin et al., 2014).

1.9 MICROCOMPUTED TOMOGRAPHY

In deploying high resolution techniques to characterize these shape change trajectories, we aim to capture how TH affects the dynamic morphology of the zebrafish skull. The first of these methods is microcomputed tomography (microCT), a 3D imaging technique for assessing phenotypes at high resolution (Charles et al., 2017). This non-destructive imaging modality uses x-ray attenuation of tissues in fixed specimens to reconstruct density images of regions of interest (Ritman, 2002). While microCT data provide researchers with valuable information, data-rich scans can require large amounts of storage space and access to costly analysis software (Tesařová et al., 2019). In recent years, open-access software and extensions have been developed, increasing the accessibility of microCT technology and analysis tools (Kikinis et al., 2014; Porto et al., 2021).

Previously, researchers have used the high sensitivity of microCT to study several aspects of zebrafish morphology, including characterizing the patterning of the axial skeleton of adult zebrafish and using it to develop a model for discriminating mutant phenotypes (Charles et al., 2017; Hur et al., 2017). Other studies have utilized this technique to quantify material properties of bones such as bone mineral density and bone volume, focusing on either larval or adult stages (Charles et al., 2017; W. N. Liao et al., 2023; Silvent et al., 2017). For my research, I chose to examine changes in bone shape, volume, and density in the zebrafish skeleton that occur during juvenile and adult development, scanning 60 individuals across these stages.

1.10 GEOMETRIC MORPHOMETRICS

After using microCT technology to generate 3D models of the zebrafish skeleton, subsequent 3D morphometrics allows for the detailed characterization of shape variation across sample populations (Caetano-Lopes et al., 2020; Hur et al., 2017). Geometric morphometrics is a methodological approach that captures shape, and can be used to measure shape changes that occur throughout development. This method uses Cartesian coordinates of geometric points, or landmarks, of specific anatomical structures or features on various organisms, organs, and components to capture shape information (Polly & Motz, 2016). Landmarks can be applied and digitized using either two dimensional (2D) images or three dimensional (3D) models using a variety of software and packages such as 3D Slicer, R, and Amira (Adams, Dean C., Collyer, M. L., Kaliontzpoulou, A. , Baken, 2022; Cardini et al., 2022; Kikinis et al., 2014).

Traditionally, landmark data collection is captured from manual annotation by trained researchers or experts, a process that can be time and labor intensive. As an alternative to manual landmarking, an extension of 3D Slicer was recently developed, called Automated Landmarking through Point cloud Alignment and Correspondence Analysis (ALPACA) (Porto et al., 2021). This approach uses point cloud registration from a specific template, aligns this template point cloud to point clouds generated from other models within a dataset, and performs a deformable registration step. After this step, the template point cloud is projected onto the target 3D model using point correspondence (Porto et al., 2021). As an approach that can increase both the scale and reproducibility of landmark-based data, this technique has broad research applications, ranging from ecology to evolution (Porto et al., 2021).

Zebrafish researchers have used morphometrics in several contexts such as measuring environmental exposure-induced phenotypes in larvae that are exposed to different toxic or mutagenic compounds (Dong et al., 2023; Gupta et al., 2018; Jarque et al., 2020). Morphometric analysis has also been utilized to generate a quantitative sex determination model and to model muscle or growth in zebrafish (Biga & Goetz, 2006; Duff et al., 2019). In this dissertation, I used a manual landmarking workflow to characterize both overall head shape and shape change of specific skeletal elements in zebrafish juveniles and adults to establish developmental trajectories at these stages. An automated landmarking workflow was developed to capture high resolution shape information of additional Danioninae species with diverse craniofacial skeletons.

1.11 ZEBRAFISH BELONG TO THE SUBFAMILY DANIONINAE

While researchers have begun to use both microCT technology and geometric morphometrics to characterize zebrafish morphology and development, these techniques have yet to be deployed for many zebrafish relatives. The Danioninae subfamily contains at least 20 genera and over 100 identified species common in India and southeast Asia (Conith et al., 2022; McCluskey & Postlethwait, 2015; Tang et al., 2010). Most species within Danioninae are endemic to several major hydrological basins across Southeast Asia; *Da. rerio* and *Da. albolineatus* being found most broadly in this region (Fang, 2003; McCluskey & Postlethwait, 2015). The organisms typically eat insects, crustaceans, algae, and detritus (McClure et al., 2006). Advances in molecular and genetic research in zebrafish has generated a growing interest in the phenotypic diversity of the broader Danioninae subfamily. This broader phylogenetic context can help provide ecological, evolutionary, and functional depth for zebrafish research, suggesting avenues for ongoing molecular and biomedical efforts and identifying informative phenotypes for further genomic and developmental analysis.

1.12 RATIONALE AND RESEARCH QUESTIONS

In this dissertation, I aim to shed light on the skeletogenic shape changes that zebrafish undergo during juvenile and adult stages of development and the influence of TH on such processes. To examine changes in the entire zebrafish skeleton during normal postembryonic development, I generated a database of microCT scans of zebrafish ranging from early juvenile through adult stages to serve as a skeletal reference of normal development (Chapter 2). I hypothesized that TH coordinates the developmental shape

changes of the craniofacial skeleton in zebrafish by influencing the behaviors of skeletogenic cell populations (Chapter 3). To assess the role of TH in regulating the developmental trajectories in which skeletal growth and shape changes occur in zebrafish, I analyzed changes in skeletal morphology for several skeletal elements and the entire craniofacial skeleton. Finally, to investigate craniofacial diversity across other Danioninae, I asked whether phenotypes that arise from modulated levels of TH mirror some of the natural craniofacial diversity seen across Danioninae skeletons (Chapter 4). My research expands on the role of TH in the regulation of bone growth and shape change during the postembryonic development stages of a widely-used vertebrate system, provides new insights into the natural craniofacial diversity of the Danioninae subfamily, and asks whether the thyroid axis may be responsible for the genetic changes that underlie phenotypic diversity among closely related organisms.

Chapter 2

Skeletal changes in wild-type zebrafish during normal juvenile and adult development

The material in this chapter was adapted from:

Nguyen, S.V., Lanni, D., Xu, Y., McMenamin, S.K. 3D dynamics of the zebrafish skeleton during postembryonic development. *Frontiers in Physiology*. 2022 May 26. doi: 10.3389/fphys.2022.875866

Raw microCT data in this chapter is available via the FaceBase repository at:

Sarah K. McMenamin, **Stacy Nguyen**, John Blythe. Thyroid hormone mediates juvenile and adult craniofacial shape change in zebrafish. *FaceBase Consortium* <https://doi.org/10.25550/1Q-X114> (2022)

2.1 INTRODUCTION

2.1.1 The zebrafish skeleton

The zebrafish skeleton is composed of the dermal skeleton (which includes teeth, scales, and fin rays) and an endoskeleton including the axial, craniofacial and appendicular elements (Tonelli et al., 2020). Several resources detail the normal anatomical development and sequence of ossification of the zebrafish skeleton, especially during early larval development (Bird & Mabee, 2003; Cabbage & Mabee, 1996; Kimmel et al., 2010b). However, less is known about skeletal changes during later juvenile and adult stages of development. Several craniofacial bones — including the dermatocranium and infraorbitals — do not become fully ossified until adult stages in zebrafish and developmental shape change of many of these skeletal elements has not been studied in detail (Chang & Franz-Odenaal, 2014; Mork & Crump, 2015).

2.1.2 Online repositories and resources

There is a growing number of online repositories of digital anatomy collections for a variety of organisms from mouse to turtle (Gray et al., 2023). In recent years, several developmental atlases have been generated from microCT scans for other models and organs, including a 3D atlas of the developing human embryo and the developing mouse heart (de Bakker et al., 2012; de Boer et al., 2012). FaceBase is a NIH-funded database of craniofacial data from mouse, human, and zebrafish that includes imaging from microCT, histological staining, and enhancer activity detection assays (Samuels et al., 2020). FishFace is the subset of FaceBase that hosts an online atlas of zebrafish craniofacial development, generated using fluorescent optical projection tomography and confocal microscopy (B. Eames et al., 2013). This database serves as a repository of confocal images

that capture the development of individual craniofacial elements up to 21 days post fertilization (dpf) (Eames et al., 2013), roughly equivalent to the AR (anal rays) and DR (dorsal rays) stages of larval development according to the postembryonic normal table (Parichy et al., 2009). FishFace also includes an interactive 3D tool for viewing the entire head at three select developmental stages.

2.1.3 Rationale for and summary of this research

To capture the changes which the zebrafish skeleton undergoes during juvenile and adult development, we generated an accessible skeletal reference from microCT scans of individuals ranging in size from 12 to 25 mm standard length (SL), ranging from J (juvenile) through A (adult) stages (Parichy et al., 2009). We show that even reproductively mature zebrafish continue to undergo substantial changes in skeletal morphology and density with continued adult growth. We demonstrate the use of this resource to quantify skeletal changes occurring with growth and development.

Using this dataset, we examined the morphological changes of vertebrae along the anterior-posterior axis of the vertebral column during juvenile and adult stages. We tested whether density and volume of the skeleton of juveniles and adults increase linearly or exponentially. Further, we asked whether patterns of skeletal density along the anterior-posterior axis of the skeleton shift are maintained with growth. This reference dataset of normal skeletal development can serve as a baseline to which disrupted developmental phenotypes can be compared. Moreover, we anticipate the dataset can be used as an anatomical reference in both educational and research settings.

2.2 RESULTS

2.2.1 Anatomical measurements from microCT cross sections

The small size of the zebrafish can pose a barrier to measuring small anatomical elements in 3D. However, microCT technology allows visualization and analysis of elements of interest. MicroCT scans generate cross sections that can be accessed using a variety of programs such as DataViewer (Bruker, Kontich, Belgium), Amira (Thermo Fisher Scientific FEI, Hillsboro, Oregon, United States) or ImageJ (National Institutes of Health, Bethesda, Maryland, United States). Any of these programs will allow a user to scroll through the stacks of cross-section images from the scans in any anatomical plane (e.g., see Fig 2.1B-D). These cross-sections capture details at a resolution of 10.5 μm , which allows anatomical measurements even in relatively small bones. To test these types of measurements, we focused on the morphological changes of vertebrae along the anterior-posterior axis. We examined sagittal cross sections (as in Fig 2.1D) from scans of adult zebrafish at four representative sizes (12, 26, 20 and 24 mm SL), measuring the diameter of the vertebral canal of vertebrae 2 through 10 (the rib-bearing vertebrae; Fig 2.1E). These widths increase markedly in more posterior vertebrae, indicating an expansion of the vertebral canal along the anterior-poster axis (Fig 2.1E).

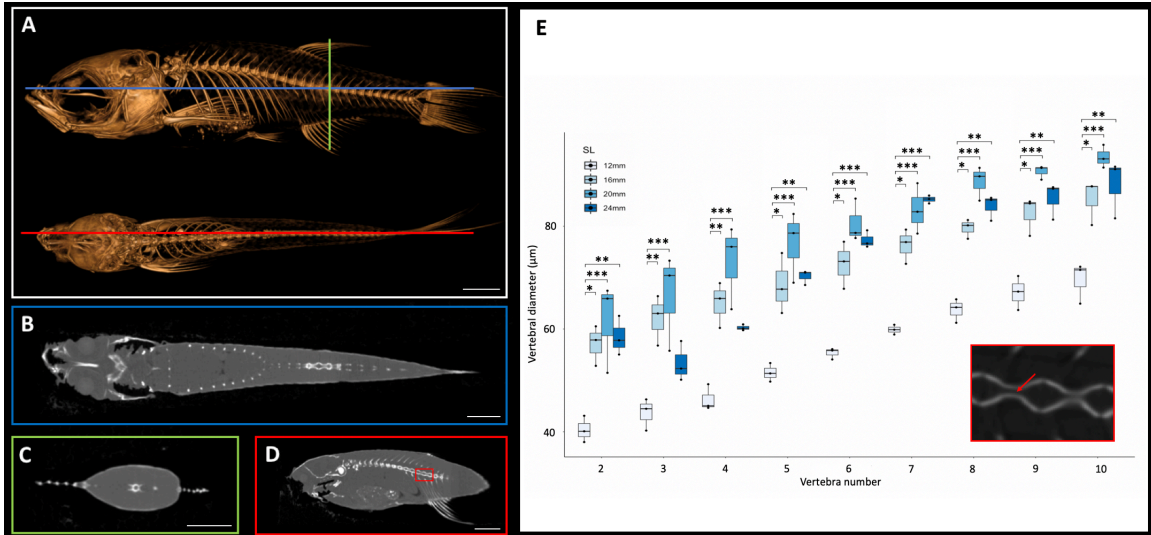


Figure 2.1 Cross sections of microCT scans visualized in 3D Slicer. (A), Surface rendering of 24 mm SL adult fish with lateral (top) and dorsal (bottom) views with coronal (blue), transverse (green), and sagittal (red) axes indicated. (B), Coronal cross section image. (C), Transverse cross section image. (D), Sagittal cross section image. (E), Quantification of vertebral canal width of 3 individual 24 mm SL adult fish; each individual is differentiated with different shapes (circle, square, triangle). Inset shows higher resolution image through vertebrate, corresponding to the boxed detail in panel D. Red arrow indicates a canal from which interior width was measure. Scale bars, 2 mm.

2.2.2 Zebrafish skeletons increase in density and volume throughout juvenile and adult growth

MicroCT datasets can be used to determine relative density. Our samples were all scanned under consistent parameters, so density can be directly compared between scans. We hypothesized that overall skeletal density would continue increasing throughout stages of adult growth. Indeed, density (as measured in mean grey values) increased markedly with increased size; regions of increasing density were particularly notable in the dermatocranium, ribs, and hypural complex (Fig 2.2A). Quantifying overall density of the skeleton as a function of body size (SL), we found that relative density increases roughly linearly throughout juvenile and adult development (Fig 2.3A). We next asked how density was distributed along the antero-posterior axis of the skeleton, and whether such patterns

change with growth. We found that density was highest in anterior regions of the body, corresponding to the craniofacial skeleton (Fig 2.2B). The high density of the head corresponds to the many plate bones in this region. The head also contains three pairs of otoliths; these dense, highly mineralized bony elements are used for hearing and vestibular function (Vasconcelos-Filho et al., 2019), and contribute to the overall density of the head. We note that while maximum density increases in increasingly large individuals, the distribution of density across the skeleton remains largely consistent (Fig 2.2B). Overall, we also see the same patterns of density distribution when comparing density to distance from the anterior portion of the zebrafish, and when normalizing density to the proportion of body length (Fig 2.2B).

MicroCT scans can be used to calculate the volume of tissues within a specified density range. Volumetric renderings of the skeleton highlighted the new appearance of bones in the skull and fins as fish continue to grow (Fig 2.2C). We further quantified the changes in overall skeletal volume, finding a roughly exponential increase in bone volume (a 3D measurement) with linear fish growth (a 2D measurement; Fig 2.3B).

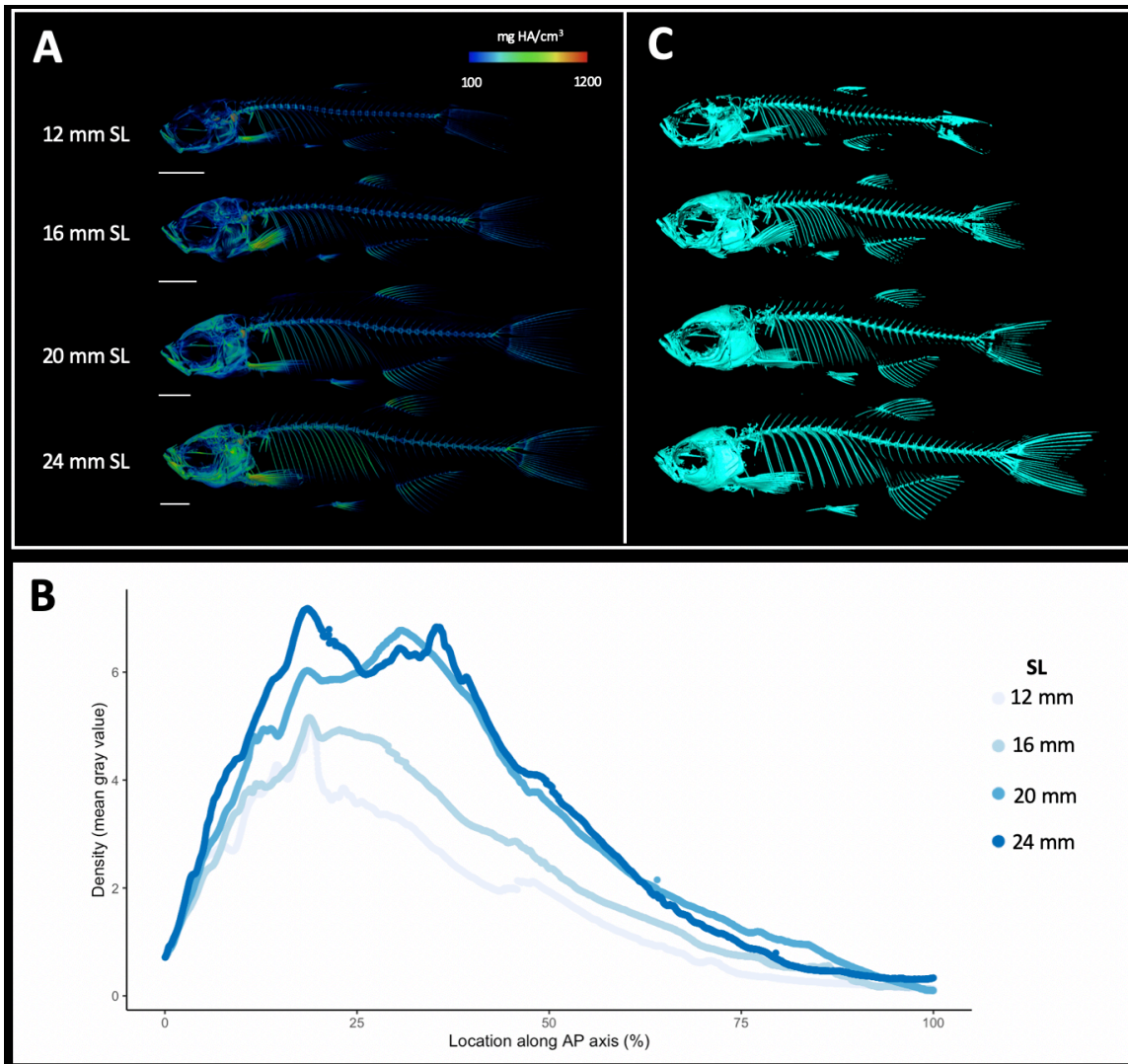


Figure 2.2 Increasing skeletal density and volume with linear growth. (A), Relative density renderings of skeletons from zebrafish at four different sizes (12, 16, 20, and 24 mm SL). Warmer colors indicate higher density regions. (B), Average density of zebrafish skeleton along the body length of individual zebrafish at four sizes. (C), Volume renderings of zebrafish at four sizes. Scale bars, 2 mm.

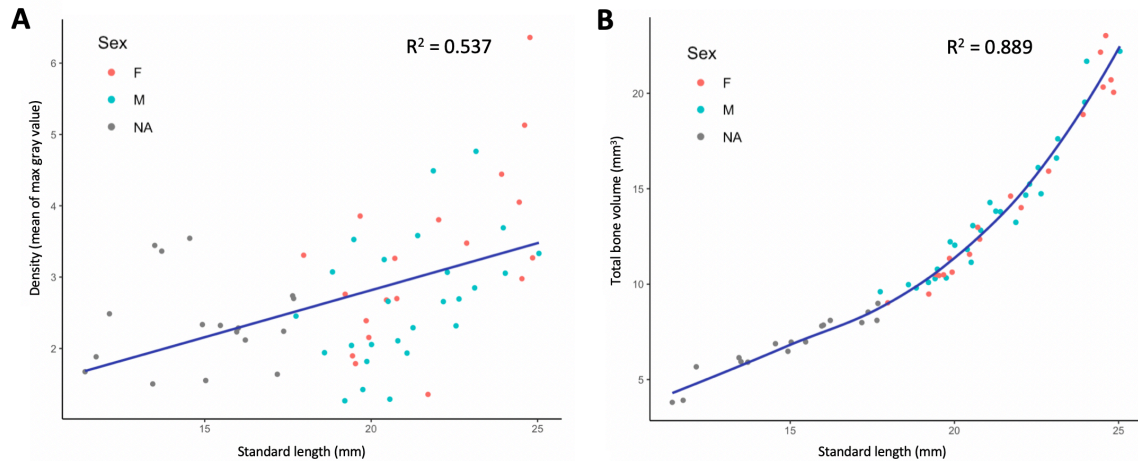


Figure 2.3. Quantified skeletal density and volume relative to linear growth. (A), Bone density relative to SL. (B), Total bone volume relative to SL. Bone volume calculated from all cross sections of scan. When possible, specimens were sexed. F, female. M, male. NA, not applicable.

2.2.3 Segmentation of individual bones captures the association of each skeletal element in relation to others in 3D space

3D models can be digitally segmented into individual elements. We segmented an adult skull into 27 individual, paired, or groups of bones (Fig 2.4). This segmented model captures the association of each element in 3D space and captures the anatomy of the adult craniofacial skeleton (Fig 2.4C). After segmentation, bones can be examined individually.

To visualize how an individual bone changes shape as development progresses, we “virtually dissected” the lower jaws and caudal vertebrae from fish at a range of sizes (Fig 2.5). We note that as adult zebrafish continue to grow, the anguloarticular prominence of the lower jaw becomes considerably more pronounced and the posterior end of the jaw widens (Fig 2.5A), while the caudal vertebrae do not undergo significant shape change during juvenile and adult development, indicating that developmental trajectories and

degrees in which shape change occurs in bones differ between skeletal elements at late stages of development (Fig 2.5B).

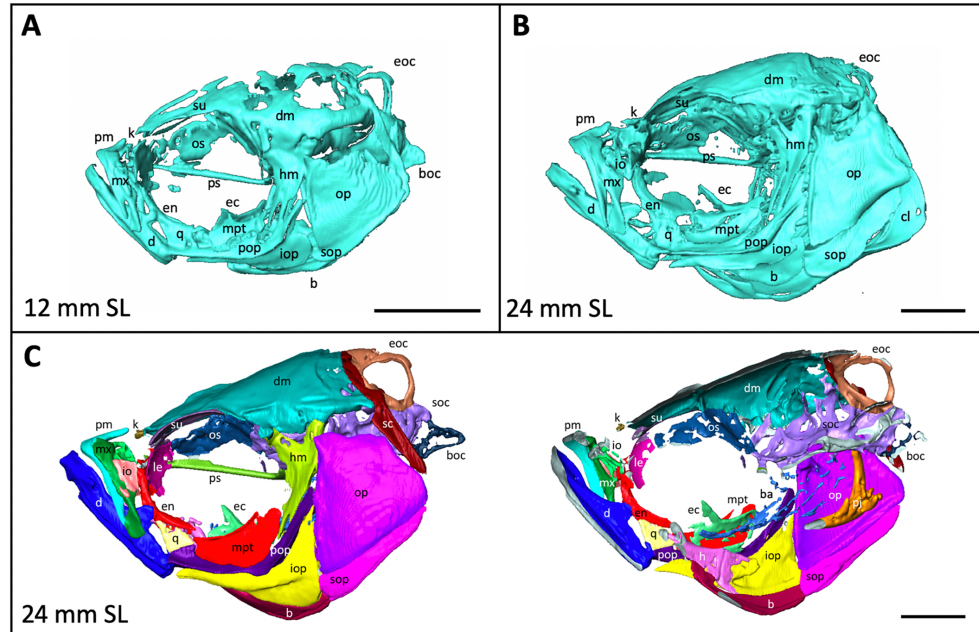


Figure 2.4. Anatomy of the craniofacial skeleton. (A), Volume rendering of the skull of a 12 mm SL zebrafish and (B), a 24 mm SL zebrafish. (C), Lateral view of skull of 24 mm SL zebrafish with segmented bones (left). Cross section of lateral view reveals some internal elements (right). b, basibranchials; ba, branchial arches; boc, basioccipital; d, dentary; dm, dermatocranium; ec, ectopterygoid; eoc, exoccipital; en, entopterygoid; h, hyoid; hm, hyomandibula; io, infraorbital; iop, interopercle; k, kinethmoid; le, lateral ethmoid; m, maxilla; mpt, metapterygoid; op, opercle; os, orbitosphenoid; pj, pharyngeal jaws; pm, premaxilla; pop, preopercle; ps, parasphenoid; q, quadrate; sc, supracleithrum; soc, supraoccipital; sop, subopercle, su, supraorbital. Scale bars, 1 mm.

2.3 DISCUSSION

2.3.1 MicroCT technology as a tool for capturing shape change across developmental stages

The ability to capture shape changes in the skeleton at a fine scale is a powerful technique now being applied to developing organisms. The sensitivity of microCT

technology makes it a powerful tool to examine subtle shape differences across developmental stages. In addition to capturing shape, we demonstrate that microCT data can be used to quantify density and volume of skeletal elements. Isolating individual elements by segmentation can provide detailed information about spatial orientation and relationships between bones within the skeleton. Using consistent microCT settings that yielded the highest resolution of skeletal elements and scanning a range of body sizes, we have shown that bone composition and morphology can be evaluated across developmental progression.

2.3.2 Progressive ossification of skeletal elements during later stages of development

Using this dataset, we assessed skeletal morphology and composition throughout juvenile and adult development in zebrafish. We showed that total bone volume and density progressively increase even during late stages of development. Additionally, we demonstrate that numerous skeletal elements continue to progressively grow and change shape during juvenile and adult growth, continuing into reproductive maturity. These results emphasize the importance of recording and matching SL between individuals. For the purposes of skeletal research, it is not sufficient to consider all “adult” zebrafish equivalent to one another: sizing and staging should be carefully considered.

2.3.3 The zebrafish skeleton continues to undergo shape changes during postembryonic development

Quantitative and qualitative assessment of the scans can highlight regions of the skeleton that are particularly dynamic during late stages of development: e.g., the

dermatocranium—which increases in density (see Fig 2.2A), and the lower jaw—which changes in shape (Fig 2.5A). These shifts can inform experimental design by suggesting specific anatomical regions for quantitative focus. Further, the labeled segmented scans (Fig 2.4C) serve as a craniofacial anatomical reference in identifying skeletal elements.

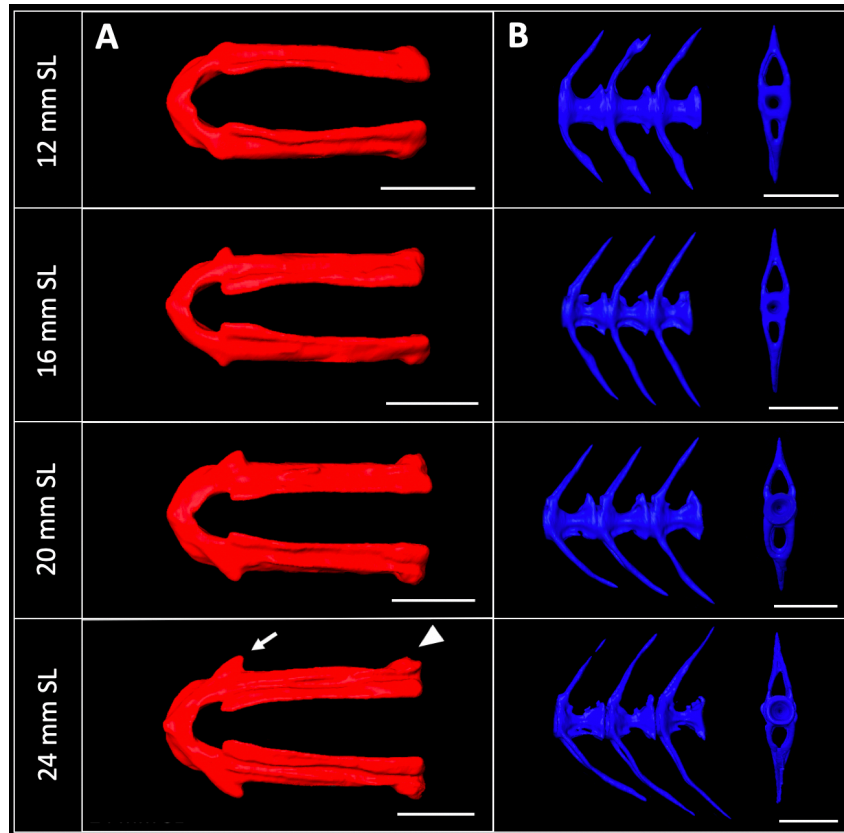


Figure 2.5. Shape changes of the lower jaw and caudal vertebrae. (A), Segmented lower jaws from 12, 16, 20, and 24 mm SL individuals, viewed from the ventral perspective. In the largest individuals, note the pronounced anguloarticular prominence (arrow) and posterior end of lower jaw (arrowhead). (B), Segmented first three caudal vertebrae from 12, 16, 20, and 24 mm SL individuals, viewed from a lateral perspective. Scale bars, 0.5 mm.

2.3.4 The skeletal reference as a normal morphological baseline

For researchers using zebrafish as a model for skeletal disease, this reference can serve as a normal baseline to which aberrant skeletons can be compared in detail, in terms

of morphology, density and skeletal volume. The reference provides a developmental framework for assessing disrupted phenotypes, allowing researchers to assess whether a model of interest shows skeletogenic processes that are accelerated or retarded relative to size. This framework can assist researchers in selecting appropriate body size ranges to evaluate and can add developmental context even when wild-type individuals (e.g., vehicle controls or non-mutant siblings) are analyzed side-by-side with a disease model. Scans from this skeletal reference were also used in both remaining chapters of this dissertation to compare normal craniofacial development and phenotypes to those of altered TH profiles and other Danioninae species. Finally, dynamic processes disrupted in a disease model can be compared to the normal rates of ossification and skeletal change established by this reference.

This dataset contributes to a growing body of resources for zebrafish researchers, and may be used to examine bone shape during juvenile and adult development at a high resolution. In addition to the interactive 3D PDFs, all of the raw data from the microCT scans have been uploaded and made available online at MorphoSource, a repository for 3D data (Boyer et al., 2016) and FaceBase, an online resource for craniofacial researchers (Supp Table 2, Samuels et al., 2020). These scans can be processed using Amira or open source 3D Slicer (Kikinis et al., 2014). Although the focus of the analyses in this manuscript is the skeleton, users of the downloadable raw scans can change the thresholds to visualize and analyze other organs and systems, including the scales, liver, and heart across late developmental stages.

2.4 MATERIALS AND METHODS

2.4.1 Fish rearing and measurement

All studies were performed on an approved protocol in accordance with the Boston College Institutional Animal Care and Use Committee (IACUC; Protocol #2020-005). Zebrafish were reared at 28°C on a 14:10 light:dark cycle and fed a diet of marine rotifers and adult pellet food flakes three times a day. Zebrafish were of the genetic background *Tg(tg:nVenus-2a-nfnB)^{wp.r18}* and originated from several matings of the same parental breeding stock (McMenamin et al., 2014). Individuals were treated with 1% DMSO at 4 dpf, which does not activate the transgenic nitroreductase system (McMenamin et al., 2014). To ensure that these individuals were representative and that the transgenic background or the DMSO treatment did not cause gross skeletal mis-patterning, we scanned representative stages from the Tübingen wild-type line for comparison. The two strains were overall comparable morphologically and in terms of relative density (Fig 2.6).

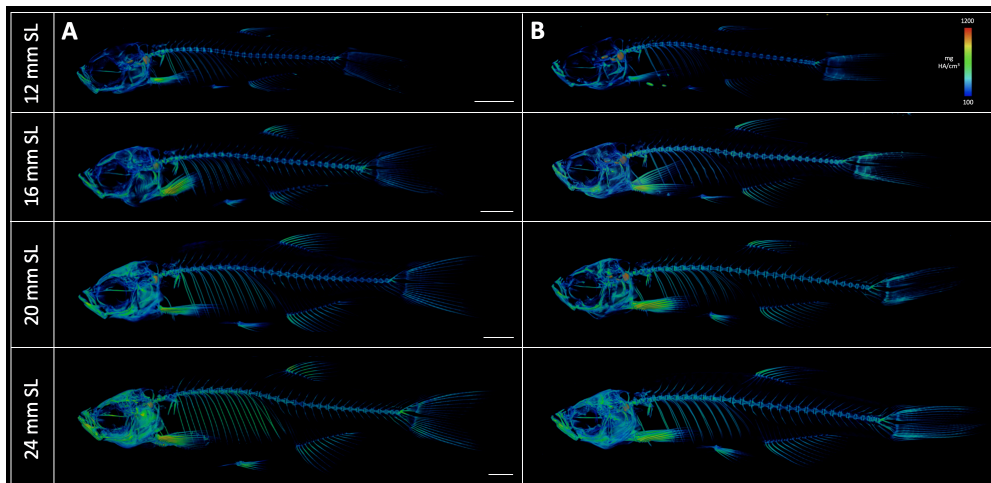


Figure 2.6. DMSO-treated *Tg(tg:nVenus-2a-nfnB)^{wp.r18}* zebrafish have similar skeleton shape and bone density compared to wild-type (Tübingen) zebrafish. (A), Relative density renderings of skeletons of zebrafish of original dataset at four different sizes (12, 16, 20, and 24 mm SL). (B), Relative density renderings of skeletons from wild-type zebrafish at the same four sizes (12, 16, 20, and 24 mm SL).

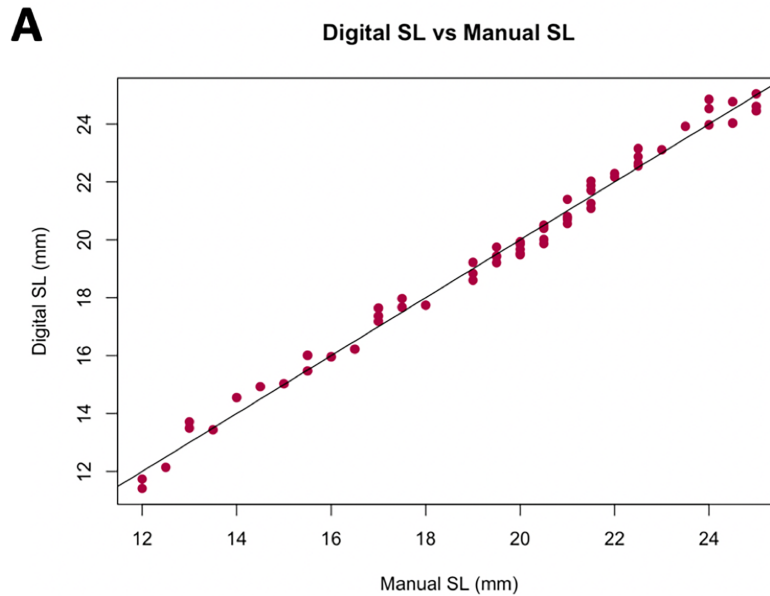


Fig 2.7. Manually measured standard lengths are closely correlated to digitally measured standard lengths. Digital length plotted against manual length for all individuals in the developmental skeletal reference dataset.

2.4.2 MicroCT scanning and reconstruction

Fish were euthanized by MS-222 and fixed in 4% paraformaldehyde for 24 hours. SL was measured in fixed samples according to Parichy et al. (2009) before scanning and was also measured digitally in the scans themselves (Fig 2.7). Fish samples shrink slightly during the fixation process; note that the reported fixed SL values may be converted to corresponding “fresh” SL by adding 0.29 mm (Parichy et al., 2009). A total of 62 specimens were scanned, ranging from 12 to 25 mm SL with a minimum of one scan for every half millimeter (Supp Table 2.1). Fixed specimens were placed in low-density foam molds and inserted into either a 1.5 ml centrifuge tube (for specimens 12-14 mm SL) or a 15 ml conical tube (for specimens >14 mm SL). Scans were performed on a SkyScan 1275 high resolution microCT system (Bruker, Kontich, Belgium) at a scanning resolution of

Relative density heatmaps were generated with the volume rendering module and physics load transfer function in Amira with a threshold range of 20–120. Mean gray value was also used to show relative density between scans. Mean gray value was calculated from imported cross section slices using the measurement tool in ImageJ (Version 1.8.0_172, National Institutes of Health, Bethesda, Maryland, United States). Volume measurements were taken with the Material Statistics module in Amira.

Individual bones were segmented using the Segmentation Editor in Amira 6.5 (Thermo Fisher Scientific FEI, Hillsboro, Oregon, United States). Briefly, the entire scan volume was loaded into the program and a pixel threshold was determined to differentiate bone from soft tissue. The lasso tool was then used to select the corresponding pixels of a specific skeletal element and added to the appropriate material label. Segmented bones include the basibrachials, branchial arches, basioccipital, dentary, dermatocranium, ectopterygoid, exoccipital, entopterygoid, hyoid, hyomandibula, infraorbital, interopercle, kinethmoid, lateral ethmoid, maxilla, metapterygoid, opercle, orbitosphenoid, pharyngeal jaws, premaxilla, preopercle, parasphenoid, quadrate, supracleithrum, supraoccipital, subopercle, and supraorbital. Pearson correlation coefficients were calculated to show the correlation between density or volume and SL.

2.4.4 Interactive 3D PDFs and data accessibility

3D models of the microCT reconstructed scans were generated in Amira 6.5 using the Segmentation Editor and Generate Surface module (Thermo Fisher Scientific FEI, Hillsboro, Oregon, United States). Meshes were simplified using MeshLab (Callieri, 2013; Cignoni et al., 2008). These models were converted to .u3d files and imported into interactive 3D PDFs using Acrobat Pro DC (Fig 2.9, Version 2021.005.20058, Adobe Inc.,

San Jose, CA, United States). Whole, raw microCT scans for individual from every 0.5 mm SL from 12 to 25 mm SL are available for download on both MorphoSource (Project URL: <https://www.morphosource.org/projects/000415918?locale=en>) and FaceBase (Project URL: <https://www.facebase.org/chaise/record/#1/isa:project/RID=1Q-X114>) repositories. When multiple scans were available for each size category, we selected the highest quality scan for upload to MorphoSource while all 62 scans are accessible on the FaceBase project page (McMenamin et al., 2022; Samuels et al., 2020).

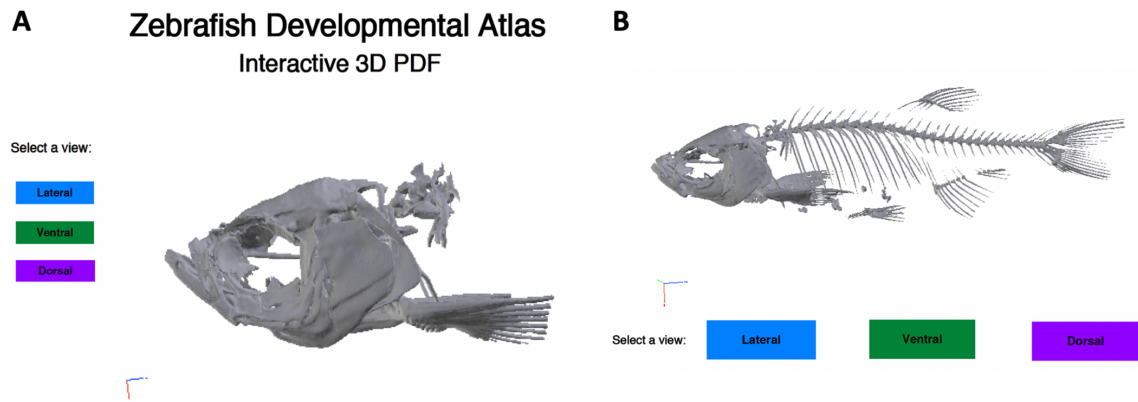


Figure 2.9 Preview of interactive PDF with freely movable 3D models for 24 mm SL individual. (A), Whole head 3D model embedded into PDF with lateral, ventral, and dorsal view options. (B), Whole body 3D model embedded into PDF with lateral, ventral, and dorsal view options.

2.5 SUPPLEMENTAL DATA

Supplemental Table 2.1. Summary of categories of sizes, sample numbers, and MorphoSource ID.

SL Category (mm)	Number of individuals scanned	MorphoSource ID of representative individual
12	2	000415877
12.5	1	000416098
13	2	000416108
13.5	1	000416117
14	1	000416167
14.5	1	000416187
15	1	000416194
15.5	2	000416225
16	1	000416236
16.5	1	000416257
17	3	000416263
17.5	2	000416291
18	1	000416305
18.5	1	000416322
19	2	000416327
19.5	4	000416332
20	5	000416337
20.5	5	000416342
21	5	000416347
21.5	5	000416357
22	2	000416367
22.5	4	000416377
23	1	000416382
23.5	1	000416387
24	3	000416395
24.5	2	000416402
25	1	000416412

Supplemental Table 2.2. Information about every individual scanned. Note that smaller individuals could not be accurately sexed. MorphoSource and FaceBase identifiers provided if available.

SL Category	Digitally measured SL (mm)	Sex	Approximate developmental Stage	MorphoSource ID	FaceBase ID
12	11.74	-	J	000415877	SE-AGT0
12	11.41	-	J	-	SE-AQVW
12.5	12.14	-	J	-	SE-E8E8
13	13.71	-	J+	000416108	SE-E8EJ
13	13.50	-	J+	000416108	SE-E8EM
13.5	13.44	-	J+	000416117	SE-E8EY
14	14.55	-	J+	000416167	SE-E8F8
14.5	14.93	-	J+	000416187	SE-E8FJ
15	15.03	-	J+	000416194	SE-E8FY
15.5	15.47	-	J+	-	SE-E8G8
15.5	16.01	-	J+	000416225	SE-E8GA
16	15.96	-	J++	000416236	SE-E8GM
16.5	16.22	-	J++	000416257	SE-E8GY
17	17.18	-	J++	-	SE-E8H8
17	17.64	-	J++	000416263	SE-E8HA
17	17.37	-	J++	-	SE-E8HC
17.5	17.67	F	J++	-	SE-EFT4
17.5	17.97	M	J++	000416291	SE-EFT6
18	17.74	F	J++	000416305	SE-EFTG
18.5	18.84	M	J++	000416322	SE-EFY2
19	19.22	M	J++	-	SE-EFY6
19	19.84	M	J++	000416327	SE-EFY8
19.5	19.41	M	J++	-	SE-EFYC
19.5	19.75	F	J++	-	SE-EFYE
19.5	19.44	M	J++	-	SE-EFYG
19.5	19.21	F	J++	000416332	SE-EFYJ
20	19.67	F	J++	-	SE-JXYC
20	19.53	F	J++	-	SE-JXYE
20	19.93	M	J++	-	SE-JXYG
20	19.48	F	J++	-	SE-JXYJ
20	19.85	F	J++	000416337	SE-JXYM
20.5	20.46	M	J++	-	SE-JXYT
20.5	20.51	M	J++	-	SE-JXYW
20.5	20.39	M	J++	000416342	SE-JXY Y
20.5	20.01	F	J++	-	SE-JXZ0
20.5	19.87	M	J++	-	SE-JXZ2
21	20.77	F	J++	-	SE-JXZ4
21	20.80	M	J++	-	SE-JXZ6

21	20.71	M	J++	-	SE-JXZ8
21	21.4	M	J++	000416347	SE-JXZA
21	20.56	M	J++	-	SE-JXZC
21.5	21.26	M	J++	-	SE-JXZE
21.5	21.87	F	J++	-	SE-JXZG
21.5	21.08	F	J++	000416357	SE-JXZJ
21.5	22.03	M	J++	-	SE-JXZM
21.5	21.71	M	J++	-	SE-JXZP
22	22.17	M	J++	000416367	SE-JXZR
22	22.29	F	J++	-	SE-JXZT
22.5	22.64	M	J++	-	SE-JXZY
22.5	22.87	M	J++	-	SE-JY00
22.5	22.55	M	J++	-	SE-JY02
22.5	23.15	F	J++	000416377	SE-JY04
23	23.11	M	A	000416382	SE-JY06
23.5	23.92	F	A	000416387	SE-JY0A
24	23.97	F	A	000416395	SE-JY0C
24	24.85	F	A	-	SE-JY0E
24	24.53	M	A	-	SE-JY0G
24.5	24.77	F	A	000416402	SE-JY0J
24.5	24.03	M	A	-	SE-JY0M
25	24.45	F	A	000416412	SE-JY0P

Supplemental Table 2.3. Summary of statistical analyses for pairwise comparisons of vertebral canal widths in 12, 16, 20 and 24 mm SL zebrafish. SE, standard error. df, degrees of freedom.

Contrast	SE	df	t ratio	p-value
V2 SL12 - V2 SL16	3.465	24.748	-4.8074048	0.01718288
V2 SL12 - V2 SL20	3.465	24.748	-6.1186902	0.00081719
V2 SL12 - V2 SL24	3.465	24.748	-5.2085831	0.00686511
V2 SL16 - V2 SL20	3.465	24.748	-1.3112853	0.99996035
V2 SL16 - V2 SL24	3.465	24.748	-0.4011783	1
V2 SL20 - V2 SL24	3.465	24.748	0.91010706	0.99999999
V3 SL12 - V3 SL16	3.465	24.748	-5.3047889	0.00549274
V3 SL12 - V3 SL20	3.465	24.748	-6.5824022	0.00027648
V3 SL12 - V3 SL24	3.465	24.748	-2.7957411	0.63599922
V3 SL16 - V3 SL20	3.465	24.748	-1.2776133	0.99997635
V3 SL16 - V3 SL24	3.465	24.748	2.5090478	0.80438546
V3 SL20 - V3 SL24	3.465	24.748	3.78666109	0.14636877
V4 SL12 - V4 SL16	3.465	24.748	-5.3952224	0.00445065
V4 SL12 - V4 SL20	3.465	24.748	-7.719555	2.06E-05
V4 SL12 - V4 SL24	3.465	24.748	-4.0204412	0.0929959
V4 SL16 - V4 SL20	3.465	24.748	-2.3243326	0.88877243
V4 SL16 - V4 SL24	3.465	24.748	1.37478117	0.99990186
V4 SL20 - V4 SL24	3.465	24.748	3.69911379	0.17208145
V5 SL12 - V5 SL16	3.465	24.748	-4.9180415	0.01337474
V5 SL12 - V5 SL20	3.465	24.748	-7.2683497	5.70E-05
V5 SL12 - V5 SL24	3.465	24.748	-5.3981086	0.00442082
V5 SL16 - V5 SL20	3.465	24.748	-2.3503082	0.87843854
V5 SL16 - V5 SL24	3.465	24.748	-0.480067	1
V5 SL20 - V5 SL24	3.465	24.748	1.87024115	0.98801495
V6 SL12 - V6 SL16	3.465	24.748	-5.0017406	0.01105016
V6 SL12 - V6 SL20	3.465	24.748	-7.2943253	5.37E-05
V6 SL12 - V6 SL24	3.465	24.748	-6.3418877	0.00048453
V6 SL16 - V6 SL20	3.465	24.748	-2.2925847	0.9006777
V6 SL16 - V6 SL24	3.465	24.748	-1.3401471	0.9999395
V6 SL20 - V6 SL24	3.465	24.748	0.95243762	0.99999997
V7 SL12 - V7 SL16	3.465	24.748	-4.7448711	0.01977645
V7 SL12 - V7 SL20	3.465	24.748	-6.7488383	0.00018788
V7 SL12 - V7 SL24	3.465	24.748	-7.3183768	5.08E-05
V7 SL16 - V7 SL20	3.465	24.748	-2.0039672	0.97302838
V7 SL16 - V7 SL24	3.465	24.748	-2.5735057	0.76959671
V7 SL20 - V7 SL24	3.465	24.748	-0.5695385	1
V8 SL12 - V8 SL16	3.465	24.748	-4.5928659	0.0277326
V8 SL12 - V8 SL20	3.465	24.748	-7.2019677	6.63E-05
V8 SL12 - V8 SL24	3.465	24.748	-5.8204521	0.00164528

V8 SL16 - V8 SL20	3.465	24.748	-2.6091018	0.74943039
V8 SL16 - V8 SL24	3.465	24.748	-1.2275863	0.99998957
V8 SL20 - V8 SL24	3.465	24.748	1.38151558	0.99989249
V9 SL12 - V9 SL16	3.465	24.748	-4.4341263	0.03922641
V9 SL12 - V9 SL20	3.465	24.748	-6.7969412	0.00016808
V9 SL12 - V9 SL24	3.465	24.748	-5.2816995	0.00579521
V9 SL16 - V9 SL20	3.465	24.748	-2.3628149	0.87327502
V9 SL16 - V9 SL24	3.465	24.748	-0.8475733	1
V9 SL20 - V9 SL24	3.465	24.748	1.51524167	0.99944824
V10 SL12 - V10 SL16	3.465	24.748	-4.5409147	0.03108924
V10 SL12 - V10 SL20	3.465	24.748	-6.9123882	0.00012875
V10 SL12 - V10 SL24	3.465	24.748	-5.3586642	0.00484609
V10 SL16 - V10 SL20	3.465	24.748	-2.3714735	0.86962952
V10 SL16 - V10 SL24	3.465	24.748	-0.8177495	1
V10 SL20 - V10 SL24	3.465	24.748	1.553724	0.99916489

Chapter 3

Thyroid hormone shapes the zebrafish craniofacial skeleton during juvenile and adult development

Some of the material in this chapter was adapted from:

Keer S., Storch J.D., **Nguyen S.**, Prado M., Singh R., Hernandez L.P., & McMenamin S.K. (2022). Thyroid hormone shapes craniofacial bones during postembryonic zebrafish development. *Evolution & Development*, 1–16. <https://doi.org/10.1111/ede.12399>

Raw microCT data in this chapter is available via the FaceBase repository at:

Sarah K. McMenamin, **Stacy Nguyen**, John Blythe. Thyroid hormone mediates juvenile and adult craniofacial shape change in zebrafish. *FaceBase Consortium* <https://doi.org/10.25550/1Q-X114> (2022)

3.1 INTRODUCTION

3.1.1 Metamorphosis in teleosts

Metamorphosis is widespread across vertebrates, and is defined as an irreversible developmental and physiological change brought about by endocrine mediators (McMenamin & Parichy, 2013). Most freshwater teleosts go through more subtle metamorphoses than their marine counterparts (McMenamin & Parichy, 2013). In zebrafish, metamorphosis brings about several changes in morphology, including changes in overall body shape and pigment pattern (Fig 3.1, McMenamin & Parichy, 2013; Parichy et al., 2009).

3.1.2 Thyroid hormone and its role during metamorphosis

The endocrine signaling factor thyroid hormone (TH) is responsible not only for amphibian metamorphosis, but also teleost metamorphosis (Brown & Cai, 2007; Campinho, 2019; S. K. McMenamin & Parichy, 2013). Previous studies from our lab and others show that TH affects the shape and ossification of different craniofacial elements in zebrafish (Galindo et al., 2019; Hu et al., 2019; Keer et al., 2019; S. McMenamin et al., 2017). Keer et al. performed an anatomical assessment of the entire adult zebrafish skeleton, finding that TH is essential for proper ossification, morphogenesis, and fusion of several bones in the anterior portions of the dermal skeleton including the dermatocranium, Weberian apparatus, and pectoral girdle (2009). In this assessment, bones were assigned a score based on severity and categorized based on embryonic germ layer origins (mesoderm or neural crest cell) and development type (intramembranous or endochondral). Overall, the hyperthyroid zebrafish skeleton was over-ossified compared to wild-type zebrafish

while the hypothyroid zebrafish was more cartilaginous with numerous malformed skeletal elements (Keer et al., 2019).

3.1.3 Skeletogenesis & skeletogenic cell types

The skeletal system continues to develop during and after zebrafish metamorphosis, with the onset of dermal bone development and the transition of cartilaginous scaffolds into ossified skeletal elements (Campinho, 2019; Parichy et al., 2009). This continuous developmental shape change - which I will call developmental trajectory - requires the coordination of different skeletogenic cell populations for proper bone development, remodeling, and maintenance. The three-dimensional shape of a bone is created by local populations of cartilage- and bone-forming cells. Osteoblasts are recognized as the cells that ossify bone, and numerous signaling pathways influence osteoblast proliferation, differentiation, localization, and mineralizing activity, thus affecting bone growth rates and patterning (Salhotra et al., 2020). The zinc finger transcription factor *sp7* is required for osteoblast differentiation and is expressed exclusively by mature osteoblasts (Ohba, 2023). There are two mechanisms in which bone formation occurs in vertebrates: intramembranous and endochondral ossification (Bassett & Williams, 2018a; Hojo et al., 2016). Intramembranous ossification is a process in which osteoblasts differentiate directly from mesenchymal cells. In contrast, during endochondral ossification, mesenchymal cells differentiate into chondrocytes, which produce cartilage. Chondrocytes express *coll1a1*, a gene that encodes a major component of type I collagen (Tsang et al., 2015). These chondrocytes create a cartilage template that osteoblasts use as a framework in which osteoblasts deposit mineralized bone (Weigle & Franz-Odenaal, 2016). During this process of endochondral bone formation, chondrocytes exit the cell cycle, becoming

hypertrophic cells that are eventually calcified, resorbed, and replaced with bone (Tsang & Cheah, 2019). There are a few differences in the composition of fish and human skeletons. Fish skeletons have 16 types of cartilage while humans only possess 3 types of cartilage (M. Benjamin, 1990). The fish vertebral column undergoes perichondral ossification and the human vertebral column forms via endochondral ossification (Arratia & Schultze, 1992). While most teleost species have mononucleated osteoclasts and bone devoid of osteocytes, zebrafish possess both multinucleated osteoclasts and osteocytic bones similar to humans (Laizé et al., 2014).

3.1.4 Responses of skeletogenic cell types to TH

During endochondral bone formation in mammals, TH inhibits chondrocyte proliferation during the transition into osteogenesis (Gomez et al., 2022). The hormone further promotes apoptosis of hypertrophic chondrocytes while stimulating vascularization of newly mineralized tissue (Gomez et al., 2022; Tsang & Cheah, 2019). This vascularization helps recruits osteoblasts to the cartilage scaffold, promoting mineralization (Leitch et al., 2020; Wojcicka et al., 2013). TH additionally regulates several pathways involved in osteoblast proliferation and differentiation (Kim & Mohan, 2013; Wojcicka et al., 2013). In mammals, hypothyroidism reduces osteoblast activity and prolongs secondary bone mineralization, which involves remodeling the primary bone into a more optimal structure (Bassett & Williams, 2018; Olszta et al., 2007). In contrast, hyperthyroidism accelerates differentiation of both mammalian chondrocytes and osteoblast *in vitro* (Gomez et al., 2022; Kim & Mohan, 2013).

3.1.5 Shape change during postembryonic development

In teleosts, components of the axial skeletal including the vertebral bodies undergo dramatic development during later stages (Campinho, 2019). The zebrafish skeleton continues to develop well beyond metamorphosis, with several elements reshaping and fully ossifying during juvenile and adult stages (Kanter et al., 2019; Xie et al., 2022). Craniofacial skeletons also continue to change shape as zebrafish grow during postembryonic development, and previously we aimed to characterize the trajectories of these normal shape changes in detail (Nguyen et al., 2022).

3.1.6 Rationale for and summary of this research

The postembryonic skeleton is dynamic and continues to undergo important, functional shape changes during juvenile and adult development. Here, to better understand how specific skeletal elements (tripus, lower jaw, hyomandibula, and pharyngeal jaw) are shaped and remodeled during normal development at postembryonic stages, we first focused on specific skeletal elements of functional and evolutionary relevance to characterize the shape change that each bone undergoes during normal, wild-type development and determine how these changes are affected by TH. I hypothesized that TH regulates developmental shape changes as zebrafish mature from larvae to adults. I predicted that hypothyroid (HypoTH) zebrafish would retain immature bone morphologies, and that hyperthyroidism would induce precocious development of adult shapes. We used both 2D and 3D geometric morphometrics to assess overall shape changes across developmental stages and TH profiles. To identify and track changes in cell populations behaviors that give rise to these altered shapes seen at juvenile and adult stages, I used

fluorescent reporters to observe preosteoblast, osteoblast, and chondrocyte populations in zebrafish developing under different TH profiles at earlier stages.

3.2 RESULTS

3.2.1 2D morphometric analysis of specific craniofacial bones reveals that TH coordinates allometric shape change during development

3.2.1a Tripus

During normal development from late larval to adult stages, the tripus undergoes several changes in morphology. The articular process of the tripus is rounded and cartilaginous at late larval stages, and gradually adopts a blunt shape during juvenile and adult development (Fig 3.1 e-h). During this developmental window, the anterior and transformator processes begin to extend away from the center of the tripus with the transformator process tapering at end (Fig 3.1 g-h). The articular process is enlarged and ventrally deflected in the HypoTH zebrafish at late larval stages while the transformator process splits with a prominent dorsal branch (Fig 3.1 a). The juvenile and adult HypoTH fish have more concave anterior margins and more concave posterior margins compared to wild-type fish (Fig 3.1 b-d). The opposite observations were made in the hyperthyroid fish, with anterior margin developing more convex while the posterior margin is more concave (Fig 3.1 i-l). At adult stages, anterior process of the tripus is less elongate in the hyperthyroid (HyperTH) condition compared to normal development (Fig 3.1 l).

Visualizing the shape variation within a morphospace (a graphical representation of all the possible shapes), the major axis of variation (the first principal component – PC1) captured 28% of the total variation while the second axis PC2 captured approximately 15%,

and the TH conditions separate from one another with the wild-type condition occupying a region in between the HypoTH and HyperTH clusters (Fig 3.3 a). Deformation grids indicate that the anterior margin and process contributes to the shape variation along PC1 and differences in the poster margin and transformator process account for much of the PC2 variation (Fig 3.3 b). To illustrate shape changes during development, we plotted PC1 scores against standard length (SL), finding differences in the allometry of the tripus between the HypoTH fish compared to both the wild-type and HyperTH fish (Fig 3.3 c).

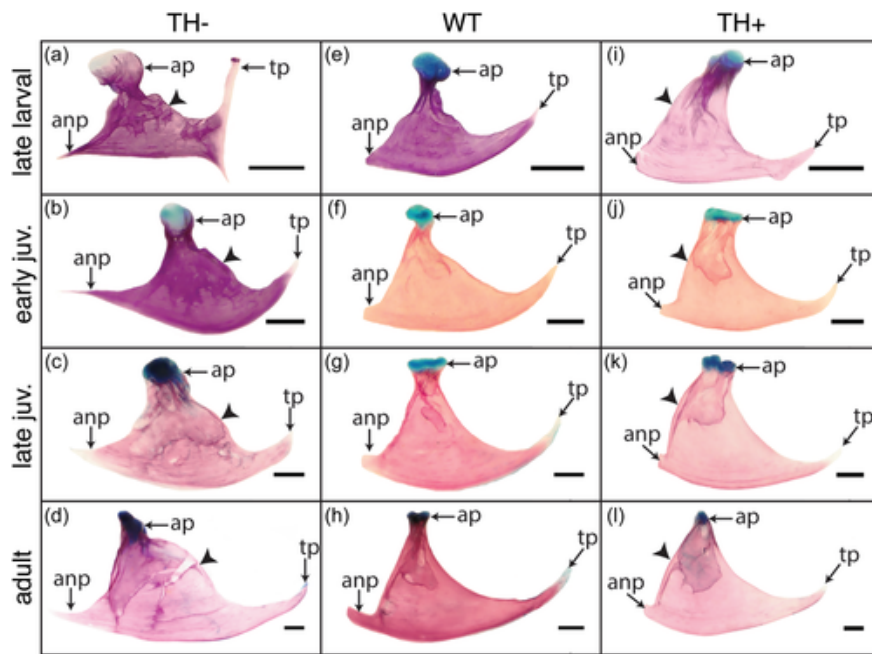


Figure 3.1 Specific features of the tripus are sensitive to developmental TH. Representative cleared and stained tripodes from late larval through adult stages. (a–d) Tripodes from HypoTH (labelled TH–) zebrafish. (e–h) Tripodes from WT zebrafish. (i–l) Tripodes from HyperTH (labeled TH+) zebrafish. The convex posterior edges of each tripus indicated with arrowheads in a–d and the convex anterior edges of each tripus indicated with arrowheads in i–l. Scale bars = 100 μ m. anp, anterior process; ap, articular process; tp, transformator process; WT, wild-type.

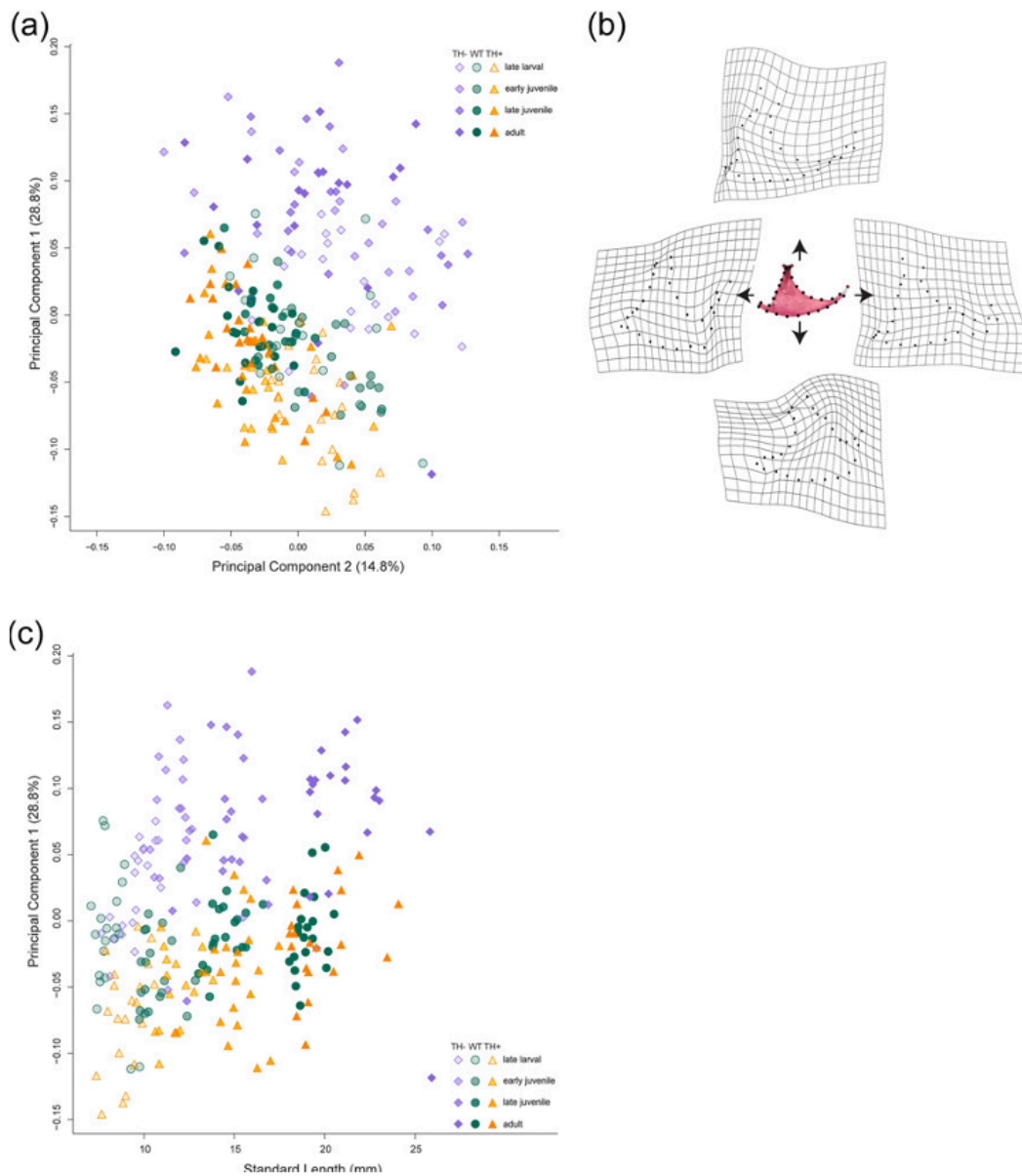


Figure 3.2 The tripus does not markedly change shape across developmental stages, but developmental TH titer changes the shape of the tripus. Principal component analysis assessing shape of each tripus from zebrafish reared under different TH conditions. (a) PCA showing wild-type (labelled WT, green circles), HypoTH (labelled TH⁻, purple diamonds), and HyperTH (labelled TH⁺, yellow triangles) tripodes. Shade of datapoints indicates developmental stages, with late larval stages being the lightest in color and the adult stage being darkest in color. Note that while wild-type and HyperTH cluster together, HypoTH clusters separately. (b) Minimum and maximum warp grids (displaying regions of high shape change) of tripus across all samples, with PC1 across the vertical axis and PC2 across the horizontal axis. (c) PC1 plotted against standard length. PCA, principal component analysis.

3.2.1b Lower Jaw

In late larval wild-type fish, the lower jaw has a partially ossified anguloarticular, retroarticular, and ventral shelf while the prominent coronoid process is fully ossified (Fig 3.3 e). The posterior margin of the coronoid process is fused with the anguloarticular at adult stages and the lower jaw is fully ossified with a prominent ventral shelf (Fig 3.3 h). Several aspects of the lower jaw are under-ossified in the HypoTH late larval and juvenile fish (Fig 3.3 a-b). Many HypoTH fish also developed ectopic endochondral growth at the mandibular symphysis (Fig 3.3 c-d). In contrast, the lower jaws of HyperTH fish exhibited premature fusion of the coronoid process and anguloarticular (Fig 3.3 i-j).

The first PC axis accounts for 23% of total shape variation and mostly captures the size of the developing ventral shelf, which becomes more pronounced as the fish develops (Fig 3.4 a-b). The second axis, which accounts for almost 21% of the total variation, captures the presence of the ectopic growth at the tip of the mandibular symphysis (Fig 3.4 a-b). Looking at the shape change in PC1 during developmental growth, each TH condition has a unique growth trajectory. Similar to the tripus, the wild-type trajectory is situated in between those of the HypoTH and HyperTH conditions (Fig 3.4 c).

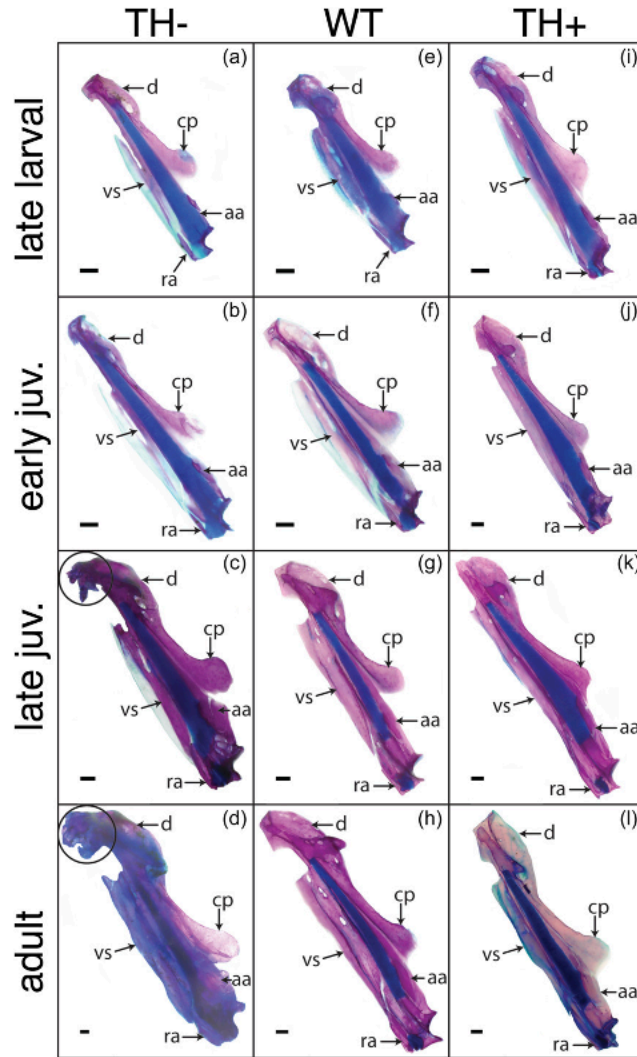


Figure 3.3 Features of the lower jaw are sensitive to developmental TH. Representative cleared and stained HypoTH (labelled TH⁻), wild-type (labelled WT), and HyperTH (labelled TH⁺) lower jaw from late larval through adult stages. (a–d) Lower jaws from TH⁻ zebrafish; (e–h) lower jaws from WT zebrafish; (i–l) lower jaws from TH⁺ zebrafish. Scale bars = 100 μ m. aa, anguloarticular; cp, coronoid process; ra, retroarticular; vs, ventral shelf; WT, wild-type.

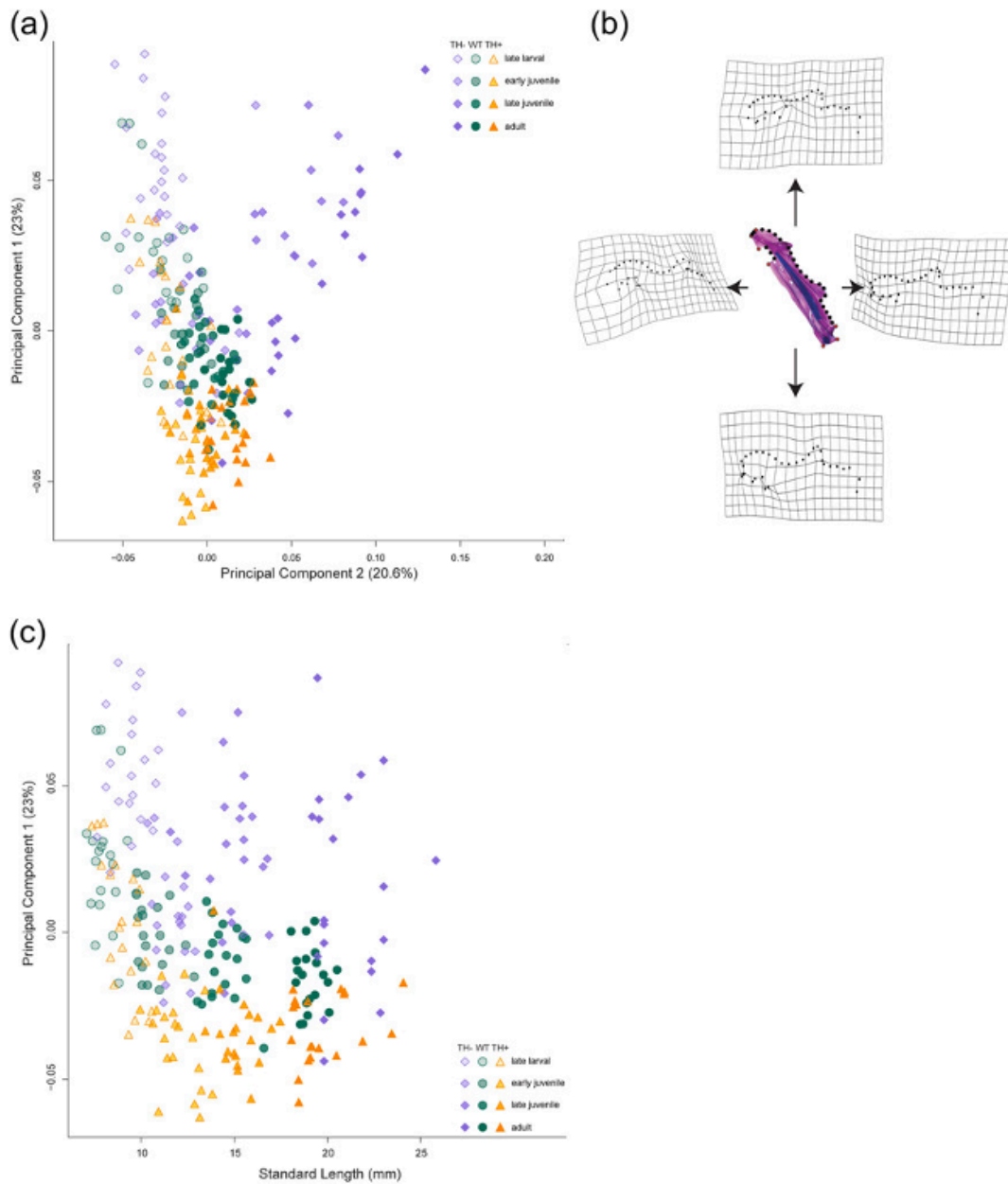


Figure 3.4. The lower jaw changes shape during larval and juvenile development and this shape change is dependent on TH. Principal component analysis of the wild-type (labelled WT, green circles), HypoTH (labelled TH-, purple diamond), and HyperTH (labelled TH+, orange triangle) lower jaw from late larval through adult stages. (a), PCA of wild-type, HypoTH, and HyperTH lower jaws. Shade of datapoints indicates developmental stages. Note that TH- late juvenile and adult samples cluster independently. (b), Minimum and maximum warp grids of lower jaws across all samples, with PC1 across the vertical axis and PC2 across the horizontal axis. (c), PC1 plotted against standard length. PCA, principal component analysis.

3.2.1c Hyomandibula

The hyomandibulae has a cross-shaped, or cruciform, body with four rami that form superficial lamina during juvenile and adult stages in wild-type zebrafish (Fig 3.6 e - h). In the HypoTH fish, there is increased cartilage present throughout development and the anterior and posterior condyles fail to separate (Fig 3.6 a-d). These hyomandibulae also show a lack of ossification between the anterior and posterior condyles while posterior shield between the opercular condyle and hyosymplectic cartilage is also less robust than in wild-type conditions (Fig 3.6 c-d). In hyomandibulae of HyperTH fish, there is a lack of cartilage present throughout juvenile and adult development, and the presence of robust shield between the anterior and posterior condyles is also missing (Fig 3.6 i-l). The shield between the opercular condyle and the hyosymplectic cartilage is more robust until the late juvenile stage (Fig 3.6 k).

Looking at the morphospace for the hyomandibulae, PC1 (39.7% of total variation) largely captures the development of the posterior ramus, which steadily increases in size as the fish grows (Fig 3.7 a-b). The second axis captures approximately 13% of the shape variation. Comparing PC1 scores across development reveals a gradual increase in PC1 score as the fish develops, with the wild-type trajectory nestled between the TH altered trajectories (Fig 3.7 c).

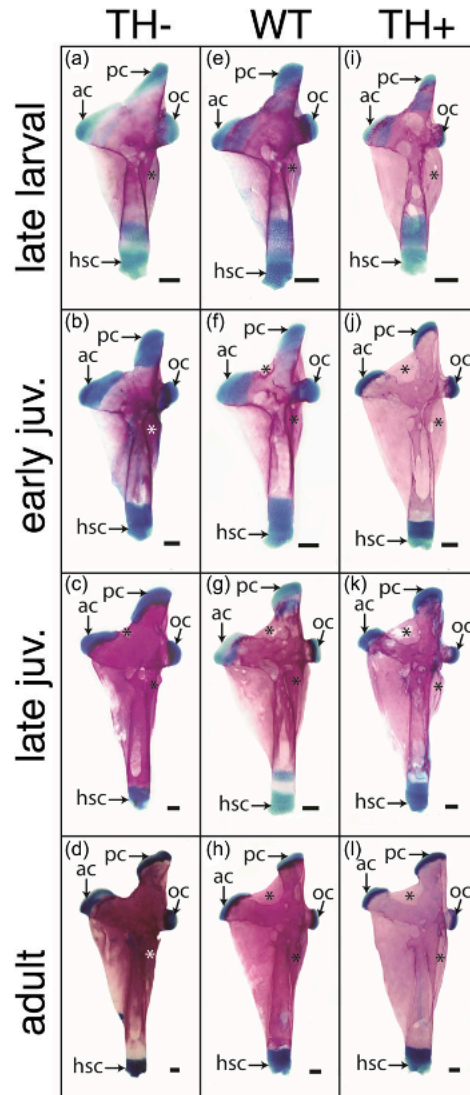


Figure 3.5 Features of the hyomandibula are dependent on developmental TH. Cleared and stained HypoTH (labelled TH-), wild-type (labelled WT), and HyperTH (labelled TH+) hyomandibulae from late larval through adult stages. (a–d) Hyomandibulae from HypoTH zebrafish; (e–h) hyomandibulae from wild-type zebrafish; (i–l) hyomandibulae from HyperTH zebrafish. Scale bars = 100 μ m. ac, anterior condyle; hsc, hyosymplectic cartilage; oc, opercular condyle; pc, posterior condyle.

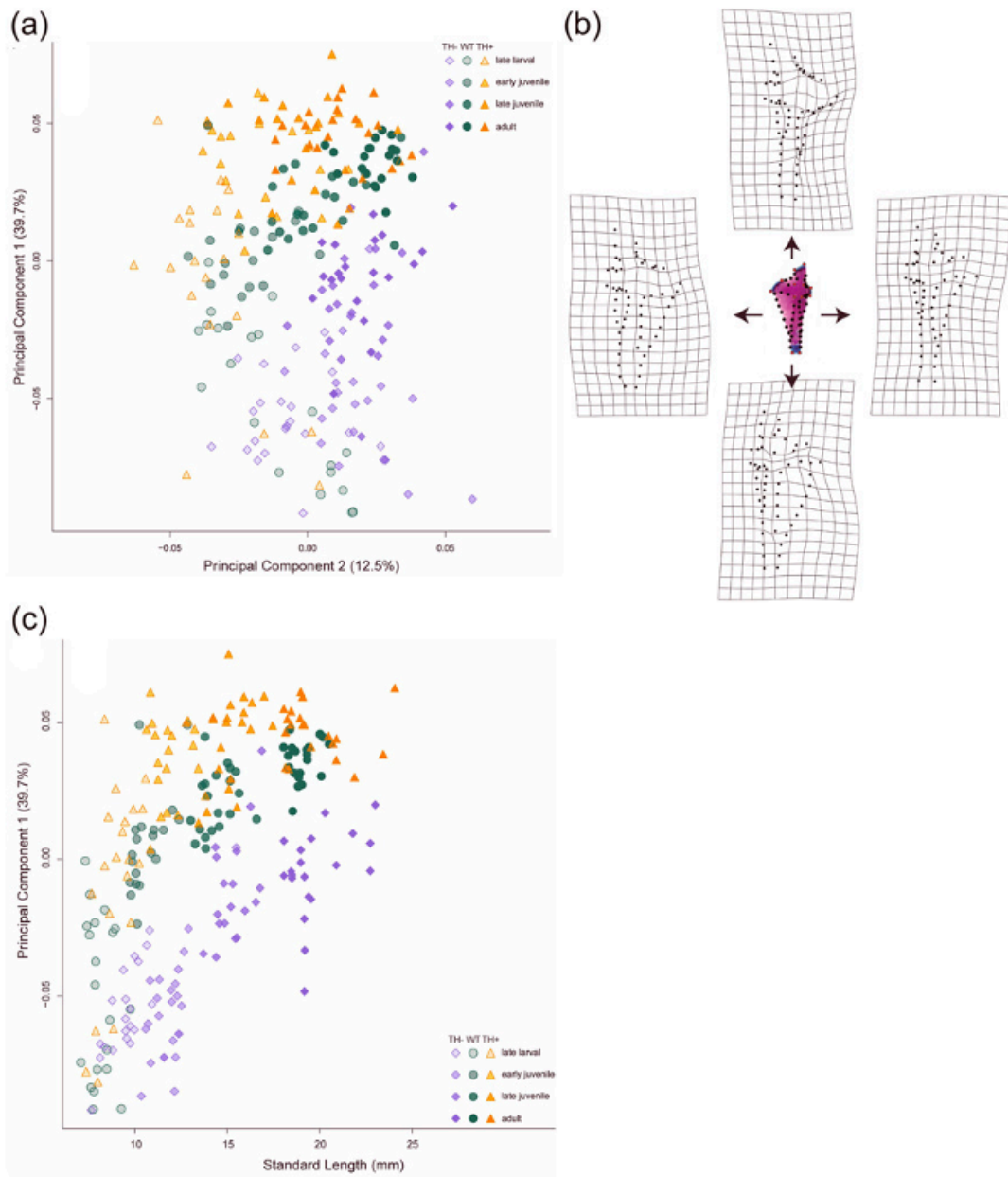


Figure 3.6 TH stimulates development of a mature shape in the hyomandibula. Principal component analysis of the wild-type (labelled WT, green circles), HypoTH (labelled TH⁻, purple diamond), and HyperTH (labelled TH⁺, orange triangle) hyomandibulae from late larval through adult stages. (a) PCA of wild-type, HypoTH, and HyperTH hyomandibulae. Shade of datapoints indicates developmental stages. Note that wild-type, HypoTH, and HyperTH all cluster separately. (b) Minimum and maximum warp grids of hyomandibulae across all samples, with PC1 across the vertical axis and PC2 across the horizontal axis. (c) PC1 plotted against standard length. PCA, principal component analysis.

3.2.1d Pharyngeal jaws

The last bone that was dissected and examined is the pharyngeal jaws, which are tooth-bearing modified ceratobranchials. While it has been shown that tooth number is altered under HypoTH and HyperTH conditions, only subtle phenotypic changes in curvature were detected in dissected pharyngeal jaws and thus not shown at different stages and TH conditions.

The PCA morphospace for the pharyngeal jaws reveal significant overlap between the wild-type and HyperTH fish (Fig 3.8 a). The first PC axis capture 35.3% of total variation, the second axis captures 15.2% of variation, and both axes are driven by subtle changes to the curvature and extension of pharyngeal jaws (Fig 3.8 a-b). The HypoTH fish occupy a region of the morphospace with lower PC2 scores compared to wild-type and HyperTH fish, and all three conditions have similar ranges in PC1 score. Plotting PC1 against SL, there is again more overlap between the wild-type and HyperTH conditions while the HypoTH condition has a unique trajectory with less increase in PC1 score (Fig 3.8 c).

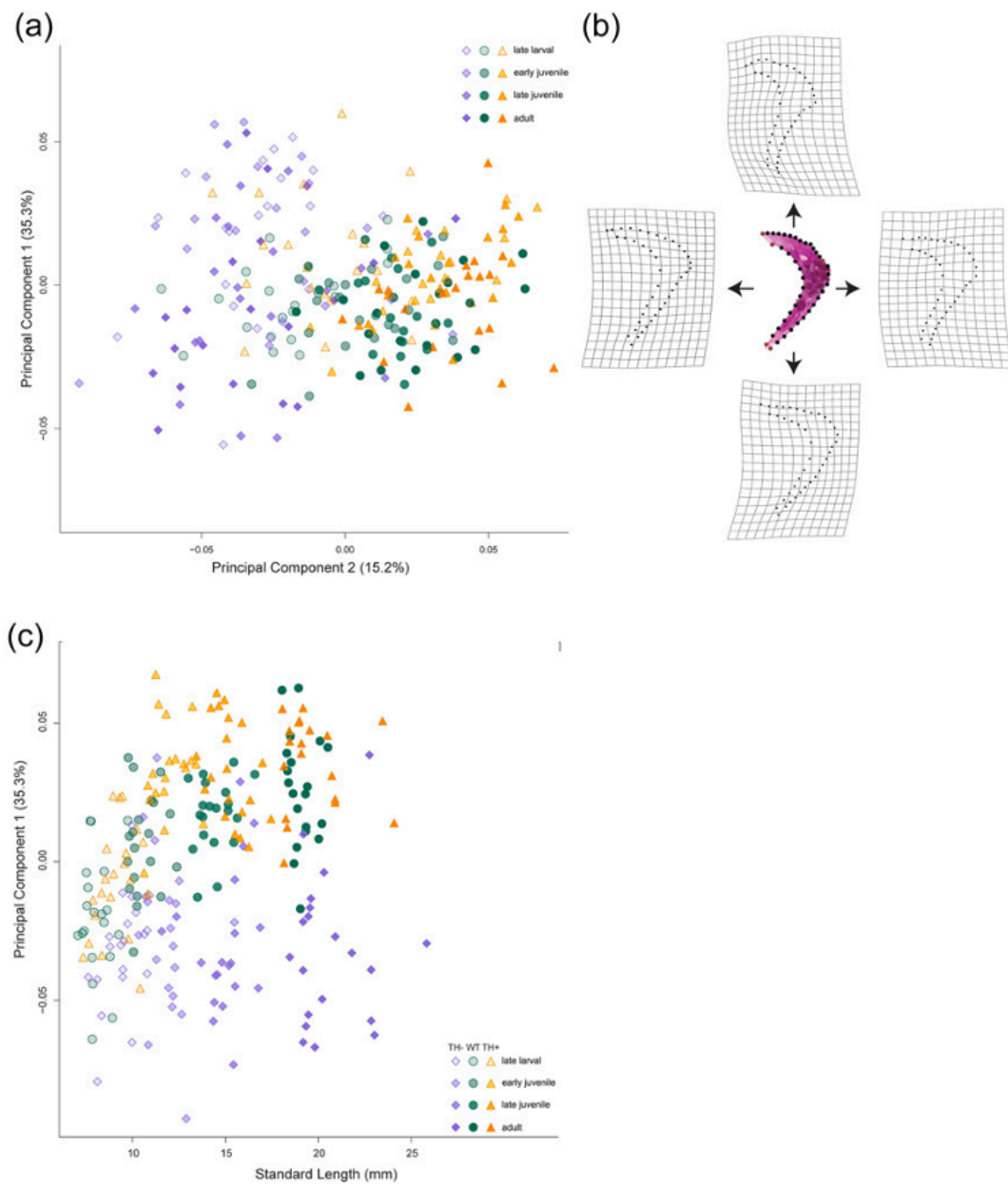


Figure 3.7 TH is required for adult shape in the pharyngeal jaws. Principal component analysis of the wild-type (labelled WT, green circles), HypoTH (labelled TH⁻, purple diamond), and HyperTH (labelled TH⁺, orange triangle) pharyngeal jaws from late larval through adult stages. (a) PCA of wild-type, HypoTH, and HyperTH pharyngeal jaws. Shade indicates developmental stage. (b) Minimum and maximum warp grids of pharyngeal jaws across all samples, with PC1 across the vertical axis and PC2 across the horizontal axis. (c) PC1 plotted against standard length. PCA, principal component analysis.

3.2.2 3D morphometric analysis reveals the role of TH in shaping the overall head shape of zebrafish during normal development

After looking at the developmental shape trajectories of four specific skeletal elements in two dimensions, we asked whether TH plays a role in sculpting of the overall head. We used microCT to capture the craniofacial shapes of zebrafish in wild-type, HypoTH, and HyperTH conditions in a slightly narrower development window, focusing on juvenile (12 mm SL) to adult (25 mm SL) stages as our 2D analyses indicate more apparent shape differences at these stages. Mirroring the shifts revealed by the single-bone, 2D analyses (see section 3.2.1), we saw a similar pattern in the morphospace in which the different TH profiles separated from one another, with the wild-type condition positioned between the TH altered conditions (Fig 3.9). PC1 (25.7% of total variation) mostly captures the widening of the frontal bone of the dermatocranium and part of the parietal bone expansion while PC2 (12.1% of total variation) captures the rest of the widening of the parietal bone as the fish grows (Fig 3.9). To examine shape trends across growth, we plotted PC1 against SL and saw the same trends for overall shape change in the head compared to the individual bones examined in two dimensions (Fig 3.10).

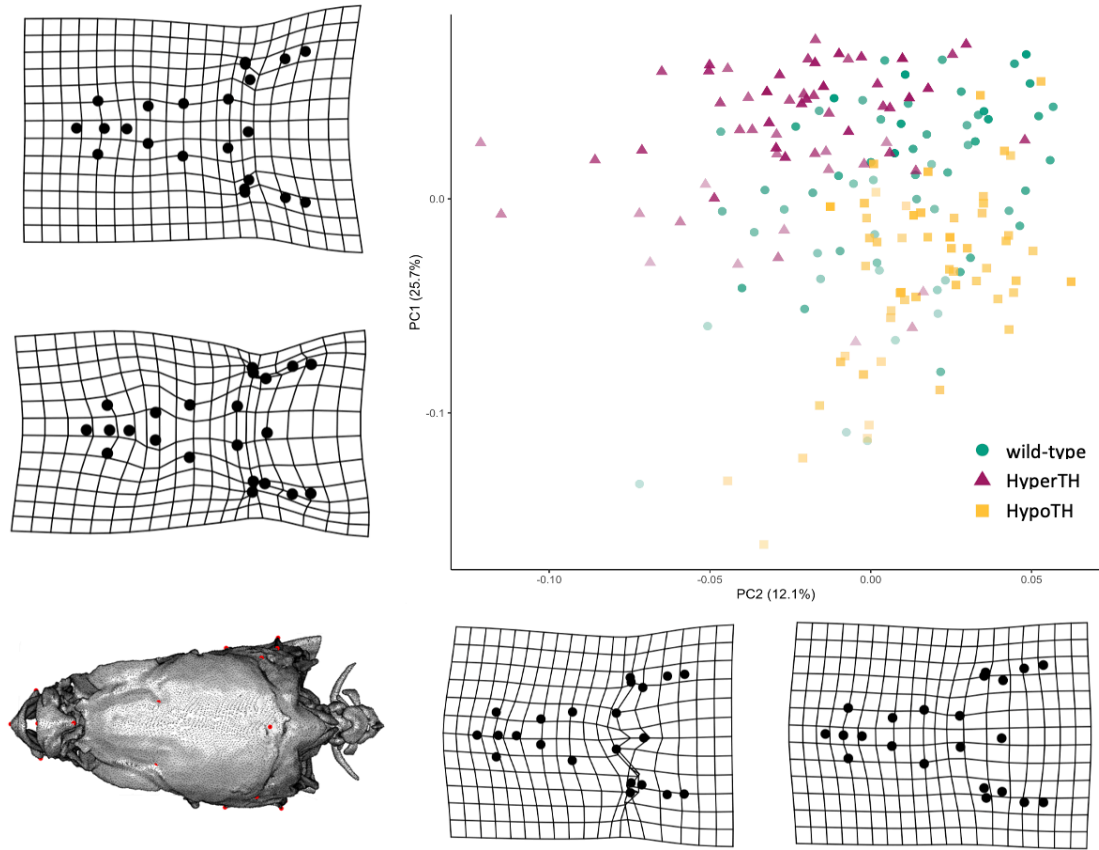


Figure 3.8 Developmental TH sculpts the adult zebrafish skull. Principal component analysis of the overall head shape of wild-type (teal), HypoTH (purple), and HyperTH (yellow) fish jaws from juvenile through adult stages. Color gradient within each condition indicates the size of each specimen, with lightest colors starting at 12 mm SL and darkest colors indicating larger fish up to 25 mm SL. Minimum and maximum warp grids of skulls across all samples, with PC1 across the vertical axis and PC2 across the horizontal axis.

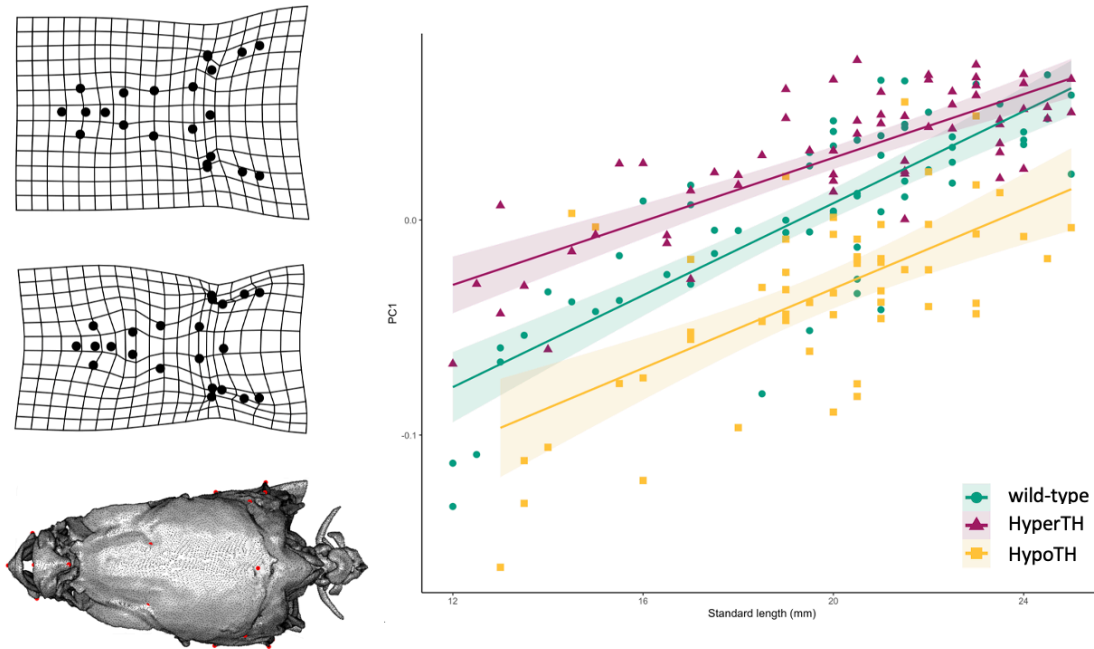


Figure 3.9 TH regulates the developmental trajectory of overall head shape in juvenile and adult zebrafish. PC1 of the overall head shape of wild-type (green), HypoTH (purple), and HyperTH (yellow) fish skulls plotted against SL.

3.2.3 The dermatocranium and jaw elements of the zebrafish craniofacial skeleton undergo the most change during juvenile and adult development

To determine which bones and regions of the zebrafish undergo the most change at juvenile and adult stages, stick and ball plots were generated to visualize the magnitude of shape variation of the manually placed landmarks. The lateral view of this plot reveals a lengthening of the skull, as the landmarks of the upper and lower jaws have expanded anteriorly across development while the landmarks of the posterior edge of the dermatocranium extended posteriorly (Fig 3.11 B). The dorsal view indicates an expansion of the posterior end of the lower jaw and dermatocranium dimensions and a condensation of the distance between the medial edges of the branchiostegal rays and the anterior edges of the opercles (Fig 3.11 D). Correlating these changes to our developmental trajectory

plots, thyroid hormone interacts with shape change and HypoTH fish have immature head shapes compared to wild-type and HyperTH fish. (Fig 3.10)

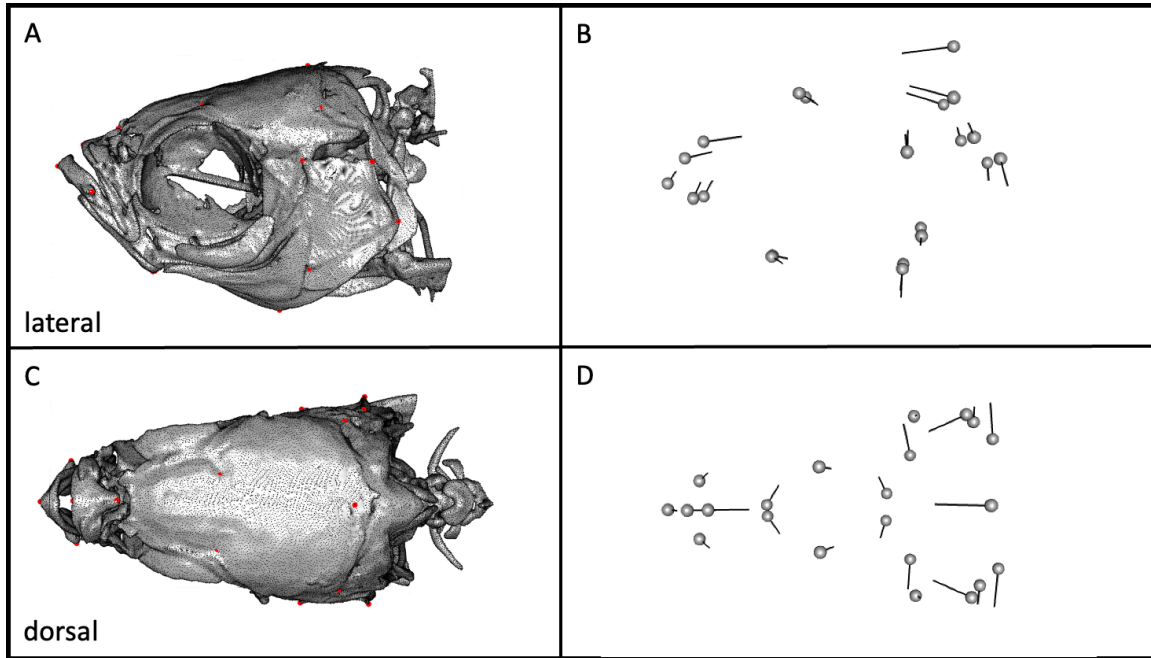


Figure 3.10 The zebrafish skull expands in several dimensions during juvenile and adult development. (A), Lateral view of manual landmarks on 3D model. (B), Lateral view of stick and ball plot of PC1 min (tip of stick segment) and PC1 max (ball end of segment). (C), Dorsal view of manual landmarks on 3D model. (D), Dorsal view of stick and ball plot of PC1 min (tip of stick segment) and PC1 max (ball end of segment).

3.2.4 Thyroid hormone influences osteoblast and chondrocyte populations during early metamorphosis

In the first part of this chapter, we identified the shape changes in specific skeletal elements and overall head shape that zebrafish undergo from late larval to adult development. Next, I used fluorescent cell reporter lines to examine the cell populations responsible for bone development in wild-type and HypoTH zebrafish during earlier stages of development as the bone shapes emerge. We examined the expression of two transgenes:

Tg(sp7:mCherry) (expressed in mature osteoblasts, Kague et al., 2016) and *Tg(-1.4coll1a1:egfp)* (expressed in chondrocytes of cartilage, Kague et al., 2012). Together, these transgenes provided cellular context during skeletogenesis in the zebrafish skull at earlier stages (Fig 3.11).

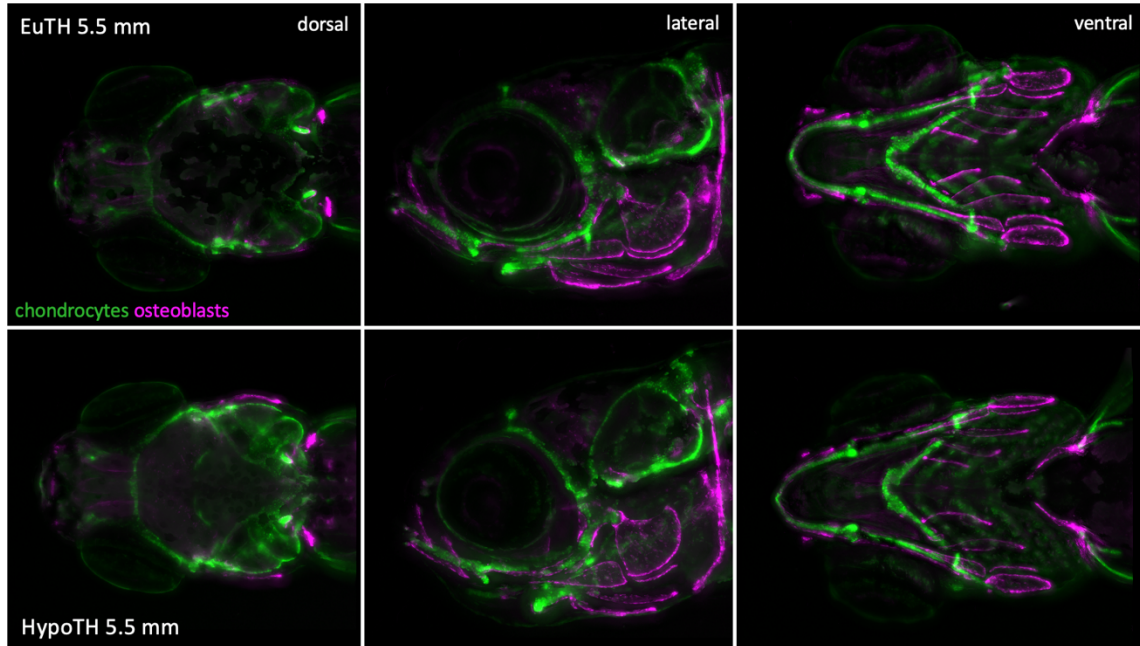


Figure 3.11 Thyroid hormone regulates osteoblast populations in zebrafish skulls. Wild-type (labelled EuTH) and hypothyroid (HypoTH) 5.5 mm SL zebrafish (top) in dorsal (left), lateral (middle), and ventral (right) views. *coll1a1* reporter in chondrocytes in green and *sp7* reporter in osteoblasts in magenta.

In HypoTH fish, there is no detectable difference in osteoblast populations in the premaxilla region of the upper jaws and ossifying edge located near the epiphyseal bar compared to wild-type siblings (Fig 3.12, Fig 3.13). The chondrocytes of Meckel's cartilage (the cartilage scaffold of the dentary) were well organized in the wild-type condition (arrows, Fig 3.14 top). Without TH, these cells appeared more disorganized (arrows, Fig 3.14 bottom). The hyomandibulae of the HypoTH fish contains more

osteoblasts and chondrocytes, but these cells appear depleted in the hyoid and branchiostegal rays relative to wild-type (Fig 3.14, Fig 3.15).

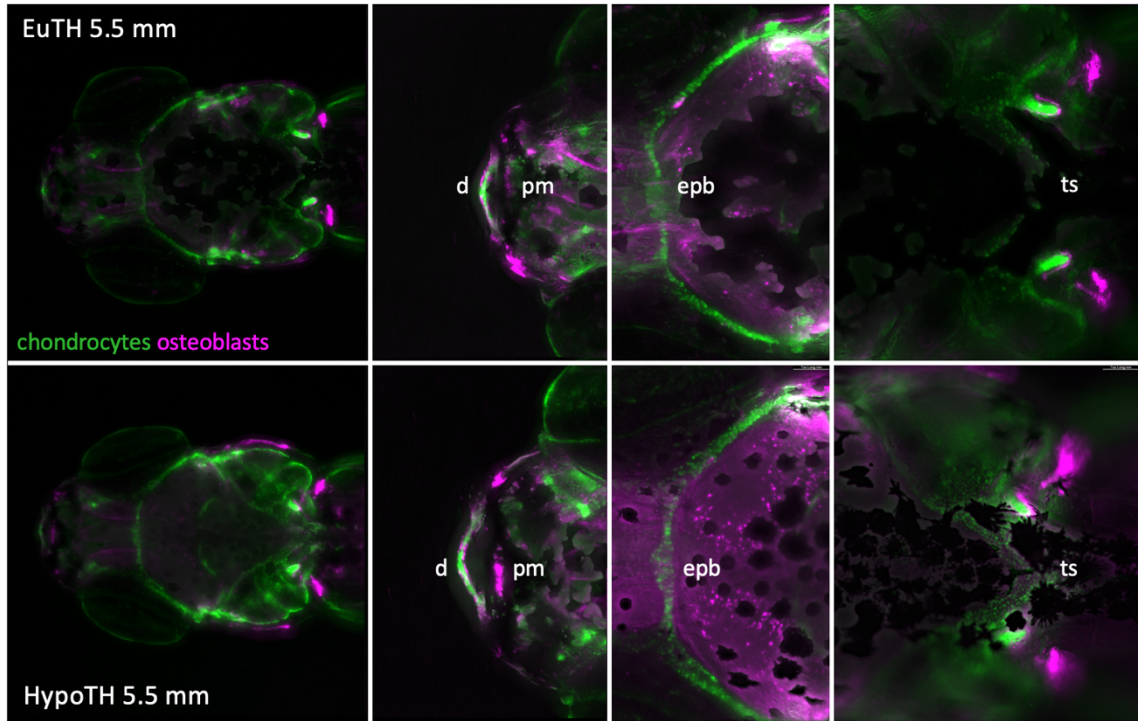


Figure 3.12 Dorsal view of *collala* & *sp7* reporter in 5.5mm SL wild-type and HypoTH zebrafish. (A), whole head view. (B), upper and lower jaws. (C), epiphyseal bar. (D), posterior end of dermatocranium. *collala* reporter in chondrocytes in green and *sp7* reporter in osteoblasts in magenta. d, dentary; pm, premaxilla; epb, epiphyseal bar; ts, tectum synoticum.

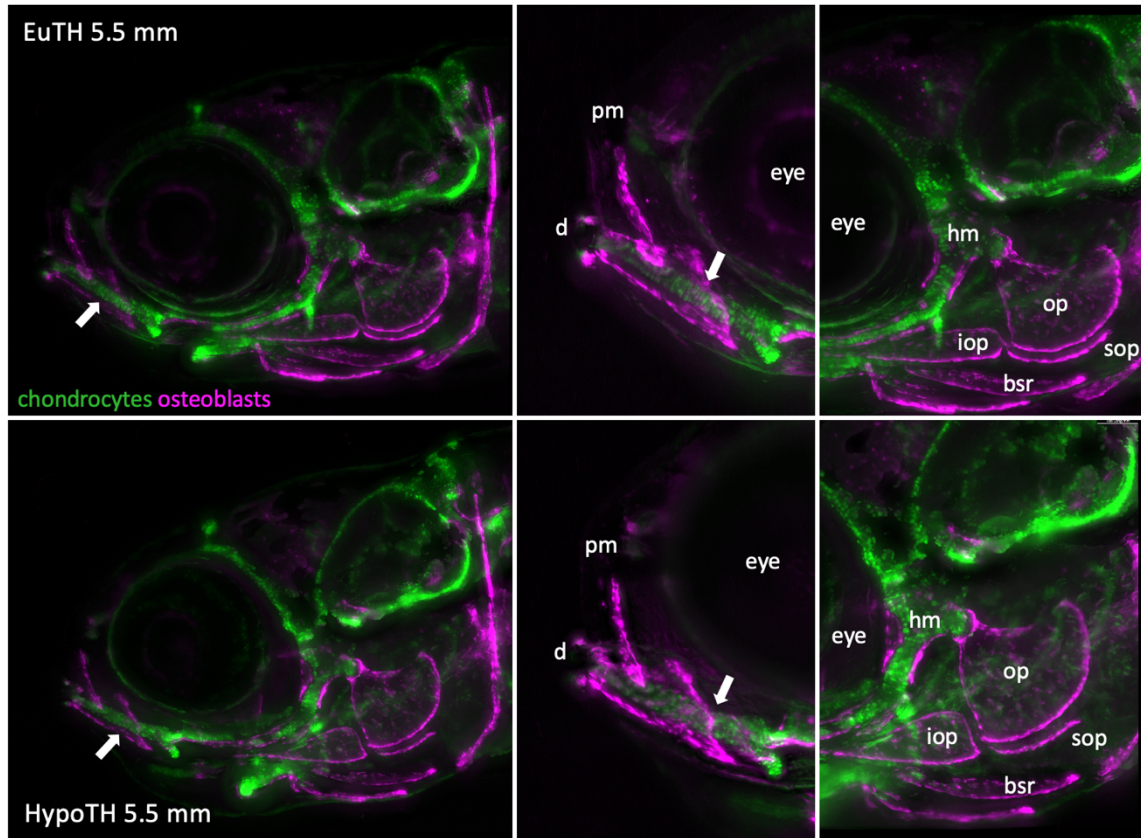


Figure 3.13 Lateral view of *collala* & *sp7* reporter in 5.5mm SL wild-type and HypoTH zebrafish. (A), whole head view. (B), upper and lower jaws. (C), opercular complex and hyomandibular. *collala* reporter in chondrocytes in green and *sp7* reporter in osteoblasts in magenta. White arrows indicate chondrocytes of Meckel's cartilage. d, dentary; pm, premaxilla; hm, hyomandibula; iop, interopercle; op, opercle; sop, subopercle; bsr, branchiostegal ray.

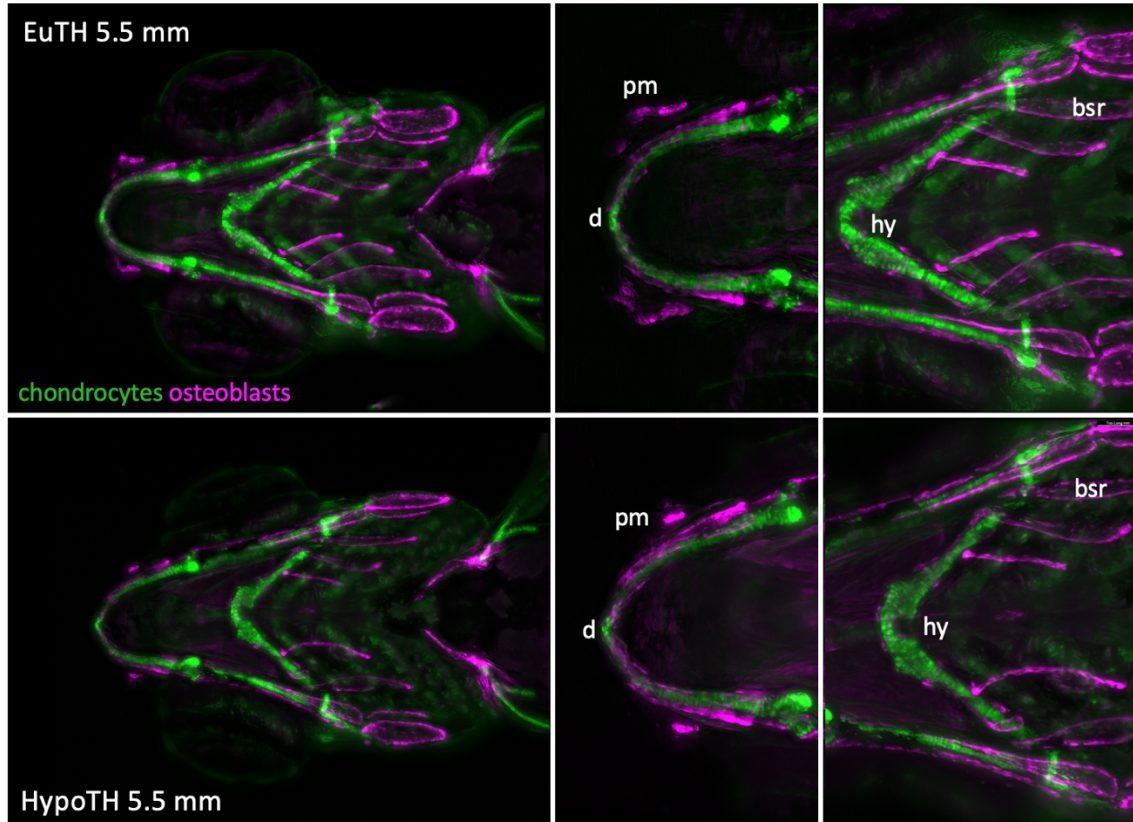


Figure 3.14 Ventral view of *collala* & *sp7* reporter in 5.5mm SL wild-type and HypoTH zebrafish. (A), whole head view. (B), upper and lower jaws. (C), hyoid and ceratohyals. *collala* reporter in chondrocytes in green and *sp7* reporter in osteoblasts in magenta. d, dentary; pm, premaxilla; hy, hyoid; bsr, branchiostegal ray.

3.3 DISCUSSION

3.3.1 TH regulates the rate of ossification of specific skeletal elements

The data from our 2D analyses suggest that TH plays a role in the morphogenesis of numerous skeletal elements in the developing postembryonic zebrafish. Notably, TH influences the shaping of the anterior and transformator processes of the tripus, the rami and lamina of the hyomandibula, and the slender overall shape of the pharyngeal jaws (Fig 3.2, Fig 3.6). The lower jaw is also sensitive to TH, and a lack of the endocrine factor results in delayed rates of ossification in numerous elements of the bone along with malformed mandibular symphyses and coronoid processes (Fig 3.4). Examining the

developmental shape trajectories of each skeletal element, the wild-type zebrafish exhibit trends in PC1 change over development that are altered in HypoTH and HyperTH fish (Fig 3.3, Fig 3.5, Fig 3.7, Fig 3.8). In most cases, the hyperthyroid fish shape trajectories are shifted forward in developmental time and the skeletal elements take on more mature shapes at earlier stages of development. In contrast, the absence of TH resulted in immature shapes in HypoTH fish compared to their size-matched wild-type and HyperTH counterparts (Fig 3.3, Fig 3.5, Fig 3.7, Fig 3.8).

3.3.2 The zebrafish skull undergoes shape changes during later stages of development that are sensitive to thyroid hormone

Visualizing the shape variation of the zebrafish entire skulls of juveniles and adults, we determined that the dermatocranium and jaw elements undergo the most change as the fish grows (Fig 3.10, Fig 3.11). The wild-type zebrafish undergo gradual widening and lengthening of the skull as they develop from juveniles into adults. In contrast, hypothyroid zebrafish retain an immature skull morphology while HyperTH conditions induce precocious development in the skull (Fig 3.10). At later stages of development, the trajectories of the wild-type and HyperTH zebrafish converge, such that the overall head shape of the two groups are similar to one another but altered in HypoTH fish (Fig 3.10).

3.3.3 Comparing 2D and 3D morphometric analyses

By using both 2D and 3D morphometric analyses in this chapter, we determined how TH works to shape both individual skeletal elements and the overall shape of the zebrafish skull. The bones used in our 2D analysis was mostly flat, making them appropriate for 2D landmarking and shape analysis. The 3D morphometric analysis

focused on the overall shape of the head, allowing us to look at several bones in association with each other and determine which bones and regions of the head underwent the most change during juvenile and adult development.

3.3.4 Thyroid hormone alters osteoblast and chondrocytes cell populations

Surveying osteoblasts and chondrocytes populations in several bones in the larval zebrafish, I observed differences in presence and organization of chondrocyte cell populations but not osteoblasts. Compared to wild-type larvae, HypoTH fish have similar populations of osteoblasts in many craniofacial bones including the premaxilla, dermatocranium, and branchiostegal rays, suggesting that TH does not play a role in stimulating this population to differentiate or proliferate during later stages of development (Fig 3.13, Fig 3.14, Fig 3.15). While the data from the 3D morphometric analyses indicated that these same bones continued to undergo shape change at juvenile and adult stages, it does appear that TH is acting upon osteoblast populations to regulate these changes (Fig 3.10, Fig 3.11). Meckel's cartilage forms a cartilaginous scaffold that acts as the template for the ossifying dentary. During normal development, chondrocytes are highly organized and tightly packed in Meckel's cartilage at 5.5 mm SL (Fig 3.14). In contrast, the chondrocytes of Meckel's cartilage in the HypoTH condition lacked this organization (Fig 3.14). This disorganization during metamorphic stages may result in an improperly formed cartilage scaffold, resulting in the ectopic malformations and growths seen on the lower jaws of hypothyroid adult zebrafish.

3.4 MATERIALS AND METHODS

3.4.1 Fish rearing and thyroid ablation

All research was performed in accordance with protocols approved by the Institutional Animal Care and Use Committee at Boston College: Institutional Animal Welfare Number Assurance Identification D16-00521; Protocol 2007-006-01. Transgenic lines used in this chapter were: *Tg(tg:nVenus-2a-nfn)^{wp.rt8}* (McMenamin et al., 2014), *opallus^{b1071}* (McMenamin et al., 2014), *Tg(-1.4co-11a1:egfp)* (Kague et al., 2012), and *Tg(sp7:mCherry)* (Kague et al., 2016). Hypothyroid zebrafish (HypoTH) were produced by treating 4-day-old *Tg(tg:nVenus-2a-nfn)^{wp.rt8}* with 10 mM metronidazole + 1% dimethyl sulfoxide to permanently ablate the thyroid follicles (as described in McMenamin et al., 2014). Treated individuals were checked for loss of nVenus signal in the thyroid follicles the next day following treatment to ensure ablation. Constitutively hyperthyroid zebrafish (HyperTH) were homozygous *opallus* mutants (McMenamin et al., 2014). For fluorescent imaging, the *Tg(tg:nVenus-2a-nfn)^{wp.rt8}* line was crossed into a *Tg(-1.4co-11a1:egfp); Tg(sp7:mCherry)* double transgenic line. All fish were reared under standard conditions (28°C, 14:10 light cycles), recirculating water was carbon-filtered. Fish were fed a combination of live marine rotifers reared with RotiGrow Plus (Reed Matriculture), live *Artemia*, and pure Spirulina flakes (Pentair).

3.4.2 MicroCT scanning and 3D modeling

Fish were euthanized by MS-222 and fixed in 4% PFA for a minimum of 24 hours. SL was measured in fixed samples according to Parichy et al. (2009) before scanning. Fish samples shrink slightly during the fixation process, and it should be noted that the reported fixed SL values may be converted to corresponding “fresh” SL by adding 0.29 mm (Parichy

et al., 2009). For the 3D morphometrics analysis, a total of 178 specimens were scanned, ranging from 12 to 25 mm SL with a minimum of one scan for every half millimeter. Fixed specimens were placed in low-density foam molds and inserted into either a 1.5 ml centrifuge tube (for specimens 12-14 mm SL) or a 15 ml conical tube (for specimens >14 mm SL). Scans were performed on a SkyScan 1275 high resolution microCT system (Bruker, Kontich, Belgium) at a scanning resolution of 10.5 μm with an x-ray source voltage of 45 kV and current of 200 mA. Projection images were generated over 360° with a 0.1° rotation step and 6 averaging frames. Thresholding, ring artifact reduction, and beam hardening corrections were consistent across all scans during reconstruction using the software NRecon (Bruker, Kontich, Belgium). Surface reconstructions were generated from the scan reconstruction slices in Amira 6.5 (Thermo Fisher Scientific FEI, Hillsboro, Oregon, United States) using the lasso tool to select and threshold the craniofacial skeleton, and 3D models were then exported using the “Generate surface” module. These models were further processed and simplified in MeshLab (Callieri, 2013; Cignoni et al., 2008).

3.4.3 Landmarking and geometric morphometrics

For 2D morphometric analyses, 240 individuals were collected, measured for standard length (SL), and binned into four developmental categories: “late larval” (7–11 mm SL), “early juvenile” (>11–15 mm SL), “late juvenile” (>15–20 mm SL), and “adult” (>20 mm SL). Samples were cleared and stained according to a modified protocol by Walker and Kimmel (2007) and SL was measured again on the fixed specimens. The tripus, lower jaw, hyomandibula, and pharyngeal jaws were manually dissected from the cleared and stained fish and imaged in lateral view. Type II landmarks, which are based on

geometrics points such as maximum or minimum curvature, were selected for each bone based on identifiable homologous characters and placed manually on digital images using the PointPicker extension in ImageJ (Fig 3.16, Schneider et al., 2012; Zelditch et al., 2004).

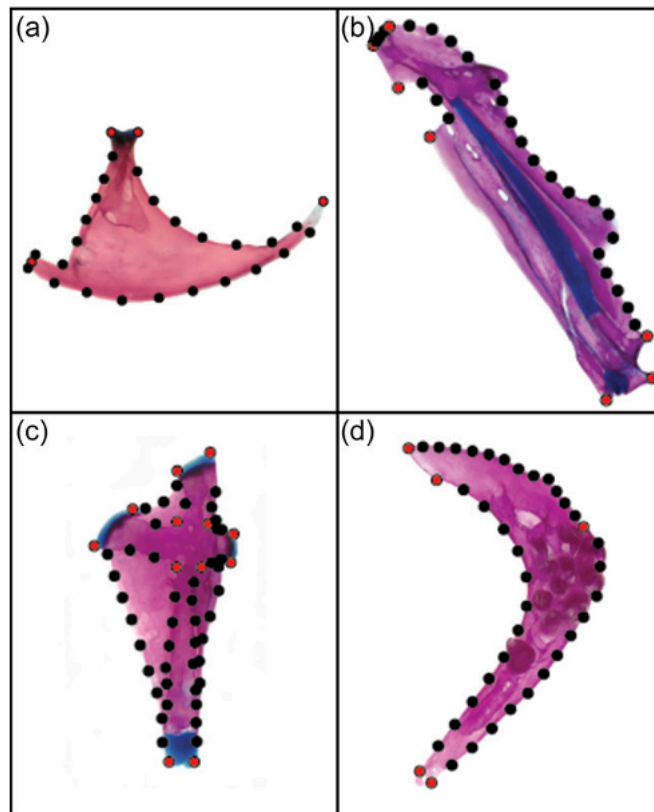


Figure 3.15 Landmarks used for developmental morphometric analysis of four craniofacial bones. Landmarks (Type I) shown in red; semilandmarks (Type II) shown in black. (A), A total of 4 landmarks and 24 semilandmarks were placed on the tripus. (B), 7 landmarks and 25 semilandmarks were placed on the lower jaw. (C), 12 landmarks and 44 semilandmarks were placed on the hyomandibula. (D), 5 landmarks and 36 semilandmarks were placed on the pharyngeal jaw.

For 3D morphometric analyses, 3D models of 178 individuals (63 wild-type, 55 HypoTH, and 60 HyperTH) were landmarked with 22 manual landmarks using the `digit.fixed()` function in the Geomorph package (v 4.0.5) in R (v 4.3.5) (Fig 3.17, Supplemental table 3.1, Adams, Dean C., Collyer, M. L., Kaliontzopoulou, A. , Baken,

2022). Landmarks were selected based on specific features of different bones and regions covering most dimensions of the zebrafish skull. Landmark coordinate information was then saved as .nts files, compiled, and converted into a .tps file format.

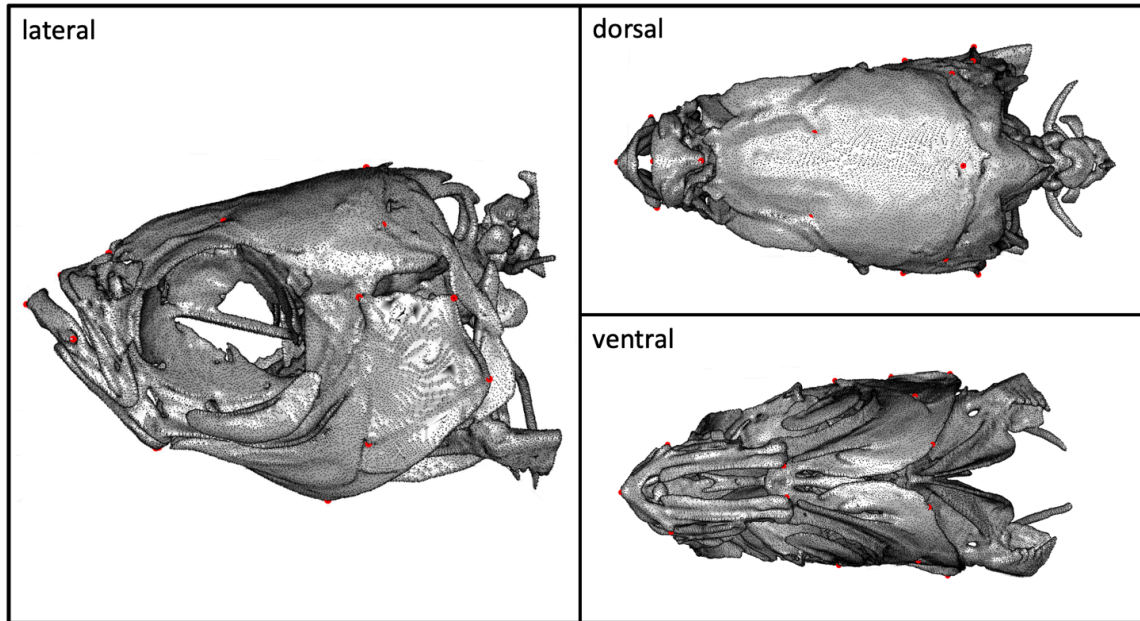


Figure 3.16 Landmarks used for developmental 3D morphometric analysis of overall head shape. Landmarks are shown in red in lateral, dorsal, and ventral views, and were manually placed using the Geomorph package in R. Full list of landmark descriptions found in Supplemental Table 3.1.

Data analysis for both 2D and 3D geometric morphometric analyses was performed using the Geomorph package (version 3.3.1) in R (version 4.0.2, Adams, Dean C., Collyer, M. L., Kaliontzpoulou, A. , Baken, 2022; Baken et al., 2021). Generalized Procrustes analysis was applied to both landmarking datasets to account for size and rotational differences among measurements, thus analyzing only bone shape. A principal component analysis (PCA) was then performed to determine major axes of shape variation. Deformation grids were generated for different principal components using the Geomorph

package (Adams, Dean C., Collyer, M. L., Kaliontzpoulou, A. , Baken, 2022; Baken et al., 2021).

3.4.4 Fluorescent Imaging

Wild-type and hypothyroid zebrafish (*Tg(tg:nVenus-2a-nfn)^{wp.rt8};Tg(-1.4collal:egfp); Tg(sp7:mCherry)*) were euthanized with Tricaine (MS-222, Sigma-Aldrich) and mounted in 2% methylcellulose in glass bottom imaging dishes. Prior to euthanasia, zebrafish were placed in water with epinephrine to shrink melanophores for clearer imaging. Z stacks of the zebrafish head were obtained using a Leica THUNDER Imaging System using a K8 camera (Leica Microsystems, Wetzlar, Germany). Raw images were parallax corrected, compressed into a single maximum project image, and then “thunderized” to remove background fluorescence. Exported images were adjusted for contrast and brightness in FIJI and all adjustments were applied to both euthyroid and hypothyroid zebrafish (Schindelin et al., 2012).

3.5 SUPPLEMENTAL DATA

Supplemental Table 3.1. Summary of 3D landmarking scheme.

Landmark	Description of landmark
1	Top anterior edge of left opercle
2	Top posterior edge of left opercle
3	Bottom anterior edge of left opercle
4	Bottom posterior edge of left opercle
5	Top anterior edge of right opercle
6	Top posterior edge of right opercle
7	Bottom anterior edge of right opercle
8	Bottom posterior edge of right opercle
9	Medial edge of left innermost branchiostegal ray
10	Medial edge of right innermost branchiostegal ray
11	Anterior edge of premaxilla
12	Tip of premaxilla ascending process/arm
13	Posterior end of right dentary
14	Tip of right dentary anterolateral process
15	Anterior tip of dentary
16	Tip of left dentary anterolateral process
17	Posterior end of left dentary
18	Center of posterior edge of parietal bone
19	Leftmost point of posterior edge of parietal bone
20	Rightmost point of posterior edge of parietal bone
21	Left lateral point of epiphyseal bar
22	Right lateral point of epiphyseal bar

CHAPTER 4

Craniofacial diversity across Danionins and effects of TH status on adult craniofacial morphology of two Danio species

This material in this chapter was adapted from:

Nguyen S.V., Lee R.S., Mohlmann E., Petrullo G., Blythe, J.O, Ranieri, I.L.,
McMenamin SK. Craniofacial diversity across Danioninae and induced by modifications
to developmental thyroid hormone. bioRxiv. <https://doi.org/10.1101/2023.08.09.552728>

4.1 INTRODUCTION

4.1.1 Using zebrafish and its relatives for research and craniofacial development

Zebrafish (*Danio rerio*) are a powerful model for developmental biology and biomedicine (Bruneel & Witten, 2015; Kwon et al., 2019a; Tonelli et al., 2020). Zebrafish have emerged as a tool for studying vertebrate skeletogenesis (Clément et al., 2008; Dietrich et al., 2021) and have been used to study skull development (Cubbage & Mabee, 1996) and craniofacial abnormalities including craniosynostosis (Laue et al., 2011; Teng et al., 2018) and cleft palate (Atukorala & Ratnayake, 2021; Raterman et al., 2020). As molecular and genetic research in zebrafish has advanced, there has been growing interest in the natural phenotypic diversity across the broader Danioninae subfamily (T. Y. Liao et al., 2011; McClure et al., 2006). Placing zebrafish into a broader phylogenetic context can help provide ecological, evolutionary, and functional depth for zebrafish research, can suggest avenues for ongoing molecular and biomedical efforts, and can identify informative phenotypes for genomic and developmental analysis.

4.1.2 Danioninae phylogeny

Within Danioninae, three major genera are described: *Danio* (27 species), *Devario* (38 species) and *Chelas* (3 species) (Kullander et al., 2017). Small, charismatic, and easy to care for, representatives from each genus are commonly used as aquarium fish (Sado & Kimura, 2005). The Danioninae phylogeny has been examined using various molecular methods (Fang, 2003; T. Y. Liao et al., 2011; Mayden et al., 2007; McCluskey & Postlethwait, 2015). Mayden et al. compared sequence information from two nuclear genes and five mitochondrial genes, generating a phylogeny that identified the *Danio* genus as monophyletic with *Da. rerio* and *Da. kyathit* as sister groups (Mayden e2007). More

recently, whole-genome restriction-associated DNA sequencing has identified *Da. aesculapii* as the sister group to *Da. rerio* (McCluskey & Postlethwait, 2015).

4.1.3 Danioninae comparative studies

Species within Danioninae show a range of morphological characteristics adapted to their slightly different ecologies. Slender-bodied *Danio* species are typically found in slower water currents compared to deep-bodied (deeper body from back to belly than wide) *Devario* species (McClure et al., 2006). Fang et al categorized 38 morphological characteristics of 18 Danioninae species, comparing morphological relationships to previously published phylogenies (2003). Studies comparing specific Danioninae have described *Da. margaritatus* and *Da. erythromicron* as morphologically similar, with similarly shaped bodies, fins, and lower jaws (Roberts, 2007). The characteristics and morphology of the pharyngeal jaws of 22 Danioninae species including *Aspidoparia morar*, *Bengala elanga*, and *Opsarius tileo* have been described and compared in detail, finding these African Danioninae likely evolved their fourth row of dentition from an ancestor with three tooth rows, as seen in Asian Danioninae (Ahnelt et al., 2015).

4.1.4 Danioninae use as research models

Zebrafish is now extremely well established as a research model, and a number of research groups have begun to ask questions using other Danioninae species. Largely due to its large and tractable size, giant danios (*Devario aequipinnatus*) have been used to study schooling behavior, pharmacological, and reproductive studies (De Jesus-Silva et al., 2018; Mekdara et al., 2021; Vorbach et al., 2019). The transparency of the Danionella and its lack

of a skull roof has made it attractive as a system for studying neurogenesis (Britz et al., 2021; Conway et al., 2021).

Aside from characteristics of different Danioninae making them tractable for certain experimental purposes, some researchers have begun to use the diversity within the subfamily to ask specific questions about evolutionary mechanisms. Most notably, different *Danio* species exhibit diverse pigmentation, and the evolution of these pigment patterns is being studied on at developmental and molecular levels (Irion & Nüsslein-Volhard, 2019; McCluskey et al., 2021; Parichy, 2021).

Although not as conspicuous as the pigment pattern diversity, the skulls of Danioninae differ between species (Conith et al., 2022; Galindo et al., 2019). These differences could form the basis for fruitful evolutionary comparisons and lay the groundwork for comparative molecular work on Danioininae skulls.

4.1.5 Fish craniofacial biology & craniofacial comparison between *Danio rerio* and other Danios

The teleost craniofacial skeleton is more elaborate and complex than the mammalian skull (Bruneel & Witten, 2015). The zebrafish skull is composed of 74 skeletal elements while the human skull has 22 bones (Cubbage & Mabee, 1996; Eames et al., 2013). Conith *et al.* examined the functional morphology of feeding behavior in zebrafish and giant danio, showing that zebrafish use jaw protrusion to produce suction while giant danios utilize jaw protrusion for prey retention (2022). Diverse upper jaw morphology, particularly in the length of the premaxilla ascending arm, and its influence on feeding

behavior has been compared between zebrafish and nine other Danioninae species (Galindo et al., 2019).

4.1.6 Role of TH in craniofacial skeleton development

Thyroid hormone (TH) regulates craniofacial development and plays a role in shaping specific craniofacial bones in zebrafish (Harper et al., 2023; Keer et al., 2019, 2022; S. McMenamin et al., 2017). TH affects the development of feeding mechanics in zebrafish, stunting the growth of the premaxilla (Galindo et al., 2019). Allometric shape change of several bones including the hyomandibula and pharyngeal jaws require developmental TH (Keer et al., 2022). Hypothyroid conditions result in immature shapes of the lower jaw and tripod of the craniofacial skeleton while zebrafish larvae reared in hyperthyroid conditions undergo precocious ossification of skull bones (Keer et al., 2022; Shkil et al., 2012). Specifically, the morphologies of the lower jaw and Weberian apparatus appeared to be most affected by increased levels of TH (Keer et al., 2019).

4.1.7 Rationale for and summary of this research

Danioninae are a subfamily of fishes that while closely related, possess diversely shaped craniofacial skeletons. Here, we aim to characterize the morphology of the craniofacial diversity across several Danioninae and compare it to the shape changes seen in TH-modulated *Danios*. We used microcomputed tomography (microCT) to capture craniofacial shape in 9 Danioninae species, including zebrafish (Charles et al., 2017). We hypothesized that some of the craniofacial differences we see among Danioninae might be due to interspecific differences in TH metabolism or TH pathways. We asked if *Da. rerio* and *Da. albolineatus* reared under altered TH profiles phenocopied the craniofacial

morphologies of other Danioninae species, and found that the hypothyroid *Danios* occupied a unique region of morphospace not occupied by other species. Our results provide insight into the natural diversity in Danioninae head shape and suggest that alterations to TH have the capacity to create unique overall craniofacial phenotypes.

4.2 RESULTS

4.2.1 Danioninae exhibit a range of craniofacial shapes

To capture overall craniofacial morphology, we scanned individuals from 9 Danioninae species (*Da. rerio*, *De. aequipinnatus*, *Da. erythromicron*, *C. dadiburjori*, *Da. albolineatus*, *Da. aesculapii*, *Da. nigrofasciatus*, *Da. margaritatus*, and *Da. kyathit*) and generated volume renderings from the microCT scans (Fig 1). We observed apparent differences in density and head shape (Fig 1). To quantitatively capture craniofacial shapes, we generated 3D models of the heads and automatically landmarked each head (Fig 2). We used 3D geometric morphometrics to define the morphospace occupied by these Danioninae craniofacial skeletons (Fig 3).

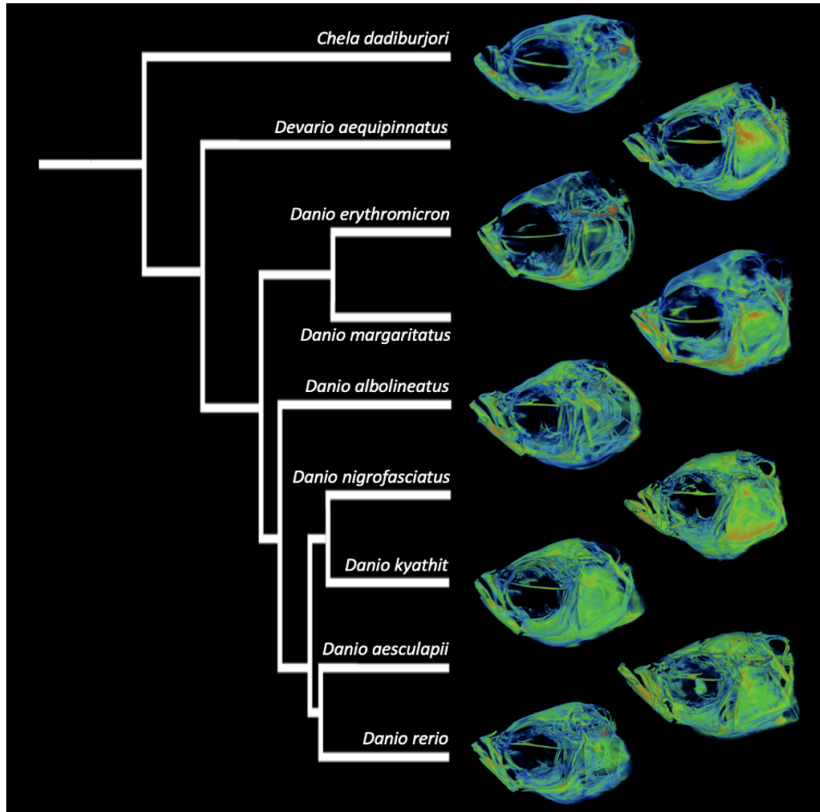


Figure 4.1 Danioninae are a subfamily of Cyprinidae. Phylogenetic tree of scanned Danioninae species, adapted from McCluskey and Postlethwait 2015. Relative density renderings of craniofacial skeletons from nine different Danioninae species. Warmer colors indicate regions of higher density.

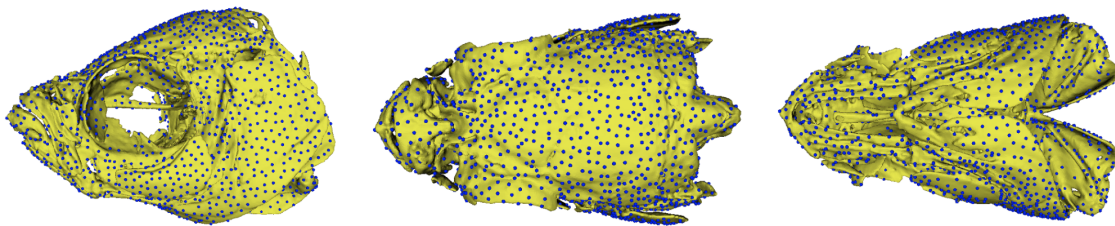


Figure 4.2 Capturing craniofacial shape information with automatic 3D landmarking. Lateral, dorsal, and ventral views of a 23.0 mm standard length *Danio rerio* head with 3000 automatic landmarks placed using ALPACA in 3D Slicer.

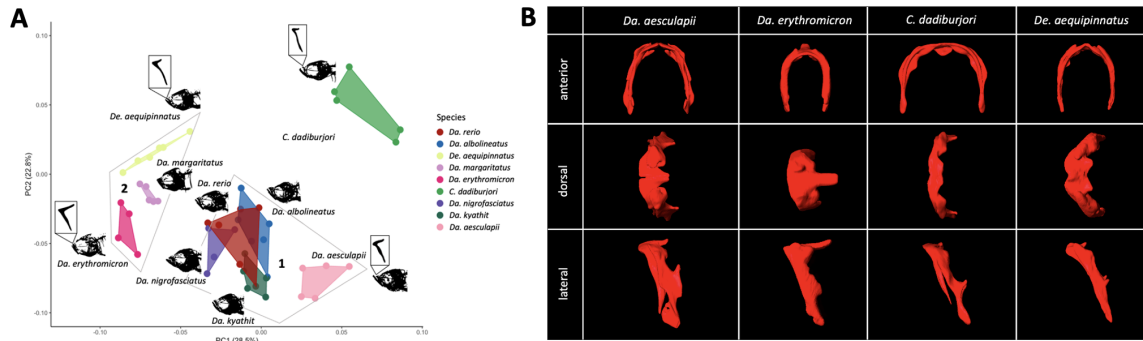


Figure 4.3 Danioninae have a spectrum of head and bone shapes. A, Morphospace for first and second principal components from principal component analysis (PCA). Two major morphological groups are numbered and outlined in gray. Specimens of the same species are colored similarly, and the morphospace occupied by each species is shaded in the same color. Silhouettes of the Danioninae heads are shown in black, based on density renderings. Silhouette of the premaxillae of four species (*Da. aesculapii*, *Da. erythromicron*, *C. dadiburjori*, and *De. aequipinnatus*) is shown in black, based on segmentation. B, The upper jaws of Danioninae heads have diverse shapes. Segmented upper jaws (premaxillae and maxillae) of *Da. aesculapii*, *Da. erythromicron*, *C. dadiburjori*, and *De. aequipinnatus* shown in anterior, dorsal, and lateral views.

4.2.2 Centroid distance is correlated with phylogenetic distance

We asked whether differences in craniofacial morphology correlated with phylogenetic relationships. We determined the centroid position of each species by calculating the mean PC1 and PC2 positions of each species and comparing this position to that of each other species (Supp Fig 1A). We found that for many of the Danioninae species (*Da. rerio*, *Da. albolineatus*, *Da. nigrofasciatus*, *Da. kyathit*, *Da. aesculapii*), centroid distance was correlated to phylogenetic distance (Supp Fig 1B, Supp Table 1). Increasing the number of automatic landmarks or changing the template species on which the automatic landmarking was based did not change overall patterns of centroid distance relationships (Supp Fig 4.2 and 4.3).

4.2.3 Thyroid hormone-altered heads have unique craniofacial skeletons

To test the roles that TH plays in shaping *Danio* skulls, we reared *Da. rerio* and *Da. albolineatus* under altered TH profiles, and we scanned hypothyroid (HypoTH) and hyperthyroid (HyperTH) *Da. rerio* and HypoTH *Da. albolineatus*. As observed previously (Galindo et al., 2019; McMenamin et al., 2014, 2017), we confirmed that HyperTH rearing conditions significantly lengthen the lower jaw in zebrafish (Fig 4). HypoTH *Da. rerio* and *Da. albolineatus* heads showed decreased relative bone density and bony lesions of the tip of the lower jaw (Fig 4A). HypoTH conditions markedly changed the shape of the skull, showing little or no overlap with euthyroid, wild-type counterparts from each respective species (Fig 5A-B).

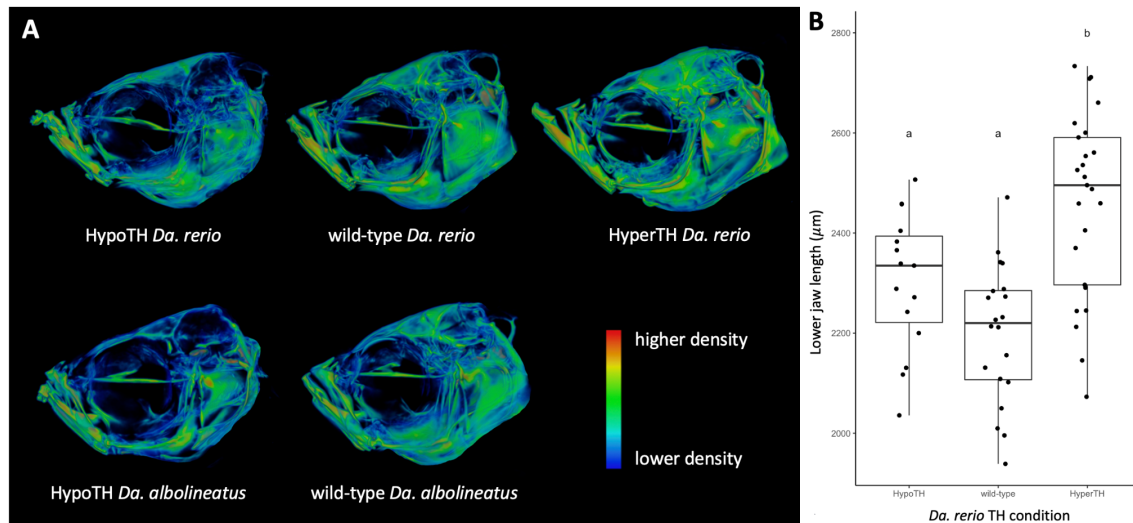


Figure 4.4 Thyroid hormone regulates craniofacial morphology in *Danio rerio* and *Danio albolineatus*. Relative density renderings of hypothyroid (HypoTH), wild-type, and hyperthyroid (HyperTH) *Da. rerio* heads. Warmer colors indicate higher density regions. B, Lower jaw lengths of HypoTH, wild-type, and HyperTH *Da. rerio*.

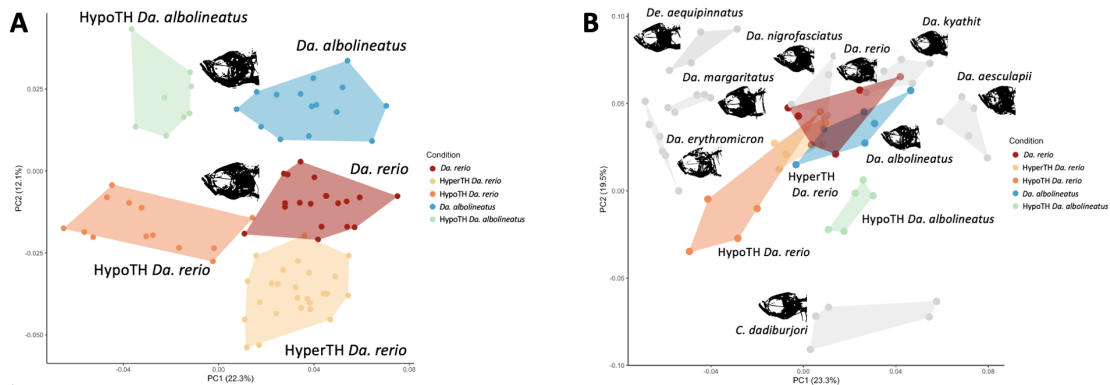


Figure 4.5 Thyroid hormone altered heads have unique craniofacial skeletons. A, Morphospace of all wild-type and TH conditions for *Da. rerio* and *Da. albolineatus*. B, Morphospace of PC1 and PC2 for head shape of nine Danioninae species in addition to HypoTH *Da. rerio* and *Da. albolineatus*, and HyperTH *Da. rerio*. Each dot represents a scanned individual specimen.

4.3 DISCUSSION

4.3.1 Diversity of Danioninae craniofacial head shapes and relationship to phylogeny

Danioninae species exhibit many differences in bone morphology and density, and these changes are also seen in TH modulated zebrafish (Keer et al., 2019, 2022; Roberts, 2007). We 3D scanned and examined the complex craniofacial shapes of the subfamily Danioninae and captured approximately 51% of variation in Danioninae head shape with two PCs. The first principal component of the morphospace (PC1) captures a continuum from elongated heads to taller, more triangular heads. There is considerable overlap between *Da. rerio*, *Da. nigrofasciatus*, *Da. kyathit*, and *Da. albolineatus*; *Da. aesculapii* (sister species to *Da. rerio*) did not overlap with *Da. rerio* in our morphospace. Aspect ratio of the head (head height relative to head length) appeared to be associated with the variation seen in the first component of the PCA, and *Da. rerio* was shown to be most

morphologically similar to *Da. nigrofasciatus*, *Da. kyathit*, and *Da. albolineatus*. Nonetheless, we found that centroid distances across the morphospace correlated with phylogenetic distance from five different species including *Da. rerio* (Supp Fig 1).

4.3.2 Detecting specific differences in upper jaw morphology

Previous work suggests that the length of the premaxilla ascending arm corresponds to protrusive ability during feeding, and that species with shorter ascending arms rely on little or no jaw protrusion (Galindo et al., 2019). To more closely examine upper jaw elements in Danioninae with the most ‘extreme’ skull shapes, we segmented the premaxillae and maxillae of *Da. aesculapii*, *Da. erythromicron*, *C. dadiburjori*, and *De. aequipinnatus* (Fig 6). There were qualitative differences in upper jaw morphology, including the relative width of the upper jaws and the length of the premaxilla ascending arm. Some of the spatial relationships present in our morphospace resemble previous 2D morphometric analyses performed on microdissected premaxillae from some of the same species (Conith et al., 2022; Galindo et al., 2019).

The feeding mechanics of several Danioninae species and altered TH-profile zebrafish have been compared and correlated to premaxilla morphology using morphometric analyses that determined that the premaxillae shape of each genus or TH condition is distinct from one another (Conith et al., 2022; Galindo et al., 2019). We see similar relationships in our dataset in which the *Danios* appear to group together, and *De. aequipinnatus* and *Da. erythromicron* are found on opposite ends of one of the principal component axes.

4.3.3 Thyroid hormone stabilizes craniofacial phenotypes

Finally, our results suggest that altering developmental TH has the capacity to create overall craniofacial phenotypes unique to other Danioninae species. In a morphospace containing *Da. rerio* and *Da. albolineatus* (Fig 5A), the first axis of variation captures the changes associated with HypoTH conditions, while the second axis appears to capture species identity. HypoTH conditions appear to result in corresponding morphological shifts in both of the species. The skull shapes we measured in TH-modulated fish did not map on to any other species we examined, inhabiting otherwise unoccupied regions of morphospace (Fig 5B). However, in both *Da. rerio* and *Da. albolineatus*, HypoTH rearing conditions shift morphology away from that of other *Danios* and closer to that of *C. dadiburjori*.

4.4 MATERIALS AND METHODS

4.4.1 Fish rearing and preparation

All experiments were performed using an approved protocol in accordance with the Institutional Animal Care and Use Committee at Boston College. *Da. rerio*, *Da. albolineatus*, *Da. nigrofasciatus* and *Da. aesculapii* were reared at 28°C on a 14:10 light:dark cycle and fed a diet of marine rotifers and adult pellet food flakes three times a day. Hypothyroid *Danio rerio* and *Danio albolineatus* were fed a diet of artemia and spirulina flakes. All other Danioninae species were purchased from local pet stores or tropical fish stores (*Da. aequipinnatus*: Petco, Shrewsbury, MA; *C. dadiburjori* & *Da. erythromicron*: Uncle Ned's Fish Factory, Millis, MA; *Da. kyathit* & *Da. margaritatus*: Lucky's Aquarium, Worcester, MA). Fish were purchased under common and scientific

species names identified by retailers; we note that species identification may be unreliable. Using species identification information that is publicly available, we were able to positively identify four of the six Danioninae obtained from the pet trade with a reasonable level of confidence (Supp. Table 4.1).

4.4.2 MicroCT scanning and 3D modeling

A total of 9 Danioninae species were scanned: *Danio rerio* (zebrafish), *Danio aesculapii* (panther danio, the likely sister species of *Da. rerio*, McCluskey and Postlethwait 2015), *Devario aequipinnatus* (giant danio), *Danio erythromicron* (emerald dwarf danio), *Chela dadiburjori* (orange hatchet danio), *Danio albolineatus* (pink pearl danio), *Danio nigrofasciatus* (spotted danio), *Danio margaritatus* (celestial pearl danio), and *Danio kyathit* (ocelot danio). All fish were euthanized in MS-222 and fixed in 4% paraformaldehyde for 24 hours. Standard length (SL) was measured on fixed specimens. Fixed samples may shrink during the fixation process and the reported SL can be converted to a fresh SL measurement by adding 0.29mm (Parichy et al., 2009). Fixed specimens were placed between low-density foam molds and scans were performed using a SkyScan 1275 high resolution microCT system (Bruker, Kontich, Belgium) with a scanning resolution of 10.5 μm and an x-ray source voltage of 45 kV and current of 200mA. Projection images were generated over 360° with a 0.2° rotation step and 4 averaging frames. Thresholding, ring artifact reduction, and beam hardening corrections were consistent across all scans during reconstruction using NRecon (Bruker, Kontich, Belgium). 3D models of the Danioninae heads were generated using the Segmentation Editor in Amira 6.5 (Thermo Fisher Scientific FEI, Hillsboro, Oregon, USA). The entire scan volume was loaded, and a pixel threshold was determined to differentiate bone from soft tissue. The lasso tool was

then used to select the corresponding pixels of the head region and added to a new material label. The generated surface module was used to create a 3D model from the corresponding material label and the model was then exported as a .ply file. 3D models were further processed and simplified using MeshLab (Cignoni et al., 2008). The upper jaws were segmented using the Segmentation Editor in Amira 6.5 (Thermo Fisher Scientific FEI, Hillsboro, Oregon, United States). The scan volume was loaded into the program and a pixel threshold was determined to differentiate bone from soft tissue. The lasso tool was then used to select the corresponding pixels of the specific skeletal elements and added to the appropriate material label.

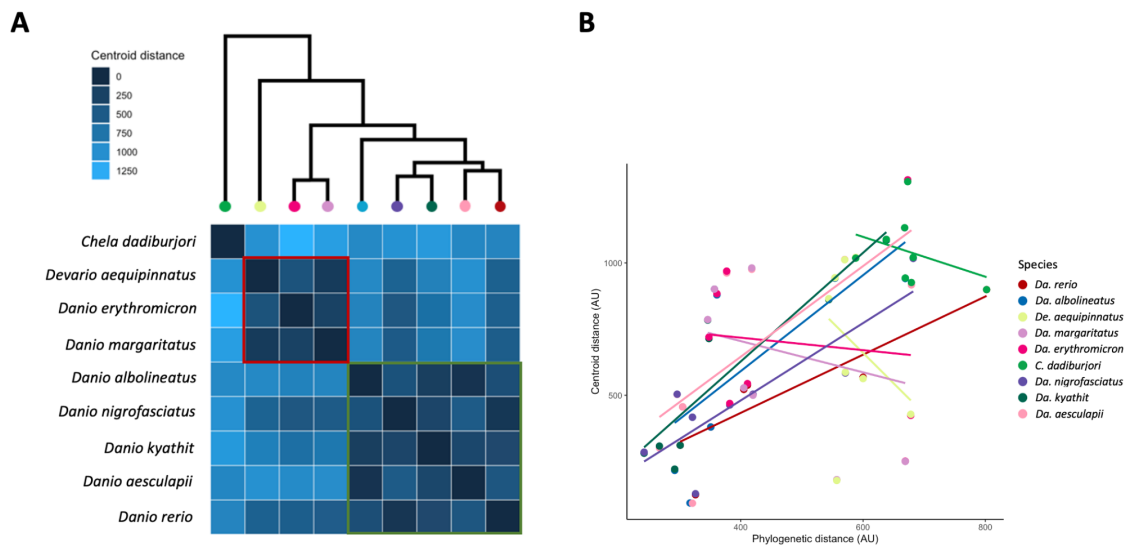
4.4.3 Automatic landmarking and geometric morphometrics

Four Danioninae species (*Da. rerio*, *Da. aesculapii*, *Da. kyathit*, and *Da. nigrofasciatus*) were used for template selection, and *Da. rerio* was determined to be the best template for automatic landmarking. All 3D models were screened for quality, and specimens in which the lower jaw was positioned underneath the upper jaw, or the mouth gape was too large were excluded from the dataset. A total of 3000 landmarks were automatically placed on 3D models using the Automated Landmarking through Pointcloud Alignment and Correspondence Analysis (ALPACA) extension in the open-source software 3D slicer (Kikinis et al., 2014; Porto et al., 2021). General Procrustes alignment (GPA) was performed to remove differences in positioning, size/scale, and orientation on the original dataset of landmark coordinates. To visualize and reduce dimensionality of shape differences among the Danioninae species in the morphospace, a Principal Component Analysis (PCA) was performed using the SlicerMorph extension of 3D Slicer (Kikinis et al., 2014). Results were plotted onto a morphospace using the Geomorph

package in RStudio (Adams, Dean C., Collyer, M. L., Kaliontzpoulou, A. , Baken, 2022; Baken et al., 2021). Centroid distances were calculated and plotted using the ggplot2 package in RStudio (Adams, Dean C., Collyer, M. L., Kaliontzpoulou, A. , Baken, 2022; Baken et al., 2021).

4.5 SUPPLEMENTAL DATA

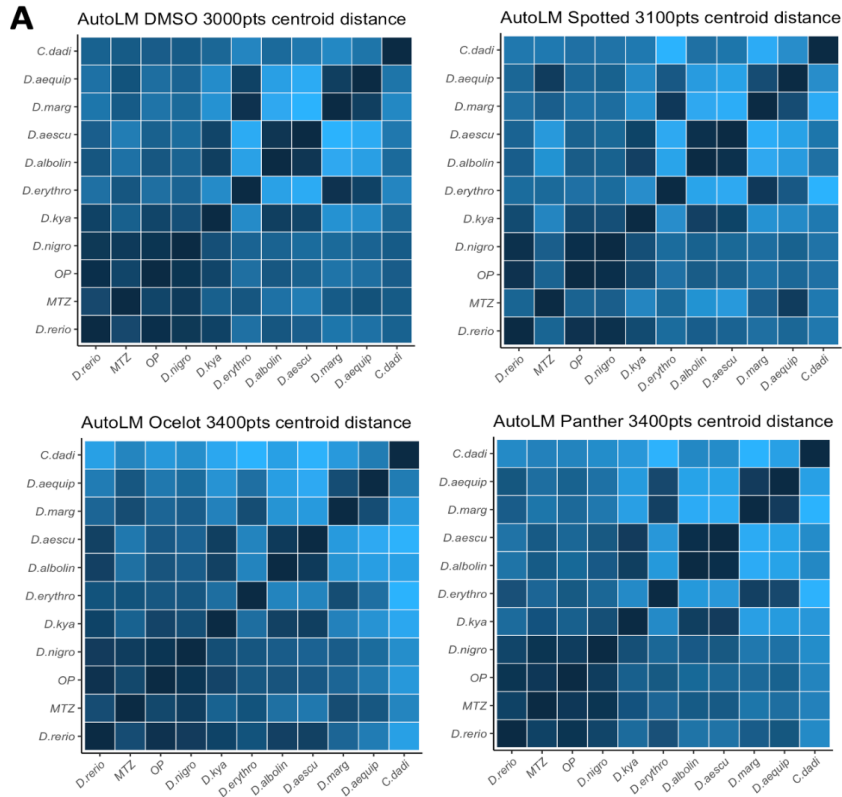
Supplemental Figure 4.1 Centroid distance (average morphospace location) is correlated with phylogenetic distance. A, Heat map of centroid distances between each of the Danioninae species. Phylogenetic tree represented at the top of the heat map. Lighter colors indicate further centroid distances. B, Relationship between phylogenetic distance and centroid distance plotted per species.



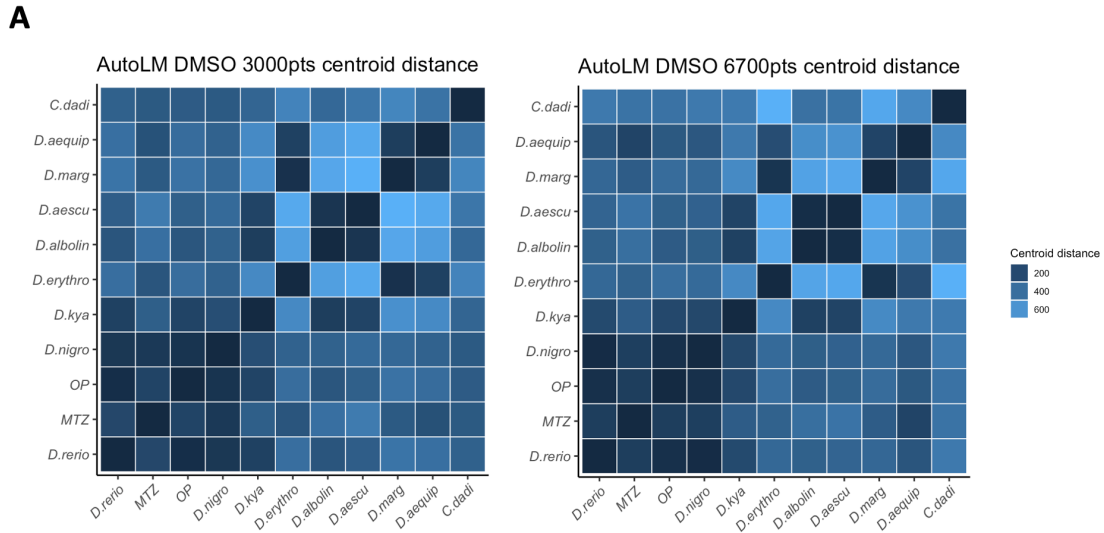
Supplemental Table 4.1 Centroid distance is correlated with phylogenetic distance. Correlation values (R^2) for each Danioninae species.

Species	Centroid-Phylogenetic Distance Correlation	Species	Centroid-Phylogenetic Distance Correlation
<i>D. rerio</i>	0.861	<i>D. aequipinnatus</i>	-0.318
<i>D. albolineatus</i>	0.684	<i>D. margaritatus</i>	-0.226
<i>D. nigrofasciatus</i>	0.847	<i>D. erythromicron</i>	-0.106
<i>D. kyathit</i>	0.886	<i>C. dadiburjori</i>	-0.338
<i>D. aesculapii</i>	0.702		

Supplemental Figure 4.2 Centroid distance relationships are maintained between different templates used for automatic 3D landmarking. Heat map of centroid distances between each of the Danioninae species using four different templates (*Da. rerio*, *Da. aesculapii*, *Da. kyathit*, and *Da. nigrofasciatus*).



Supplemental Figure 4.3 Centroid distance relationships are maintained between 3000 and 6700 automatically placed 3D landmarks. Heat map of centroid distances between each of the Danioninae species using different amounts of automatic landmarks.



Supplemental Table 4.2. Summary of species identification of species obtained from the pet trade.

Species	Established species attribute	Study species attribute	Reference
<i>Danio aequipinnatus</i>	9.5-10.5 dorsal rays upper jaw length: 9.2-12% SL	10-11 dorsal rays upper jaw length: 8.75-9.26% SL	Kullander et al., 2017
<i>Chela dadiburjori</i>	dark blue lateral stripe with 2-5 circular spots along length	dark blue lateral stripe with 2-5 circular spots along length	Menon, 1952
<i>Danio erythromicron</i>	long ascending arm relative to premaxilla length	long ascending arm relative to premaxilla length	Galindo et al., 2019
<i>Danio kyathit</i>	9 dorsal soft rays 19-20 anal soft rays 33 vertebrae	9 dorsal soft rays 16 anal soft rays 27 vertebrae	FishBase
<i>Danio margaritatus</i>	3 anal spines 30-32 vertebrae	3 anal spines 28 vertebrae	FishBase

CHAPTER 5

Discussion: Research summary and future directions

5.1 RESEARCH SUMMARY & FUTURE DIRECTIONS

5.1.1 Research goals

My goals in this dissertation were threefold: 1) To explore the normal changes that the zebrafish skeleton undergoes during postembryonic development, 2) To determine the roles of TH in bringing about these changes in the skull, 3) To capture the diversity of craniofacial phenotypes across relatives of the zebrafish and test for evidence that shifts in TH metabolism could underlie Danioninae adaptation.

5.1.2 A developmental framework for assessing disrupted phenotypes

In this dissertation, I investigated the dynamic changes the zebrafish skeleton undergoes during juvenile and adult development (Chapter 2). I used microCT due its sensitivity and ability to capture shape information at a high resolution, showing that during postembryonic stages of development, the specific elements of the zebrafish skeleton continue to undergo changes in morphology. In the context of our research, microCT technology enabled us to segment out specific bones of interest throughout juvenile and adult development in order to study shape change in great detail. Segmenting out specific elements such as the lower jaw and vertebral bodies, I demonstrated the continual growth and shape change that occurs into reproductive maturity.

I demonstrated some of the applications of this skeletal reference, using our scans to make both qualitative and quantitative observations. Our results highlight the dynamic nature of the zebrafish skeleton during metamorphosis and later stages of development, showing that while these changes are not as drastic as the bone remodeling of amphibian metamorphosis, the skeleton progressively increases in bone volume and density at these

stages. Working with and processing our high resolution scans, we provided more resolution on the developmental anatomical context and spatial information of the zebrafish skeleton.

While microCT data provide researchers with valuable information, data-rich scans can require large amounts of storage space and access to costly analysis software (Tesařová et al., 2019). I generated interactive 3D PDFs, embedding fully processed 3D models with preset views into files that can be easily accessed by all interested users without cost (Nguyen et al., 2022). In addition to the generated 3D PDFs, all raw data from the microCT scans have been uploaded and are readily available on both MorphoSource, a repository for 3D data and FaceBase, an online resource for craniofacial researchers (Boyer et al., 2016; McMenamin et al., 2022; Samuels et al., 2020). These resources provide other researchers full access to our unprocessed scans from which numerous qualitative and quantitative measurements can be taken. This dataset contributes to a growing body of resources for zebrafish researchers, providing a developmental framework in which dynamic processes disrupted in a disease model can be compared to the normal rates of ossification and skeletal change established by this reference, as demonstrated by the application of the dataset to Chapters 3 and 4 of this dissertation.

5.1.3 Advancement of the understanding of the role of thyroid hormone in zebrafish skeletogenesis during postembryonic development

In Chapter 3, we determined that the zebrafish skeleton continues to change and develop during metamorphosis and juvenile and adult stages. In other prior studies, TH has been shown to regulate developmental transitions and the development of adult morphologies (Campinho, 2019; Campinho et al., 2014; Hu et al., 2019; Keer et al., 2019).

In Chapter 3, we examined how thyroid hormone shapes the zebrafish craniofacial skeleton across developmental time and what shifts in developmental timing occur in HypoTH and HyperTH conditions. Using 2D geometric morphometrics, we showed that these specific skeletal elements undergo structural remodeling during normal development, and that TH is required for the proper structural remodeling of these bones. We demonstrate that TH not only influences dermal and endochondral ossification but also stimulates developmental shape changes in these bones.

Further, the remodeling and continued growth of multiple craniofacial elements must be coordinated in a spatiotemporal manner through adult development for the proper formation of the entire zebrafish skull as a single structure. Using the skeletal reference from the previous chapter and 3D geometric morphometrics, we deployed a manual landmarking scheme that outlined several bones of interests on all sides and aspects of the zebrafish head. Here, we showed that during later stages of development, the zebrafish skull continues to elongate and widen. After characterizing these shape changes during normal development, we then compared this development trajectory to those of hypothyroid and hyperthyroid fish. We found heterochronic shifts in developmental timing in which skulls of hypothyroid fish retain immature skull morphologies compared to equally sized wild-type counterparts. In contrast, we determined that hyperthyroid fish underwent precocious shape change when compared to the wild-type condition.

After determining which bones and regions are most sensitive to TH titer, we used fluorescent reporters to observe osteoblast and chondrocyte populations during larval developing, asking whether altering the presence of these cell types gives rise to the observed shape differences in each TH condition. Comparing wild-type and HypoTH

conditions, we found no differences in osteoblast populations in numerous bones including the premaxilla, dermatocranium, and branchiostegal rays. Meckel's cartilage of the lower jaw in HypoTH fish was composed of disorganized chondrocytes while the wild-type zebrafish had tightly packed and organized chondrocytes in Meckel's cartilage. Together, this body of work advances the understanding of the TH regulation of skeletal morphogenesis during metamorphic and postmetamorphic development, highlighting specific elements that can be assayed for changes in functional morphology comparing different TH conditions.

Other research suggests that the TH signaling axis acts a target of major selection during fish speciation. In arctic charr, a cold-water fish from the Salmonidae family, thyroid hormone signaling has been shown to play a role in lineage specification (Woronowicz et al., 2023). Differences in thyroid hormone concentration and lower levels of thyroid-stimulating hormone-beta2 gene expression have been found in stream-resident threespine stickleback compared to marine sticklebacks, indicating that allelic variation of TH genes may play a role in the evolution of phenotypic traits in closely related species (Kitano et al., 2010). Further, changes in the degree of integration and modularity across developmental time and under different TH conditions can also be examined, providing insight into whether TH plays a role in these patterns of integration and modularity in zebrafish.

5.1.4 Insight into the craniofacial diversity of the Danioninae subfamily

The last research chapter of this dissertation asked whether phenotypes induced by changing TH concentration mirrors some of the natural evolutionary diversity seen across Danioninae craniofacial skeletons. Heterochronic shifts in the rate or timing of

developmental processes contribute to evolutionary diversity and transformation (Goswami et al., 2013; McNamara, 2012). Danioninae relatives of the zebrafish have seen a growing interest in recent years, as they have the potential to serve as comparative counterpoints to zebrafish in genomic and evolutionary studies (McCluskey & Postlethwait, 2015). For example, the evolution of pigment patterns of Danios has been extensively studied (Irion & Nüsslein-Volhard, 2019; McCluskey et al., 2021; Parichy, 2021).

In this chapter, we characterized the craniofacial diversity across several Danioninae species and then compared these skulls to those of TH-modulated *Da. rerio* and *Da. albolineatus*. Specifically, we asked whether the heterochronic shifts observed in the altered TH profiles underpin the natural diversity of Danioninae. Our study found most of the craniofacial variation in the shape the jaw elements and dermatocranium, and in the aspect ratio of craniofacial skeletons (ratio of head length to head depth). These data also suggest that altering TH condition has the capacity to create unique craniofacial phenotypes, as the skull shapes we measured in TH-altered profiles of *Da. rerio* and *Da. albolineatus* did not directly map onto any other species examined. We conclude that TH-modulated *Danio* heads do not exactly mirror the natural diversity of these Danioninae species. However, this body of work surveys the species diversification of Danioninae head shape, obtaining the first high resolution scans for many of these Danioininae species and laying the groundwork for future comparative cellular and molecular work.

5.1.5 Conclusion and future directions

In summary, my work demonstrated that TH is indeed essential in bringing about postembryonic developmental changes during zebrafish metamorphosis. The hormone is also essential for development of a normal craniofacial shape in a relative of the zebrafish, *Da. albolineatus*. Further, I captured a range of natural phenotypic variation present across Danioninae. I showed that while the phenotypic shifts brought about by shifts in thyroid concentration do not exactly mirror the head shapes of the Danioninae species studied in this dissertation, these TH-modulated heads more closely resemble other Danioninae species, indicating that TH could be a possible substrate for evolution. While little is known about TH signaling in these species, I have shown that modulating TH levels in the Danioninae species *Da. rerio* and *Da. albolineatus* results in altered craniofacial phenotypes.

These findings suggest that TH can be further assessed for its roles in skeletogenesis by measuring differences in TH physiology or expression of TH-related genes, shedding light on how genetic changes can modify phenotypic traits such as craniofacial morphologies. Future work may focus on measuring TH concentration and metabolic rates in Danioninae, as well as determining the genetic differentiation of TH genes among these species. Heterochronic shifts in developmental timing are responsible for many specialized morphologies and because TH plays an important role in regulating many physiological changes associated with teleost metamorphosis, this work suggests that the TH pathway maybe be a target for adaptive radiation.

REFERENCES

- Adams, Dean C., Collyer, M. L., Kaliontzopoulou, A., Baken, E. (2022, June 23). *Geomorph: Software for geometric morphometric analyses. R package version 4.0.4*. Comprehensive R Archive Network (CRAN). <https://cran.r-project.org/package=geomorph>
- Ahnelt, H., Herdina, A. N., & Metscher, B. D. (2015). Unusual pharyngeal dentition in the African Chedrin fishes (Teleostei: Cyprinidae): Significance for phylogeny and character evolution. *Zoologischer Anzeiger - A Journal of Comparative Zoology*, 255, 85–102. <https://doi.org/10.1016/J.JCZ.2015.02.007>
- Alberch, P., Gould, S. J., Oster, G. F., & Wake, D. B. (1979). Size and Shape in Ontogeny and Phylogeny. *Paleobiology*, 5(3), 296–317. <http://www.jstor.org/stable/2400262>
- Alt, B., Reibe, S., Feitosa, N. M., Elsalini, O. A., Wendl, T., & Rohr, K. B. (2006). Analysis of origin and growth of the thyroid gland in zebrafish. *Developmental Dynamics*, 235(7), 1872–1883. <https://doi.org/10.1002/DVDY.20831>
- Arratia, G., & Schultze, H. -P. (1992). Reevaluation of the caudal skeleton of certain actinopterygian fishes: III. Salmonidae. Homologization of caudal skeletal structures. *Journal of Morphology*, 214(2), 187–249. <https://doi.org/10.1002/JMOR.1052140209>
- Atukorala, A. D. S., & Ratnayake, R. K. (2021). Cellular and molecular mechanisms in the development of a cleft lip and/or cleft palate; insights from zebrafish (*Danio rerio*). *The Anatomical Record*, 304(8), 1650–1660. <https://doi.org/10.1002/AR.24547>
- Baken, E. K., Collyer, M. L., Kaliontzopoulou, A., & Adams, D. C. (2021). geomorph v4.0 and gmShiny: Enhanced analytics and a new graphical interface for a comprehensive morphometric experience. *Methods in Ecology and Evolution*, 12(12), 2355–2363. <https://doi.org/10.1111/2041-210X.13723>
- Bakos, B., Takacs, I., Stern, P. H., & Lakatos, P. (2018). *Skeletal Effects of Thyroid Hormones*. <https://doi.org/10.1007/s12018-018-9246-z>
- Bassett, J. H. D., & Williams, G. R. (2018a). Thyroid Hormone in Bone and Joint Disorders. *Genetics of Bone Biology and Skeletal Disease*, 547–569. <https://doi.org/10.1016/B978-0-12-804182-6.00031-9>
- Bassett, J. H. D., & Williams, G. R. (2018b). Thyroid Hormone in Bone and Joint Disorders. *Genetics of Bone Biology and Skeletal Disease*, 547–569. <https://doi.org/10.1016/B978-0-12-804182-6.00031-9>
- Biga, P. R., & Goetz, F. W. (2006). Zebrafish and giant danio as models for muscle growth: Determinate vs. indeterminate growth as determined by morphometric analysis. *American Journal of Physiology - Regulatory Integrative and Comparative Physiology*, 291(5), 1327–1337. <https://doi.org/10.1152/AJPREGU.00905.2005/ASSET/IMAGES/LARGE/ZH60110654560009.JPEG>
- Bird, N. C., & Mabee, P. M. (2003). Developmental Morphology of the Axial Skeleton of the Zebrafish, *Danio rerio* (Ostariophysi: Cyprinidae). In *Developmental Dynamics* (Vol. 228, Issue 3, pp. 337–357). John Wiley & Sons, Ltd. <https://doi.org/10.1002/dvdy.10387>

- Bonett, R. M. (2021). Heterochrony. *Evolutionary Developmental Biology*, 15–28. https://doi.org/10.1007/978-3-319-32979-6_71
- Bonett, R. M., Steffen, M. A., & Robison, G. A. (2014). Heterochrony repolarized: A phylogenetic analysis of developmental timing in plethodontid salamanders. *EvoDevo*, 5(1), 1–18. <https://doi.org/10.1186/2041-9139-5-27/FIGURES/7>
- Boyer, D. M., Gunnell, G. F., Kaufman, S., & McGeary, T. M. (2016). MORPHOSOURCE: ARCHIVING AND SHARING 3-D DIGITAL SPECIMEN DATA. *The Paleontological Society Papers*, 22, 157–181. <https://doi.org/10.1017/scs.2017.13>
- Britz, R., Conway, K. W., & Rüber, L. (2021). The emerging vertebrate model species for neurophysiological studies is *Danionella cerebrum*, new species (Teleostei: Cyprinidae). *Scientific Reports 2021 11:1*, 11(1), 1–11. <https://doi.org/10.1038/s41598-021-97600-0>
- Brown, D. D., & Cai, L. (2007). Amphibian metamorphosis. *Developmental Biology*, 306(1), 20–33. <https://doi.org/10.1016/J.YDBIO.2007.03.021>
- Bruneel, B., & Witten, P. E. (2015). Power and challenges of using zebrafish as a model for skeletal tissue imaging. *The American Society for Bone and Mineral Research*, 56(2), 161–173. <https://doi.org/10.3109/03008207.2015.1013193>
- Caetano-Lopes, J., Henke, K., Urso, K., Duryea, J., Charles, J. F., Warman, M. L., & Harris, M. P. (2020). Unique and non-redundant function of *csf1r* paralogs in regulation and evolution of post-embryonic development of the zebrafish. *Development (Cambridge)*, 147(2). <https://doi.org/10.1242/dev.181834>
- Callieri, M. (2013). *Meshlab as a Complete Open Tool for the Integration of Photos and Colour with High-Resolution 3D Geometry Data*.
- Campinho, M. A. (2019). Teleost metamorphosis: The role of thyroid hormone. *Frontiers in Endocrinology*, 10(JUN). <https://doi.org/10.3389/fendo.2019.00383>
- Campinho, M. A., Saraiva, J., Florindo, C., & Power, D. M. (2014). Maternal thyroid hormones are essential for neural development in zebrafish. *Molecular Endocrinology*, 28(7), 1136–1149. <https://doi.org/10.1210/me.2014-1032>
- Cardini, A., de Jong, Y. A., & Butynski, T. M. (2022). Can morphotaxa be assessed with photographs? Estimating the accuracy of two-dimensional cranial geometric morphometrics for the study of threatened populations of African monkeys. *Anatomical Record*, 305(6). <https://doi.org/10.1002/ar.24787>
- Chang, C., & Franz-Odenaal, T. A. (2014). The zebrafish infraorbital bones: a descriptive study. *Zebrafish*, 11(1), 50–56. <https://doi.org/10.1089/ZEB.2013.0907>
- Charles, J. F., Sury, M., Tsang, K., Urso, K., Henke, K., Huang, Y., Russell, R., Duryea, J., & Harris, M. P. (2017). Utility of quantitative micro-computed tomographic analysis in zebrafish to define gene function during skeletogenesis. *Bone*, 101, 162–171. <https://doi.org/10.1016/j.bone.2017.05.001>
- Chen, C., Zhou, Z., Zhong, M., Li, M., Yang, X., Zhang, Y., Wang, Y., Wei, A., Qu, M., Zhang, L., Xu, S., Chen, S., & Yu, Z. (2011). Excess Thyroid Hormone Inhibits Embryonic Neural Stem/Progenitor Cells Proliferation and Maintenance through STAT3 Signalling Pathway. *Neurotoxicity Research*, 20(1), 15–25. <https://doi.org/10.1007/s12640-010-9214-y>

- Cignoni, P., Callieri, M., Corsini, M., Dellepiane, M., Ganovelli, F., & Ranzuglia, G. (2008). *MeshLab: an Open-Source Mesh Processing Tool*.
- Clément, A., Wiweger, M., von der Hardt, S., Rusch, M. A., Selleck, S. B., Chien, C.-B., & Roehl, H. H. (2008). Regulation of Zebrafish Skeletogenesis by *ext2/dackel* and *papst1/pinscher*. *PLoS Genetics*, *4*(7), e1000136. <https://doi.org/10.1371/journal.pgen.1000136>
- Conith, M. R., Ringo, D., Conith, A. J., Deleon, A., Wagner, M., McMenamin, S., Cason, C., & Cooper, W. J. (2022). The Evolution of Feeding Mechanics in the Danioninae, or Why Giant Danios Don't Suck Like Zebrafish. *Integrative Organismal Biology*, *4*(1), 1–20. <https://doi.org/10.1093/IOB/OBAC049>
- Conway, K. W., M. Kubicek, K., & Britz, R. (2021). Extreme evolutionary shifts in developmental timing establish the miniature Danionella as a novel model in the neurosciences. *Developmental Dynamics*, *250*(4), 601–611. <https://doi.org/10.1002/DVDY.280>
- Cubbage, C. C., & Mabee, P. M. (1996). Development of the cranium and paired fins in the zebrafish *Danio rerio* (Ostariophysi, Cyprinidae). *Journal of Morphology*, *229*(2), 121–160. [https://doi.org/10.1002/\(SICI\)1097-4687\(199608\)229:2<121::AID-JMOR1>3.0.CO;2-4](https://doi.org/10.1002/(SICI)1097-4687(199608)229:2<121::AID-JMOR1>3.0.CO;2-4)
- de Bakker, B. S., de Jong, K. H., Hagoort, J., Oostra, R. J., & Moorman, A. F. M. (2012). Towards a 3-dimensional atlas of the developing human embryo: The Amsterdam experience. *Reproductive Toxicology*, *34*(2), 225–236. <https://doi.org/10.1016/j.reprotox.2012.05.087>
- de Boer, B. A., van den Berg, G., de Boer, P. A. J., Moorman, A. F. M., & Ruijter, J. M. (2012). Growth of the developing mouse heart: An interactive qualitative and quantitative 3D atlas. *Developmental Biology*, *368*(2), 203–213. <https://doi.org/10.1016/j.ydbio.2012.05.001>
- De Jesus-Silva, L. M., De Oliveira, P. V., Da Silva Ribeiro, C., Ninhaus-Silveira, A., & Veríssimo-Silveira, R. (2018). Ovarian cycle in *Devario aequipinnatus* with emphasis on oogenesis. *Zygote*, *26*(2), 168–176. <https://doi.org/10.1017/S0967199418000060>
- Delaurier, A., Eames, B. F., Blanco-Sánchez, B., Peng, G., He, X., Swartz, M. E., Ullmann, B., Westerfield, M., & Kimmel, C. B. (n.d.). *Zebrafish sp7:EGFP: a transgenic for studying otic vesicle formation, skeletogenesis, and bone regeneration*. <https://doi.org/10.1002/dvg.20639>
- Denoël, M., Drapeau, L., & Winandy, L. (2019). Reproductive fitness consequences of progenesis: Sex-specific pay-offs in safe and risky environments. *Journal of Evolutionary Biology*, *32*(6). <https://doi.org/10.1111/jeb.13449>
- Denoel, M., & Joly, P. (2000). Neoteny and progenesis as two heterochronic processes involved in paedomorphosis in *Triturus alpestris* (Amphibia: Caudata). *Proceedings of the Royal Society of London. Series B: Biological Sciences*, *267*(1451), 1481–1485. <https://doi.org/10.1098/RSPB.2000.1168>
- Dietrich, K., Fiedler, I. A. K., Kurzyukova, A., López-Delgado, A. C., McGowan, L. M., Geurtzen, K., Hammond, C. L., Busse, B., & Knopf, F. (2021). Skeletal Biology and Disease Modeling in Zebrafish. *Journal of Bone and Mineral Research*, *36*(3), 436–458. <https://doi.org/10.1002/JBMR.4256>

- Dong, G., Wang, N., Xu, T., Liang, J., Qiao, R., Yin, D., & Lin, S. (2023). Deep Learning-Enabled Morphometric Analysis for Toxicity Screening Using Zebrafish Larvae. *Environmental Science and Technology*, *57*(46), 18127–18138.
https://doi.org/10.1021/ACS.EST.3C00593/ASSET/IMAGES/LARGE/ES3C00593_0004.JPEG
- Duboule, D. (1994). Temporal colinearity and the phylotypic progression: a basis for the stability of a vertebrate Bauplan and the evolution of morphologies through heterochrony. *Development*, *1994*(Supplement), 135–142.
<https://doi.org/10.1242/DEV.1994.SUPPLEMENT.135>
- Duff, N. M., Sommerfeld, R. E., & Litvak, M. K. (2019). Discriminating Sex in Zebrafish (*Danio rerio*) Using Geometric Morphometrics. *Zebrafish*, *16*(2), 207–213.
<https://doi.org/10.1089/ZEB.2018.1664/ASSET/IMAGES/LARGE/FIGURE6.JPEG>
- Eames, B., DeLaurier, A., Ullmann, B., Huycke, T. R., Nichols, J. T., Dowd, J., McFadden, M., Sasaki, M. M., & Kimmel, C. B. (2013). FishFace: interactive atlas of zebrafish craniofacial development at cellular resolution. *BMC Developmental Biology*, *13*(1), 23. <https://doi.org/10.1186/1471-213X-13-23>
- Esteve-Altava, B., & Rasskin-Gutman, D. (2015). Evo-Devo insights from pathological networks: exploring craniosynostosis as a developmental mechanism for modularity and complexity in the human skull. *Journal of Anthropological Sciences = Rivista Di Antropologia : JASS*, *93*, 103–117.
<https://doi.org/10.4436/JASS.93001>
- Fang, F. (2003). Phylogenetic Analysis of the Asian Cyprinid Genus *Danio* (Teleostei, Cyprinidae). <https://doi.org/10.1643/IA03-131.1>, *2003*(4), 714–728. <https://doi.org/10.1643/IA03-131.1>
- Fazzalari, N. L. (2008). Bone remodeling: A review of the bone microenvironment perspective for fragility fracture (osteoporosis) of the hip. *Seminars in Cell & Developmental Biology*, *19*, 467–472.
<https://doi.org/10.1016/j.semdb.2008.08.003>
- Fricke, R., Eschmeyer, W. N., & Van der Laan, R. (2023, June 6). *ESCHMEYER'S CATALOG OF FISHES: GENERA, SPECIES, REFERENCES*. California Academy of Sciences.
- Galindo, D., Sweet, E., DeLeon, Z., Wagner, M., DeLeon, A., Carter, C., McMenamin, S. K., & Cooper, W. J. (2019). Thyroid hormone modulation during zebrafish development recapitulates evolved diversity in danionin jaw protrusion mechanics. *Evolution & Development*, *21*(5), 231–246.
<https://doi.org/10.1111/ede.12299>
- Gomez, G. A., Aghajanian, P., Pourteymoor, S., Larkin, D., & Mohan, S. (2022). Differences in pathways contributing to thyroid hormone effects on postnatal cartilage calcification versus secondary ossification center development. *ELife*, *11*. <https://doi.org/10.7554/ELIFE.76730>
- Goswami, A., Foley, L., & Weisbecker, V. (2013). Patterns and implications of extensive heterochrony in carnivoran cranial suture closure. *Journal of Evolutionary Biology*, *26*(6), 1294–1306. <https://doi.org/10.1111/JEB.12127>

- Gray, J. A., Gignac, P. M., Stanley, E. L., & Jaimi Gray, C. A. (2023). The first full body diffusible iodine-based contrast-enhanced computed tomography dataset and teaching materials for a member of the Testudines. *The Anatomical Record*. <https://doi.org/10.1002/AR.25282>
- Gupta, T., Marquart, G. D., Horstick, E. J., Tabor, K. M., Pajevic, S., & Burgess, H. A. (2018). Morphometric analysis and neuroanatomical mapping of the zebrafish brain. *Methods*, *150*, 49–62. <https://doi.org/10.1016/J.YMETH.2018.06.008>
- Hammond, C. L., Moro, E., Eames, B., & Roehl, H. (2012). Using transgenic reporters to visualize bone and cartilage signaling during development in vivo. *Frontiers in Endocrinology*. <https://doi.org/10.3389/fendo.2012.00091>
- Harper, M., Hu, Y., Donahue, J., Acosta, B., Braes, F. D., Nguyen, S., Zeng, J., Barbaro, J., Lee, H., Bui, H., & McMenamin, S. K. (2023). Thyroid hormone regulates proximodistal patterning in fin rays. *Proceedings of the National Academy of Sciences of the United States of America*, *120*(21), e2219770120. https://doi.org/10.1073/PNAS.2219770120/SUPPL_FILE/PNAS.2219770120.SD02.XLSX
- Harris, M. P., Henke, K., Hawkins, M. B., & Witten, P. E. (2014). Fish is Fish: The use of experimental model species to reveal causes of skeletal diversity in evolution and disease. *Journal of Applied Ichthyology*, *30*(4), 616–629. <https://doi.org/10.1111/jai.12533>
- Henke, K., Farmer, D. T., Niu, X., Kraus, J. M., Galloway, J. L., & Youngstrom, D. W. (2023). Genetically engineered zebrafish as models of skeletal development and regeneration. *Bone*, *167*, 116611. <https://doi.org/10.1016/J.BONE.2022.116611>
- Hernandez, L. P., & Staab, K. L. (2015). Bottom Feeding and Beyond: How the Premaxillary Protrusion of Cypriniforms Allowed for a Novel Kind of Suction Feeding. *Integrative and Comparative Biology*, *55*(1), 74–84. <https://doi.org/10.1093/ICB/ICV038>
- Hoyo, H., McMahon, A. P., & Ohba, S. (2016). An Emerging Regulatory Landscape for Skeletal Development. *Trends in Genetics*, *32*(12), 774–787. <https://doi.org/10.1016/j.tig.2016.10.001>
- Hu, Y., Mauri, A., Donahue, J., Singh, R., Acosta, B., & McMenamin, S. (2019). Thyroid hormone coordinates developmental trajectories but does not underlie developmental truncation in danionins. *Developmental Dynamics*, *248*(11), 1144–1154. <https://doi.org/10.1002/dvdy.76>
- Hur, M., Gistelinck, C. A., Huber, P., Lee, J., Thompson, M. H., Monstad-Rios, A. T., Watson, C. J., McMenamin, S. K., Willaert, A., Parichy, D. M., Coucke, P., & Kwon, R. Y. (2017). MicroCT-Based phenomics in the zebrafish skeleton reveals virtues of deep phenotyping in a distributed organ system. *ELife*, *6*. <https://doi.org/10.7554/eLife.26014>
- Irion, U., & Nüsslein-Volhard, C. (2019). The identification of genes involved in the evolution of color patterns in fish. *Current Opinion in Genetics & Development*, *57*, 31–38. <https://doi.org/10.1016/J.GDE.2019.07.002>

- Iwai, N., & Tachiki, Y. (2023). Species-specific model to predict amphibian metamorphosis. *Scientific Reports 2023 13:1*, 13(1), 1–8. <https://doi.org/10.1038/s41598-023-43639-0>
- Jarque, S., Rubio-Brotons, M., Ibarra, J., Ordoñez, V., Dyballa, S., Miñana, R., & Terriente, J. (2020). Morphometric analysis of developing zebrafish embryos allows predicting teratogenicity modes of action in higher vertebrates. *Reproductive Toxicology*, 96, 337–348. <https://doi.org/10.1016/J.REPROTOX.2020.08.004>
- Kague, E., Gallagher, M., Burke, S., Parsons, M., Franz-Odenaal, T., & Fisher, S. (2012). Skeletogenic Fate of Zebrafish Cranial and Trunk Neural Crest. *PLoS ONE*, 7(11), e47394. <https://doi.org/10.1371/journal.pone.0047394>
- Kague, E., Roy, P., Asselin, G., Hu, G., Simonet, J., Stanley, A., Albertson, C., & Fisher, S. (2016). Osterix/Sp7 limits cranial bone initiation sites and is required for formation of sutures. *Developmental Biology*, 413(2), 160–172. <https://doi.org/10.1016/J.YDBIO.2016.03.011>
- Kanther, M., Scalici, A., Rashid, A., Miao, K., Van Deventer, E., & Fisher, S. (2019). Initiation and early growth of the skull vault in zebrafish. *Mechanisms of Development*, 160, 103578. <https://doi.org/10.1016/j.mod.2019.103578>
- Keer, S., Cohen, K., May, C., Hu, Y., McMenamin, S., & Hernandez, L. P. (2019). Anatomical Assessment of the Adult Skeleton of Zebrafish Reared Under Different Thyroid Hormone Profiles. *Anatomical Record*, 302(10), 1754–1769. <https://doi.org/10.1002/ar.24139>
- Keer, S., Storch, J. D., Nguyen, S., Prado, M., Singh, R., Hernandez, L. P., & McMenamin, S. K. (2022). Thyroid hormone shapes craniofacial bones during postembryonic zebrafish development. *Evolution & Development*, 24(1–2), 61–76. <https://doi.org/10.1111/EDE.12399>
- Kikinis, R., Pieper, S. D., & Vosburgh, K. G. (2014). 3D Slicer: A Platform for Subject-Specific Image Analysis, Visualization, and Clinical Support. In *Intraoperative Imaging and Image-Guided Therapy* (pp. 277–289). Springer New York. https://doi.org/10.1007/978-1-4614-7657-3_19
- Kim, H.-Y., & Mohan, S. (2013). Role and Mechanisms of Actions of Thyroid Hormone on the Skeletal Development. *Bone Research*, 1(2), 146–161. <https://doi.org/10.4248/BR201302004>
- Kimmel, C. B., DeLaurier, A., Ullmann, B., Dowd, J., & McFadden, M. (2010a). Modes of developmental outgrowth and shaping of a craniofacial bone in zebrafish. *PLoS One*, 5(3), e9475. <https://doi.org/10.1371/journal.pone.0009475>
- Kimmel, C. B., DeLaurier, A., Ullmann, B., Dowd, J., & McFadden, M. (2010b). Modes of Developmental Outgrowth and Shaping of a Craniofacial Bone in Zebrafish. *PLoS ONE*, 5(3), e9475. <https://doi.org/10.1371/journal.pone.0009475>
- Kitano, J., Lema, S. C., Luckenbach, J. A., Mori, S., Kawagishi, Y., Kusakabe, M., Swanson, P., & Peichel, C. L. (2010). Adaptive Divergence in the Thyroid Hormone Signaling Pathway in the Stickleback Radiation. *Current Biology*, 20(23), 2124–2130. <https://doi.org/10.1016/J.CUB.2010.10.050>

- Kullander, S. O., Rahman, M. M., Norén, M., & Mollah, A. R. (2017). Devario in Bangladesh: Species diversity, sibling species, and introgression within danionin cyprinids (Teleostei: Cyprinidae: Danioninae). *PLoS ONE*, *12*(11). <https://doi.org/10.1371/journal.pone.0186895>
- Kwon, R. Y., Watson, C. J., & Karasik, D. (2019a). Using zebrafish to study skeletal genomics. *Bone*, *126*, 37–50. <https://doi.org/10.1016/J.BONE.2019.02.009>
- Kwon, R. Y., Watson, C. J., & Karasik, D. (2019b). Using zebrafish to study skeletal genomics. *Bone*, *126*, 37–50. <https://doi.org/10.1016/J.BONE.2019.02.009>
- Kyomen, S., Murillo-Rincón, A. P., & Kaucká, M. (2023). Evolutionary mechanisms modulating the mammalian skull development. *Philosophical Transactions of the Royal Society B*, *378*(1880). <https://doi.org/10.1098/RSTB.2022.0080>
- Laizé, V., Gavaia, P. J., & Cancela, M. L. (2014). Fish: a suitable system to model human bone disorders and discover drugs with osteogenic or osteotoxic activities. *Drug Discovery Today: Disease Models*, *13*, 29–37. <https://doi.org/10.1016/J.DDMOD.2014.08.001>
- Laue, K., Pogoda, H. M., Daniel, P. B., Van Haeringen, A., Alanay, Y., Von Ameln, S., Rachwalski, M., Morgan, T., Gray, M. J., Breuning, M. H., Sawyer, G. M., Sutherland-Smith, A. J., Nikkels, P. G., Kubisch, C., Bloch, W., Wollnik, B., Hammerschmidt, M., & Robertson, S. P. (2011). Craniosynostosis and multiple skeletal anomalies in humans and zebrafish result from a defect in the localized degradation of retinoic acid. *American Journal of Human Genetics*, *89*(5), 595–606. <https://doi.org/10.1016/J.AJHG.2011.09.015>
- Leitch, V. D., Bassett, J. H. D., & Williams, G. R. (2020). Role of thyroid hormones in craniofacial development. *Nature Reviews Endocrinology*, *16*(3), 147–164. <https://doi.org/10.1038/s41574-019-0304-5>
- Liao, T. Y., Kullander, S. O., & Fang, F. (2011). Phylogenetic position of rasborin cyprinids and monophyly of major lineages among the Danioninae, based on morphological characters (Cypriniformes: Cyprinidae). *Journal of Zoological Systematics and Evolutionary Research*, *49*(3), 224–232. <https://doi.org/10.1111/J.1439-0469.2011.00621.X>
- Liao, W. N., You, M. S., Ulhaq, Z. S., Li, J. P., Jiang, Y. J., Chen, J. K., & Tse, W. K. F. (2023). Micro-CT analysis reveals the changes in bone mineral density in zebrafish craniofacial skeleton with age. *Journal of Anatomy*, *242*(3), 544–551. <https://doi.org/10.1111/JOA.13780>
- Mayden, R. L., Tang, K. L., Conway, K. W., Freyhof, J., Chamberlain, S., Haskins, M., Schneider, L., Sudkamp, M., Wood, R. M., Agnew, M., Bufalino, A., Sulaiman, Z., Miya, M., Saitoh, K., & He, S. (2007). Phylogenetic relationships of Danio within the order cypriniformes: A framework for comparative and evolutionary studies of a model species. *Journal of Experimental Zoology Part B: Molecular and Developmental Evolution*, *308*(5), 642–654. <https://doi.org/10.1002/JEZ.B.21175>
- McClure, M. M., McIntyre, P. B., & McCune, A. R. (2006). Notes on the natural diet and habitat of eight danionin fishes, including the zebrafish *Danio rerio*.

- Journal of Fish Biology*, 69(2), 553–570. <https://doi.org/10.1111/J.1095-8649.2006.01125.X>
- McCluskey, B. M., & Postlethwait, J. H. (2015). Phylogeny of Zebrafish, a “Model Species,” within Danio, a “Model Genus.” *Molecular Biology and Evolution*, 32(3), 635–652. <https://doi.org/10.1093/MOLBEV/MSU325>
- McCluskey, B. M., Uji, S., Mancusi, J. L., Postlethwait, J. H., & Parichy, D. M. (2021). A complex genetic architecture in zebrafish relatives *Danio quagga* and *D. kyathit* underlies development of stripes and spots. *PLOS Genetics*, 17(4), e1009364. <https://doi.org/10.1371/JOURNAL.PGEN.1009364>
- McMenamin, S., Carter, C., & Cooper, W. J. (2017). Thyroid Hormone Stimulates the Onset of Adult Feeding Kinematics in Zebrafish. *Zebrafish*, 14(6), 517–525. <https://doi.org/10.1089/ZEB.2017.1453>
- McMenamin, S. K., Bain, E. J., McCann, A. E., Patterson, L. B., Eom, D. S., Waller, Z. P., Hamill, J. C., Kuhlman, J. A., Eisen, J. S., & Parichy, D. M. (2014). Thyroid hormone-dependent adult pigment cell lineage and pattern in zebrafish. *Science*, 345(6202), 1358–1361. <https://doi.org/10.1126/science.1256251>
- McMenamin, S. K., Nguyen, S. V., & Blythe, J. O. (2022, December 8). *Thyroid hormone mediates juvenile and adult craniofacial shape change in zebrafish*. FaceBase Consortium. <https://www.facebase.org/id/1Q-X114>
- McMenamin, S. K., & Parichy, D. M. (2013). Metamorphosis in Teleosts. *Current Topics in Developmental Biology*, 103, 127–165. <https://doi.org/10.1016/B978-0-12-385979-2.00005-8>
- McNamara, K. J. (2012). Heterochrony: The Evolution of Development. *Evolution: Education and Outreach*, 5(2), 203–218. <https://doi.org/10.1007/S12052-012-0420-3/FIGURES/12>
- Mekdara, P. J., Nasimi, F., Schwalbe, M. A. B., & Tytell, E. D. (2021). Tail Beat Synchronization during Schooling Requires a Functional Posterior Lateral Line System in Giant Danios, *Devario aequipinnatus*. *Integrative and Comparative Biology*, 61(2), 427–441. <https://doi.org/10.1093/ICB/ICAB071>
- Menon, A. G. K. (1952). Notes on Fishes in the Indian Museum. XLVI. On a New Fish of the Genus *Laubuca* from Cochin. *Records of the Zoological Survey of India*, 49(1), 1–4. <https://doi.org/10.26515/RZSI/V49/I1/1952/162080>
- Mork, L., & Crump, G. (2015). Zebrafish Craniofacial Development: A Window into Early Patterning. *Current Topics in Developmental Biology*, 115, 235. <https://doi.org/10.1016/BS.CTDB.2015.07.001>
- Nguyen, S. V., Lanni, D., Xu, Y., Michaelson, J. S., & McMenamin, S. K. (2022). Dynamics of the Zebrafish Skeleton in Three Dimensions During Juvenile and Adult Development. *Frontiers in Physiology*, 13, 1027. <https://doi.org/10.3389/FPHYS.2022.875866/BIBTEX>
- Ohba, S. (2023). Regulatory landscape of Runx2 and Sp7 in osteoblast and chondrocyte lineages: Recent findings from next-generation sequencer-based studies. *Oral Science International*. <https://doi.org/10.1002/OSI2.1184>
- Okamiya, H., Sugime, R., Furusawa, C., Inoue, Y., & Kishida, O. (2021). Paedomorphosis in the Ezo salamander (*Hynobius retardatus*) rediscovered

- after almost 90 years. *Zoological Letters*, 7(1). <https://doi.org/10.1186/s40851-021-00183-x>
- Olszta, M. J., Cheng, X., Jee, S. S., Kumar, R., Kim, Y. Y., Kaufman, M. J., Douglas, E. P., & Gower, L. B. (2007). Bone structure and formation: A new perspective. *Materials Science and Engineering: R: Reports*, 58(3–5), 77–116. <https://doi.org/10.1016/J.MSER.2007.05.001>
- Parichy, D. M. (2006). Evolution of danio pigment pattern development. *Heredity* 2006 97:3, 97(3), 200–210. <https://doi.org/10.1038/sj.hdy.6800867>
- Parichy, D. M. (2021). Evolution of pigment cells and patterns: recent insights from teleost fishes. *Current Opinion in Genetics & Development*, 69, 88–96. <https://doi.org/10.1016/J.GDE.2021.02.006>
- Parichy, D. M., Elizondo, M. R., Mills, M. G., Gordon, T. N., & Engeszer, R. E. (2009). Normal table of postembryonic zebrafish development: Staging by externally visible anatomy of the living fish. *Developmental Dynamics*, 238(12), 2975–3015. <https://doi.org/10.1002/dvdy.22113>
- Polly, P. D., & Motz, G. J. (2016). Patterns and Processes in Morphospace: Geometric Morphometrics of Three-Dimensional Objects. *The Paleontological Society Papers*, 22(October), 71–99. <https://doi.org/10.1017/scs.2017.9>
- Porto, A., Rolfe, S., & Maga, A. M. (2021). ALPACA: A fast and accurate computer vision approach for automated landmarking of three-dimensional biological structures. *Methods in Ecology and Evolution*, 12(11), 2129–2144. <https://doi.org/10.1111/2041-210X.13689>
- Ranieri, I. L. (2023). *Thyroid Hormone Modulates Zebrafish Pectoral Fin Development*. Boston College.
- Raterman, S. T., Metz, J. R., Wagener, F. A. D. T. G., & Von den Hoff, J. W. (2020). Zebrafish Models of Craniofacial Malformations: Interactions of Environmental Factors. *Frontiers in Cell and Developmental Biology*, 8, 1346. <https://doi.org/10.3389/FCCELL.2020.600926/BIBTEX>
- Ritman, E. L. (2002). Molecular imaging in small animals—roles for micro-CT. *Journal of Cellular Biochemistry*, 87(S39), 116–124. <https://doi.org/10.1002/JCB.10415>
- Roberts, T. R. (2007). The celestial pearl danio, a new genus and species of colourful minute cyprinid fish from Myanmar (Pisces: Cypriniformes). *The Raffles Bulletin of Zoology*, 55(1), 131–140. <http://repository.si.edu/xmlui/handle/10088/12143>
- Ruthsatz, K., Dausmann, K. H., Paesler, K., Babos, P., Sabatino, N. M., Peck, M. A., & Glos, J. (2020). Shifts in sensitivity of amphibian metamorphosis to endocrine disruption: the common frog (*Rana temporaria*) as a case study. *Conservation Physiology*, 8(1). <https://doi.org/10.1093/CONPHYS/COAA100>
- Sado, T., & Kimura, S. (2005). Developmental morphology of the cyprinid fish *Chela dadiburjori*. *Ichthyological Research*, 52(1), 20–26. <https://doi.org/10.1007/S10228-004-0249-Z/METRICS>
- Salhotra, A., Shah, H. N., Levi, B., & Longaker, M. T. (2020). Mechanisms of bone development and repair. *Nature Reviews Molecular Cell Biology* 2020 21:11, 21(11), 696–711. <https://doi.org/10.1038/s41580-020-00279-w>

- Samuels, B. D., Aho, R., Brinkley, J. F., Bugacov, A., Feingold, E., Fisher, S., Gonzalez-Reiche, A. S., Hacia, J. G., Hallgrimsson, B., Hansen, K., Harris, M. P., Ho, T. V., Holmes, G., Hooper, J. E., Jabs, E. W., Jones, K. L., Kesselman, C., Klein, O. D., Leslie, E. J., ... Chai, Y. (2020). FaceBase 3: Analytical tools and FAIR resources for craniofacial and dental research. *Development (Cambridge)*, 147(18). <https://doi.org/10.1242/DEV.191213/225842>
- Schindelin, J., Arganda-Carreras, I., Frise, E., Kaynig, V., Longair, M., Pietzsch, T., Preibisch, S., Rueden, C., Saalfeld, S., Schmid, B., Tinevez, J. Y., White, D. J., Hartenstein, V., Eliceiri, K., Tomancak, P., & Cardona, A. (2012). Fiji: an open-source platform for biological-image analysis. *Nature Methods* 2012 9:7, 9(7), 676–682. <https://doi.org/10.1038/nmeth.2019>
- Schneider, C. A., Rasband, W. S., & Eliceiri, K. W. (2012). NIH Image to ImageJ: 25 years of image analysis. *Nature Methods* 2012 9:7, 9(7), 671–675. <https://doi.org/10.1038/nmeth.2089>
- Shibusawa, N., Endo, Y., Morimoto, N., Takahashi, I., & Miura, T. (2021). Mathematical modeling of palatal suture pattern formation: morphological differences between sagittal and palatal sutures. *Scientific Reports* 2021 11:1, 11(1), 1–14. <https://doi.org/10.1038/s41598-021-88255-y>
- Shkil, F. N., Kapitanova, D. V., Borisov, V. B., Abdissa, B., & Smirnov, S. V. (2012). Thyroid hormone in skeletal development of cyprinids: Effects and morphological consequences. *Journal of Applied Ichthyology*, 28(3), 398–405. <https://doi.org/10.1111/j.1439-0426.2012.01992.x>
- Silvent, J., Akiva, A., Brumfeld, V., Reznikov, N., Rechav, K., Yaniv, K., Addadi, L., & Weiner, S. (2017). Zebrafish skeleton development: High resolution micro-CT and FIB-SEM block surface serial imaging for phenotype identification. *PLOS ONE*, 12(12), e0177731. <https://doi.org/10.1371/journal.pone.0177731>
- Staab, K. L., Holzman, R., Hernandez, L. P., & Wainwright, P. C. (2012). Independently evolved upper jaw protrusion mechanisms show convergent hydrodynamic function in teleost fishes. *Journal of Experimental Biology*, 215(9), 1456–1463. <https://doi.org/10.1242/JEB.066308>
- Tang, K. L., Agnew, M. K., Hirt, M. V., Sado, T., Schneider, L. M., Freyhof, J., Sulaiman, Z., Swartz, E., Vidthayanon, C., Miya, M., Saitoh, K., Simons, A. M., Wood, R. M., & Mayden, R. L. (2010). Systematics of the subfamily Danioninae (Teleostei: Cypriniformes: Cyprinidae). *Molecular Phylogenetics and Evolution*, 57(1), 189–214. <https://doi.org/10.1016/J.YMPEV.2010.05.021>
- Teng, C. S., Ting, M. C., Farmer, D. T., Brockop, M., Maxson, R. E., & Crump, J. G. (2018). Altered bone growth dynamics prefigure craniosynostosis in a zebrafish model of Saethre-Chotzen syndrome. *ELife*, 7. <https://doi.org/10.7554/ELIFE.37024>
- Tesařová, M., Heude, E., Comai, G., Zikmund, T., Kaucká, M., Adameyko, I., Tajbakhsh, S., & Kaiser, J. (2019). An interactive and intuitive visualisation method for X-ray computed tomography data of biological samples in 3D Portable Document Format. *Scientific Reports*, 9(1), 1–8. <https://doi.org/10.1038/s41598-019-51180-2>

- Thambirajah, A. A., Koide, E. M., Imbery, J. J., & Helbing, C. C. (2019). Contaminant and environmental influences on thyroid hormone action in amphibian metamorphosis. *Frontiers in Endocrinology*, *10*(MAY), 451610. <https://doi.org/10.3389/FENDO.2019.00276/BIBTEX>
- Tonelli, F., Bek, J. W., Besio, R., De Clercq, A., Leoni, L., Salmon, P., Coucke, P. J., Willaert, A., & Forlino, A. (2020). Zebrafish: A Resourceful Vertebrate Model to Investigate Skeletal Disorders. *Frontiers in Endocrinology*, *11*, 489. <https://doi.org/10.3389/FENDO.2020.00489/BIBTEX>
- Tsang, K. Y., Chan, D., & Cheah, K. S. E. (2015). Fate of growth plate hypertrophic chondrocytes: Death or lineage extension? *Development, Growth & Differentiation*, *57*(2), 179–192. <https://doi.org/10.1111/DGD.12203>
- Tsang, K. Y., & Cheah, K. S. (2019). The extended chondrocyte lineage: implications for skeletal homeostasis and disorders. *Current Opinion in Cell Biology*, *61*, 132–140. <https://doi.org/10.1016/J.CEB.2019.07.011>
- Tuchendler, D., & Bolanowski, M. (2014). The influence of thyroid dysfunction on bone metabolism. *Thyroid Research*, *7*(1), 1–5. <https://doi.org/10.1186/s13044-014-0012-0>
- Vancamp, P., & Darras, V. M. (2018). From zebrafish to human: A comparative approach to elucidate the role of the thyroid hormone transporter MCT8 during brain development. *General and Comparative Endocrinology*, *265*, 219–229. <https://doi.org/10.1016/J.YGCEN.2017.11.023>
- Vancamp, P., Houbrechts, A. M., & Darras, V. M. (2018). Insights from zebrafish deficiency models to understand the impact of local thyroid hormone regulator action on early development. *General and Comparative Endocrinology*. <https://doi.org/10.1016/J.YGCEN.2018.09.011>
- Vasconcelos-Filho, J. E., Thomsen, F. S. L., Stosic, B., Antonino, A. C. D., Duarte, D. A., Heck, R. J., Lessa, R. P. T., Santana, F. M., Ferreira, B. P., & Duarte-Neto, P. J. (2019). Peeling the Otolith of Fish: Optimal Parameterization for Micro-CT Scanning. *Frontiers in Marine Science*, *6*, 728. <https://doi.org/10.3389/fmars.2019.00728>
- Vassilieva, A. B., & Smirnov, S. V. (2021). Increasing Hormonal Control of Skeletal Development: An Evolutionary Trend in Amphibians. *Frontiers in Ecology and Evolution*, *9*. <https://doi.org/10.3389/fevo.2021.733947>
- Vorbach, B. S., Chandasana, H., Derendorf, H., & Yanong, R. P. E. (2019). Pharmacokinetics of Oxytetracycline in the Giant Danio (*Devario aequipinnatus*) following bath immersion. *Aquaculture*, *498*, 12–16. <https://doi.org/10.1016/J.AQUACULTURE.2018.08.027>
- Wahl, R., Mudri, D., Bilić curčić, I., Bilić, B., Bilić curčić, B., Meštrović, L. M., Mihaljević mihaljević, I., & Kizivat, T. (2023). Hyperthyroidism and Wnt Signaling Pathway: Influence on Bone Remodeling. *Metabolites 2023, Vol. 13, Page 241*, *13*(2), 241. <https://doi.org/10.3390/METABO13020241>
- Walker, M. B., & Kimmel, C. B. (2007). A two-color acid-free cartilage and bone stain for zebrafish larvae. *Biotechnic and Histochemistry*, *82*(1), 23–28. <https://doi.org/10.1080/10520290701333558>
- Waung, J. A., Bassett, J. H. D., & Williams, G. R. (2012). Thyroid hormone metabolism in skeletal development and adult bone maintenance. *Trends in*

- Endocrinology & Metabolism*, 23(4), 155–162.
<https://doi.org/10.1016/J.TEM.2011.11.002>
- Weigele, J., & Franz-Odenaal, T. A. (2016). Functional bone histology of zebrafish reveals two types of endochondral ossification, different types of osteoblast clusters and a new bone type. *Journal of Anatomy*, 229(1), 92–103.
<https://doi.org/10.1111/JOA.12480>
- Witten, P. E., Hansen, A., & Hall, B. K. (2001). Features of mono- and multinucleated bone resorbing cells of the zebrafish *Danio rerio* and their contribution to skeletal development, remodeling, and growth. *Journal of Morphology*, 250(3), 197–207. <https://doi.org/10.1002/jmor.1065>
- Wojcicka, A., Bassett, J. H. D., & Williams, G. R. (2013). Mechanisms of action of thyroid hormones in the skeleton. *Biochimica et Biophysica Acta (BBA) - General Subjects*, 1830(7), 3979–3986.
<https://doi.org/10.1016/J.BBAGEN.2012.05.005>
- Woronowicz, K. C., Esin, E. V., Markevich, G. N., Daane, J. M., Harris, M. P., & Shkil, F. N. (2023). Phylogenomic analysis of the Lake Kronotskoe species flock of Dolly Varden charr reveals genetic signatures of sympatric radiation. *BioRxiv*, 2023.02.24.529919. <https://doi.org/10.1101/2023.02.24.529919>
- Xie, H., Li, M., Kang, Y., Zhang, J., & Zhao, C. (2022). Zebrafish: an important model for understanding scoliosis. *Cellular and Molecular Life Sciences* 2022 79:9, 79(9), 1–16. <https://doi.org/10.1007/S00018-022-04534-5>
- Yelick, P. C., & Schilling, T. F. (2002). Molecular dissection of craniofacial development using zebrafish. *Critical Reviews in Oral Biology and Medicine : An Official Publication of the American Association of Oral Biologists*, 13(4), 308–322. <https://doi.org/10.1177/154411130201300402>
- Zelditch, M., Swiderski, D., Sheets, H., & Fink, W. (2004). Geometric Morphometrics for Biologists. *Geometric Morphometrics for Biologists*, 1–443.
<https://doi.org/10.1016/B978-0-12-778460-1.X5000-5>